

UNCLASSIFIED

Copy

5

~~RESTRICTED~~

RM A9H11a

NACA RM A9H11a

CLASSIFICATION CHANGED

To UNCLASSIFIED

~~RESTRICTED~~
NACA

By authority of *H. L. Dryden* Date *6-11-53*

per NACA Release form #1505
By HLR, 7-20-53

RESEARCH MEMORANDUM

TESTS OF A MODEL HORIZONTAL TAIL OF ASPECT RATIO 4.5 IN
THE AMES 12-FOOT PRESSURE WIND TUNNEL. II - ELEVATOR
HINGE LINE NORMAL TO THE PLANE OF SYMMETRY

By Bruce E. Tinling and Jerald K. Dickson

Ames Aeronautical Laboratory
Moffett Field, Calif.

CLASSIFIED DOCUMENT

This document contains classified information affecting the National Defense of the United States within the meaning of the Espionage Act, USC 5031 and 5041. Its transmission or the revelation of its contents in any manner to an unauthorized person is prohibited by law. Information so classified may be imparted only to persons in the military and naval services of the United States, appropriate civilian officers and employees of the Federal Government who have a legitimate interest therein, and to United States citizens of known loyalty and discretion who of necessity must be informed thereof.

NATIONAL ADVISORY COMMITTEE FOR AERONAUTICS

WASHINGTON
October 17, 1949

~~RESTRICTED~~

UNCLASSIFIED



NATIONAL ADVISORY COMMITTEE FOR AERONAUTICS

RESEARCH MEMORANDUM

TESTS OF A MODEL HORIZONTAL TAIL OF ASPECT RATIO 4.5 IN

THE AMES 12-FOOT PRESSURE WIND TUNNEL. II - ELEVATOR

HINGE LINE NORMAL TO THE PLANE OF SYMMETRY

By Bruce E. Tinling and Jerald K. Dickson

SUMMARY

Wind-tunnel tests have been conducted to evaluate the independent effects of Reynolds and Mach numbers on the aerodynamic characteristics of a horizontal tail equipped with a 0.30-chord, plain, sealed elevator with a tab. The elevator hinge line was normal to the plane of symmetry. The airfoil sections parallel to the plane of symmetry were the NACA 64A010.

The Reynolds number was varied from 2,000,000 to 11,000,000 at a Mach number of 0.21, and the Mach number was varied from 0.21 to 0.88 at a Reynolds number of 2,000,000. Lift, drag, pitching moment, elevator hinge moment, tab hinge moment, chordwise distribution of static pressure at the midsemispan, and pressure difference across the elevator-nose seal were measured.

An increase of Reynolds number from 2,000,000 to 11,000,000 increased the angle of attack for the stall by approximately 2° . Changes in Reynolds number from 2,000,000 to 11,000,000 had little effect on the aerodynamic characteristics of the tail at angles of attack below the stall.

Abrupt decreases in the lift-curve slope and in the elevator effectiveness occurred at a Mach number of about 0.85. The Mach numbers at which marked changes in the elevator hinge-moment coefficients occurred were dependent upon the magnitude of angle of attack and elevator deflection. In general, however, the changes of elevator hinge-moment coefficient were gradual as the Mach number was increased to 0.80. The tab was effective in reducing the elevator hinge moments throughout the Mach number range. Calculations indicated that incorporation of sufficient sealed internal balance to reduce the variation of elevator hinge moment with elevator deflection by 50 percent at a Mach number of 0.21 would cause only a 10-percent reduction for elevator deflections greater than 5° at a Mach number of 0.85.

UNCLASSIFIED

Comparison of the results of this investigation with those for a horizontal tail of the same aspect ratio, taper ratio, and airfoil section but with the quarter-chord line swept back 35° showed that the abrupt decrease in lift-curve slope occurred at a Mach number about 0.08 greater for the swept-back horizontal tail. The Mach numbers at which a decrease in elevator effectiveness occurred were very nearly the same for both horizontal tails, but the rate of decrease of elevator effectiveness with further Mach number increase was much less for the swept-back horizontal tail. Abrupt changes in the elevator hinge-moment coefficients occurred at higher Mach numbers for the swept-back horizontal tail than for the horizontal tail without sweep.

INTRODUCTION

A systematic investigation has been undertaken at the Ames Aeronautical Laboratory to determine experimentally the control-effectiveness and hinge-moment parameters of horizontal tails. References 1 through 5 present results of low-speed wind-tunnel tests of both swept and unswept horizontal tails of several aspect ratios, all having the same taper ratio and airfoil section.

The tests reported herein were conducted to evaluate the effects of compressibility and dynamic scale on a horizontal tail with elevator hinge line normal to the plane of symmetry, the low-speed aerodynamic characteristics of which have been reported in reference 2. The results of the tests of the horizontal tail without sweepback are compared with the results of tests of a horizontal tail of the same aspect ratio, taper ratio, and airfoil section but with 35° of sweepback of the quarter-chord line (reference 6).

NOTATION

C_D	drag coefficient	$\left(\frac{\text{drag}}{qS} \right)$
C_L	lift coefficient	$\left(\frac{\text{lift}}{qS} \right)$
C_{he}	elevator hinge-moment coefficient	$\left(\frac{\text{elevator hinge moment}}{2q M_{Ae}} \right)$
C_{ht}	tab hinge-moment coefficient	$\left(\frac{\text{tab hinge moment}}{2q M_{At}} \right)$

- C_m pitching-moment coefficient about a lateral axis passing through the quarter point of the mean aerodynamic chord
- $$\left(\frac{\text{pitching-moment}}{qS\bar{c}} \right)$$
- M Mach number $\left(\frac{V}{a} \right)$
- P pressure coefficient $\left(\frac{p_l - p}{q} \right)$
- P_{Cr} critical pressure coefficient, pressure coefficient corresponding to a local Mach number of 1.0 in a streamwise direction
- $$\left\{ \frac{2}{\gamma M^2} \left[\left(\frac{2}{\gamma+1} + \frac{\gamma-1}{\gamma+1} M^2 \right)^{\frac{\gamma}{\gamma-1}} - 1 \right] \right\}$$
- R Reynolds number $\left(\frac{\rho V \bar{c}}{\mu} \right)$
- $\frac{\Delta p}{q}$ pressure coefficient across the elevator-nose seal
- $$\left(\frac{\text{pressure below the seal} - \text{pressure above the seal}}{\text{free-stream dynamic pressure}} \right)$$
- M_{Ae} first moment of the elevator area behind the elevator hinge line about the hinge line, feet cubed
- M_{At} first moment of the tab area behind the tab hinge line about the tab hinge line, feet cubed
- S semispan horizontal-tail model area, square feet
- V airspeed, feet per second
- a speed of sound, feet per second
- $b/2$ semispan, measured perpendicular to the plane of symmetry, feet
- c chord, measured parallel to the plane of symmetry, feet
- \bar{c} mean aerodynamic chord $\left(\frac{\int_0^{b/2} c^2 dy}{\int_0^{b/2} c dy} \right)$, feet

c_e	chord of the elevator behind the hinge line measured perpendicular to the elevator hinge line, feet
p_t	local static pressure, pounds per square foot
p	free-stream static pressure, pounds per square foot
q	free-stream dynamic pressure, pounds per square foot
y	lateral distance normal to plane of symmetry, feet
α	corrected angle of attack, degrees
α_u	angle of attack, uncorrected for tunnel-wall interference and angle-of-attack counter correction, degrees
γ	ratio of specific heats $\left(\frac{\text{specific heat at constant pressure}}{\text{specific heat at constant volume}} \right)$
δ_e	elevator deflection (positive to increase lift) measured in a plane normal to the elevator hinge line, degrees
δ_t	tab deflection (positive to increase lift) measured in a plane normal to the tab hinge line, degrees
ρ	density of air, slugs per cubic foot
μ	absolute viscosity of air, slugs per foot-second

$$C_{L\alpha} = \left(\frac{\partial C_L}{\partial \alpha} \right)_{\delta_e = \delta_t = 0} \quad (\text{measured through } \alpha=0), \text{ per degree}$$

$$C_{L\delta_e} = \left(\frac{\partial C_L}{\partial \delta_e} \right)_{\alpha = \delta_t = 0} \quad (\text{measured through } \delta_e=0), \text{ per degree}$$

$$\alpha_{\delta_e} = - \left(\frac{C_{L\delta_e}}{C_{L\alpha}} \right)_{C_L=0}$$

$$C_{he\alpha} = \left(\frac{\partial C_{he}}{\partial \alpha} \right)_{\delta_e = \delta_t = 0} \quad (\text{measured through } \alpha=0), \text{ per degree}$$

$$C_{he\delta_e} = \left(\frac{\partial C_{he}}{\partial \delta_e} \right)_{\alpha = \delta_t = 0} \quad (\text{measured through } \delta_e=0), \text{ per degree}$$

$$C_{he\delta_t} = \left(\frac{\partial C_{he}}{\partial \delta_t} \right)_{\alpha = \delta_e = 0} \quad (\text{measured through } \delta_t=0), \text{ per degree}$$

The subscripts outside the parentheses represent the factors held constant during the measurement of the parameters.

MODEL

The semispan model tested in this investigation represented a horizontal tail of aspect ratio 4.5 and taper ratio 0.5 (fig. 1). The airfoil section parallel to the plane of symmetry was the NACA 64A010 (table I). The 70-percent-chord line of the tail was perpendicular to the plane of symmetry. The tip shape was formed by rotating the section parallel to the undisturbed stream about a line inboard of the tip a distance equal to the maximum tip ordinate.

The model was equipped with a full-span, radius-nose, sealed elevator, the chord of which was 30 percent of the model chord. The elevator was hinged to the stabilizer at 28, 81, and 95 percent of the semispan. These hinges and a close-fitting block at the plane of symmetry divided the sealed balance chamber into three separate sections. The seals were fitted closely to the ends of each section to reduce leakage to a minimum. The elevator was equipped with an unsealed tab, the area of which was 5.9 percent of the elevator area and which extended from 23.7 to 44.8 percent of the semispan. The elevator and the tab hinge gaps are shown in figure 1.

The stabilizer was constructed of solid steel and the elevator of aluminum alloy. The model was mounted vertically with the wind-tunnel floor serving as a reflection plane as shown in figure 2. The rotating turntable upon which the model was mounted is directly connected to the force-measuring apparatus. The elevator and the tab hinge moments were measured with resistance-type electric strain gages. The elevator gage was beneath the turntable cover plates, and the tab gage was contained within the elevator. The elevator deflection was remotely controlled, and the tab deflection was set by means of an indexing system built into the tab and elevator. The gap between the elevator and the reflection plane was approximately 0.02 inch.

A chordwise row of orifices was provided at 50 percent of the semispan to measure the chordwise distribution of static pressure. Six orifices to measure the pressure difference across the elevator-nose seal were located in the balance chamber, one on either side of the seal at 13, 49, and 91 percent of the semispan.

CORRECTIONS TO DATA

The data have been corrected for the effects of tunnel-wall interference, for constriction due to the presence of the tunnel walls, and for model-support tare forces.

Tunnel-Wall Interference

Corrections to the data for the effects of tunnel-wall interference have been evaluated by the methods of reference 7 using the theoretical span loading for incompressible flow calculated by the methods of reference 8. The corrections added to the drag coefficient and to the angle of attack were:

$$\Delta \alpha = 0.329 C_L, \text{ degrees}$$

$$\Delta C_D = 0.00502 C_L^2$$

No attempt was made to separate the tunnel-wall interference effects resulting from lift due to elevator deflection and lift due to angle of attack. No corrections were applied to the pitching-moment or hinge-moment data.

Constriction Effects

The data have been corrected for the constriction effects due to the presence of the tunnel walls by the methods of reference 9. The following table shows the magnitude of the corrections to Mach number and to dynamic pressure:

<u>Corrected Mach number</u>	<u>Uncorrected Mach number</u>	<u>q uncorrected q corrected</u>
0.210	0.210	1.001
.600	.600	1.001
.750	.749	1.002
.800	.798	1.002
.850	.848	1.003
.880	.876	1.004

Tares

A correction to the drag data was necessary to allow for forces on the exposed surface of the turntable. This correction was determined from tests with the model removed from the tunnel. The correction was found to vary with Reynolds number only and is presented in the following table:

<u>R × 10⁻⁶</u>	<u>C_D tare</u>
1.00	0.0071
2.00	.0063
5.00	.0058
11.00	.0056

No attempt was made to evaluate the tares due to possible interference effects between the model and the turntable. No account was taken of the tunnel floor boundary layer which at the location of the model had a displacement thickness of $1/2$ inch.

TESTS

Reynolds Number Effects

To determine the effects of Reynolds number on the aerodynamic characteristics of the horizontal tail, the lift, drag, pitching moment, and elevator hinge moment were measured for a Mach number of 0.21 at Reynolds numbers of 2,000,000, 5,000,000, and 11,000,000. For these tests the angle-of-attack range was from -10° to 20° , the elevator deflections were 0° , -10° , and -20° , and the tab was undeflected. For Mach numbers of 0.60, 0.80, and 0.88, similar data were obtained at Reynolds numbers of 1,000,000 and 2,000,000 with the elevator and the tab undeflected.

Mach Number Effects

To determine the effects of compressibility on the aerodynamic characteristics of the horizontal tail, the lift, drag, pitching moment, elevator hinge moment, tab hinge moment, pressure difference across the elevator-nose seal, and chordwise distribution of static pressure were measured at a Reynolds number of 2,000,000 at Mach numbers of 0.21, 0.60, 0.75, 0.80, 0.85, and 0.88. The angle-of-attack range was from -10° to 20° except at Mach numbers greater than 0.80 where the angle-of-attack range was limited by wind-tunnel power. For the greater part of the tests, the range of elevator deflection was from -20° to 4° . Lift and hinge-moment measurements were made for tab deflections of 0° , 5° , 10° , and 15° for the complete range of Mach numbers and elevator deflections at uncorrected angles of attack of 0° and 4° .

Effects of Standard Roughness and Removal of the Elevator-Nose Seal

Tests were also made to evaluate the separate effects of standard leading-edge roughness (reference 10), and of removing the elevator-nose seal. Data were obtained at a Reynolds number of 2,000,000 over the angle-of-attack range for elevator deflections of 4° , 0° , and -15° with the tab undeflected at Mach numbers of 0.21, 0.80, and 0.88.

RESULTS AND DISCUSSION

The results of tests conducted to evaluate the effects of Reynolds number on the aerodynamic characteristics of the horizontal tail are

presented in figures 3 and 4, and the results of tests conducted to evaluate the effects of Mach number are presented in figures 5 through 12. The data from tests conducted to evaluate the separate effects of leading-edge roughness and of removal of the elevator-nose seal are presented in figures 13 through 16. An index to the figures presenting the results is given in the appendix.

Certain data are presented for values of uncorrected angle of attack α_u where

$$\alpha = 0.99\alpha_u + \Delta\alpha$$

The constant 0.99 is the ratio between the geometric angle of attack and the uncorrected angle of attack indicated by the angle-of-attack counter. The uncorrected angle of attack does not differ from the corrected value by more than 0.30° for any of the test points presented.

Effect of Reynolds Number

Low speed.—The effects of increasing the Reynolds number from 2,000,000 to 11,000,000 at a Mach number of 0.21 are presented in figure 3. Increasing the Reynolds number from 2,000,000 to 5,000,000 increased the angle of attack at which the stall occurred when the elevator was undeflected by approximately 2° and increased the maximum lift coefficient by about 0.10; no further increase in this maximum lift coefficient occurred when the Reynolds number was increased to 11,000,000. Increasing the Reynolds number from 2,000,000 to 11,000,000 had no important effect on any of the aerodynamic characteristics at angles of attack less than that for stall.

The slope parameters measured from results of tests of a geometrically similar model conducted in the Ames 7- by 10-foot wind tunnel are presented for comparison with those evaluated from results of the present tests in the following table:

Slope parameter	Ames 7- by 10-foot wind tunnel (Reference 2) R = 3,000,000	Ames 12-foot pressure wind tunnel R = 2,000,000
$C_{L\alpha}$	0.066	0.063
$C_{L\delta_e}$.045	.044
$C_{he\alpha}$	- .0020	- .0032
$C_{he\delta_e}$	- .0093	- .0100
Aerodynamic center, percent \bar{c} ($C_L = 0, \delta_e = 0$)	22.9	25.0

The large difference in the values of $C_{he\alpha}$ is due to the non-linearity near 0° angle of attack of the data shown in figure 3(b) for a Reynolds number of 2,000,000 with the elevator undeflected. The values of $\frac{\partial C_{he}}{\partial \alpha}$ for 0° elevator deflection measured between 2° and 4° angle of attack from the data from the Ames 12-foot pressure wind tunnel for a Reynolds number of 2,000,000 and from the Ames 7-by-10-foot wind-tunnel data were about the same, having a value of approximately -0.0020 . The reason for the difference of 2.1 percent of the mean aerodynamic chord in the location of the aerodynamic center is not known.

High subsonic speeds.— Figure 4 presents a comparison between data obtained at Reynolds numbers of 2,000,000 and 1,000,000 at Mach numbers of 0.60, 0.80, and 0.88. At Mach numbers of 0.60 and 0.80 the decrease in Reynolds number had little effect other than to decrease the lift at angles of attack greater than about 6° . At a Mach number of 0.88, decreasing the Reynolds number from 2,000,000 to 1,000,000 resulted in a decrease of lift-curve slope of 0.015 per degree at small angles of attack, a forward movement of the aerodynamic center at zero lift of 8.4 percent of the mean aerodynamic chord, and a more rapid increase of drag coefficient with lift coefficient.

Effect of Mach Number

The aerodynamic characteristics of the horizontal tail at a Reynolds number of 2,000,000 for Mach numbers from 0.21 to 0.88 are presented in figures 5 through 12.

Lift.— The variation of lift coefficient with angle of attack is presented in figure 5. With the elevator undeflected, increasing the Mach number from 0.21 to 0.80 reduced the maximum angle of attack for which stabilizer effectiveness was maintained from approximately 12° to 8° . Further increase of Mach number increased the angle of attack for which the stabilizer remained effective. At a Mach number of 0.88, the stabilizer was effective (for $\delta_e = 0$) to an angle of attack of at least 12° ; wind-tunnel power limitations prevented further increase in angle of attack at this Mach number.

The elevator was effective in producing changes in lift at Mach numbers of 0.21 and 0.60 throughout the angle-of-attack range for all negative elevator deflections. As the Mach number was increased beyond 0.60, the range of elevator deflection and the range of angle of attack for which the elevator was effective was progressively reduced. At a Mach number of 0.88, the elevator was not effective when deflected negatively more than 4° if the angle of attack was greater than about 4° . The variation of lift coefficient with elevator deflection at an uncorrected angle of attack of 0° is presented in figure 17. These data show that the range of elevator deflection for which the elevator effectiveness

was constant diminished as the Mach number was increased to 0.85.

The effects of Mach number on the values of the stabilizer-effectiveness parameter $C_{L\alpha}$, the elevator-effectiveness parameter $C_{L\delta_e}$, and α_{δ_e} are shown in figure 18. Gradual increases in $C_{L\alpha}$ and $C_{L\delta_e}$ occurred as the Mach number was increased from 0.21 to 0.85, $C_{L\alpha}$ increasing from 0.063 to 0.088 and $C_{L\delta_e}$ increasing from 0.044 to 0.061. Increasing the Mach number had little effect on the value of α_{δ_e} until a Mach number of 0.85 was exceeded. Further increase in Mach number to 0.88 caused an abrupt decrease in the value of α_{δ_e} .

Elevator hinge moment.— The elevator hinge-moment coefficients for various Mach numbers up to 0.88 are presented in figure 6 as a function of angle of attack and in figure 7 as a function of elevator deflection. At the higher Mach numbers the slopes of the curves vary considerably with angle of attack and with elevator deflection. It is apparent, therefore, that at the higher Mach numbers the hinge-moment parameters $C_{he\delta_e}$ and $C_{he\alpha}$ are not indicative of the hinge-moment characteristics of the horizontal tail and that any discussion in terms of these parameters would be misleading. The data of figure 19 show that, at Mach numbers less than about 0.80, increasing the Mach number caused gradual changes in the hinge-moment coefficients for elevator deflections and angles of attack between $\pm 6^\circ$. The Mach numbers at which rapid changes in the elevator hinge-moment coefficients occurred were dependent upon the angle of attack and elevator deflection.

Effect of tab.— The variation of elevator hinge-moment coefficient with elevator deflection for several tab deflections is presented in figure 7. The tab-effectiveness parameter $C_{he\delta_t}$, measured at 0° angle of attack and 0° elevator deflection, had a value of approximately -0.0040 and was little affected by compressibility. This is evident from the data of figure 20, which present the increment of elevator hinge-moment coefficient produced by tab deflection ΔC_{he} as a function of Mach number. However, with the elevator deflected more than -6° , little increase in balancing hinge moment was obtained as the tab was deflected to more than 10° at a Mach number of 0.88. The change in lift coefficient due to deflection of the tab is shown in figure 17.

The tab hinge-moment coefficients are presented in figure 8 to permit application of the tab-effectiveness data to the design of a simple or spring-tab installation.

Pressure difference across the elevator-nose seal.— The variation of the pressure coefficient across the elevator-nose seal with elevator deflection is presented in figure 9. Leakage around the ends of the

seal in each section of the balance chamber may have had an effect on these data, especially those for the tip section of the balance chamber where the ratio of leakage area to vent area between the curtains and the elevator was the greatest. The data of figure 9(a) are in fair agreement with those presented in reference 2 for elevator deflections up to -9° .

Inspection of the data presented in figure 9 reveals that, in general, the rate of change of pressure coefficient across the elevator-nose seal with elevator deflection, measured at 0° elevator deflection, became more positive (greater balancing effect) as the Mach number was increased. At a Mach number of 0.21, the rate of change of balancing pressure with elevator deflection decreased at large negative elevator deflections. At 0° angle of attack, for example, the balancing pressure in the middle section of the balance chamber decreased as the elevator was deflected more than -15° . As the Mach number was increased, a decrease of balancing effectiveness occurred at progressively smaller elevator deflections. At a Mach number of 0.85, the rate of change of balancing pressure with elevator deflection in the middle section of the balance chamber decreased markedly at an elevator deflection of approximately -4° when the angle of attack was 0° .

In order to evaluate the reduction of elevator hinge moment obtainable through the use of a sealed internal aerodynamic balance, the hinge-moment coefficients have been computed for an elevator with a balance plate having a chord equal to 0.35 of the elevator chord and extending from 0 to 96 percent of the semispan. The total elevator-deflection range would be limited to approximately 36° if this amount of internal balance were employed. In computing the hinge-moment characteristics of the balanced elevator, it was assumed that the pressure difference indicated by each pair of orifices existed uniformly over the balance plate between the center lines of the hinges which limited that section of the balance chamber wherein the orifices were located. The computed hinge moments of the balanced elevator are presented with the measured hinge moments of the radius-nose, sealed elevator in figure 21. These computations show that, at a Mach number of 0.21, use of the sealed internal balance would result in a 50-percent reduction in $\frac{\partial C_{h_e}}{\partial \delta_e}$ for elevator deflections less than about -15° . As the Mach number was increased, the range of elevator deflection for which $\frac{\partial C_{h_e}}{\partial \delta_e}$ would be reduced by the internal balance was progressively decreased. At a Mach number of 0.85, for example, the calculated value of $\frac{\partial C_{h_e}}{\partial \delta_e}$ was reduced by only about 10 percent when the elevator was deflected more than -5° . At this Mach number, the calculated value of $\frac{\partial C_{h_e}}{\partial \delta_e}$ was approximately zero between elevator deflections of $\pm 2^\circ$. Any greater amount of internal balance would result in overbalance for small elevator deflections at a Mach number of 0.85.

The effect of the sealed internal aerodynamic balance on the variation of elevator hinge-moment coefficient with angle of attack (fig. 21) was small.

Pitching moment.— The pitching-moment coefficients about the quarter point of the mean aerodynamic chord are presented in figure 10. These data show that the static longitudinal stability increased markedly at the stall.

The rate of change of pitching-moment coefficient with lift coefficient indicates that the aerodynamic center (for $\delta_e = 0$ and $C_L = 0$) moved gradually forward from 25 to 23 percent of the mean aerodynamic chord as the Mach number was increased from 0.21 to 0.77 (fig. 22). Further Mach number increase to about 0.86 resulted in a rapid rearward shift of the aerodynamic center to about 28 percent of the mean aerodynamic chord.

Drag.— The drag data of figure 11 are summarized in figure 23, where the minimum drag coefficient, maximum lift-drag ratio, and the lift coefficient for maximum lift-drag ratio are presented as a function of Mach number. The Mach number for drag divergence, defined as the Mach number at which $\frac{\partial C_D}{\partial M} = 0.10$, was approximately 0.84 when the elevator was undeflected. The maximum lift-drag ratio was 24.8 at a Mach number of 0.21 and was decreased to 23.0 by an increase in Mach number to 0.75. Further Mach number increase caused an abrupt decrease of maximum lift-drag ratio, the value for a Mach number of 0.88 being roughly one-third of that at a Mach number of 0.75.

Pressure distribution.— The chordwise distribution of static pressure at the midsemispan was measured to correlate the effects of Mach number on the aerodynamic characteristics, as evaluated from force measurements, with the changes in surface pressures, and to provide data for structural design. The pressure-distribution data are presented in figure 12 for various angles of attack and elevator deflections for which force data are presented.

Inspection of the data of figure 12 reveals that regions of supersonic flow existed over the horizontal tail at the higher Mach numbers. Deflection of the elevator had little effect on the surface pressures forward of any point on the stabilizer where the flow was supersonic. This affords an explanation of the loss of elevator effectiveness at the higher Mach numbers. The abrupt increase with increasing Mach number of the elevator hinge-moment coefficient for small elevator deflections (fig. 19(b)) may be correlated with the change in pressure distribution which occurred when the flow over the elevator became supersonic.

Effects of Leading-Edge Roughness

Results of tests conducted with standard roughness, as defined in reference 10, are presented in figures 13 through 16 for Mach numbers of 0.21, 0.80, and 0.88. Results of tests conducted without leading-edge roughness are also presented in these figures.

Leading-edge roughness caused reductions in the lift at large angles of attack at all Mach numbers for which data were obtained and caused the stall to be less abrupt at a Mach number of 0.21. (See fig. 13(a).) Both the stabilizer-effectiveness parameter and the elevator-effectiveness parameter were reduced when leading-edge roughness was applied. This effect was greatest at a Mach number of 0.88 where $C_{L\alpha}$ was reduced by 0.017 per degree and $C_{L\delta_e}$ was reduced by 0.019 per degree. It was assumed in measuring $C_{L\delta_e}$ that the elevator effectiveness was constant between deflections of 0° and 4° .

Inspection of the data of figure 14 shows that leading-edge roughness caused sizable reductions in the variation of elevator hinge-moment coefficient with elevator deflection.

The data of figure 15 indicate that leading-edge roughness caused the aerodynamic center (for $\delta_e = 0$ and $C_L = 0$) to shift forward at Mach numbers of 0.80 and 0.88. This effect was greatest at a Mach number of 0.88 where the aerodynamic center (for $\delta_e = 0$ and $C_L = 0$) was shifted from 28.0 to 17.4 percent of the mean aerodynamic chord.

Effect of Removal of the Elevator-Nose Seal

The effect of removal of the elevator-nose seal is shown in figures 13 through 15 where comparison is made between data obtained with the elevator nose sealed and with the elevator nose unsealed.

Unsealing the elevator nose had no important effect on the variation of lift with angle of attack, but did reduce the elevator effectiveness. (See fig. 13.) This reduction was greatest at a Mach number of 0.88 where the value of $C_{L\delta_e}$ decreased by 0.011 per degree.

Unsealing the elevator nose had small effects on the elevator hinge-moment coefficients as is shown by the data of figure 14.

Comparison of the Effects of Mach Number on Two Horizontal Tails Which Differed Primarily in the Angle of Sweepback

Comparison of the effects of compressibility on the aerodynamic characteristics of the horizontal tail of this investigation with those of a similar horizontal tail which differed primarily in the angle of

sweepback may be made from the data presented in figures 22 through 25. The NACA 64A010 airfoil sections of the swept-back horizontal tail were inclined 35° to the plane of symmetry and the quarter-chord line of these airfoil sections was swept back 35° . The elevator chord was 30 percent of the chord of the airfoil section in each case, which resulted in the elevator area of the swept-back horizontal tail being smaller by 2.8 percent of the total model area. Comparison of the low-speed aerodynamic characteristics of these horizontal tails has been made in reference 2, and the effects of Reynolds and Mach numbers on the aerodynamic characteristics of the swept-back horizontal tail have been reported in reference 6.

The Mach number at which an abrupt decrease in the stabilizer-effectiveness parameter $C_{L\alpha}$ occurred was greater by about 0.08 for the swept-back horizontal tail. (See fig. 22.) The Mach number at which the elevator-effectiveness parameter $C_{L\delta_e}$ began to decrease was nearly the same for both horizontal tails; however, the value of $C_{L\delta_e}$ for the unswept horizontal tail decreased much more rapidly with further increase of Mach number than did that for the swept-back horizontal tail.

The data of figure 23 show that the Mach numbers for which abrupt changes in the elevator hinge-moment coefficients occurred were greater for the swept-back horizontal tail. It should be noted that the moment of the area of the unswept elevator was greater than that of the swept-back elevator by a factor of 1.413. This fact must be considered if a comparison of the hinge moments of the two elevators is to be made.

The aerodynamic-center location (at $C_L = 0$ for $\delta_e = 0$) of the swept-back horizontal tail changed very little as the Mach number was increased to 0.85 and moved rapidly rearward with further increase in Mach number. (See fig. 24.) For the unswept tail, the aerodynamic center (at $C_L = 0$ for $\delta_e = 0$) moved forward 2 percent of the mean aerodynamic chord as the Mach number was increased from 0.21 to 0.78 and then moved rapidly rearward with further increase of Mach number.

The Mach number for drag divergence was greater by about 0.07 for the swept-back horizontal tail. The minimum drag coefficient of the unswept horizontal tail, however, was less than that of the swept-back horizontal tail at Mach numbers less than about 0.81 (fig. 25).

SUMMARY OF RESULTS

The results of wind-tunnel tests conducted to evaluate the independent effects of Reynolds and Mach numbers on the aerodynamic characteristics of a horizontal tail of aspect ratio 4.5 with the hinge line normal to the plane of symmetry have been presented.

Results of tests at a Mach number of 0.21 at Reynolds numbers of 2,000,000, 5,000,000, and 11,000,000 indicated that:

1. An increase in Reynolds number from 2,000,000 to 5,000,000 increased the angle of attack for the stall by approximately 2° and increased the maximum lift coefficient by about 0.10; no further increases occurred when the Reynolds number was increased to 11,000,000.

2. Change in Reynolds number from 2,000,000 to 11,000,000 had little effect on the aerodynamic characteristics at angles of attack below the stall.

Results of tests at a Reynolds number of 2,000,000 over a range of Mach numbers from 0.21 to 0.88 indicated that:

1. Increasing the Mach number from 0.21 to 0.85 increased the lift-curve slope from 0.063 to 0.088 per degree; further increase of Mach number caused an abrupt decrease in lift-curve slope.

2. The elevator-effectiveness parameter $C_{L\delta_e}$ increased from 0.044 to 0.061 per degree between Mach numbers of 0.21 and 0.85 and decreased abruptly as the Mach number was increased to 0.88.

3. The Mach number at which a marked change in the elevator hinge-moment coefficient occurred was dependent upon the angle of attack and the elevator deflection; however, the changes in the elevator hinge-moment coefficients at angles of attack and elevator deflections between $\pm 6^\circ$ were gradual as the Mach number was increased to 0.80.

4. The tab was effective in producing a balancing increment of elevator hinge moment throughout the Mach number range.

5. Incorporation of a sealed internal balance sufficient to cause a 50-percent reduction in the variation of elevator hinge moment with elevator deflection at a Mach number of 0.21 caused only a 10-percent reduction at a Mach number of 0.85 for elevator deflections more negative than -5° .

Results of tests to evaluate the effect of leading-edge roughness indicated that:

1. Leading-edge roughness caused reductions in the lift-curve slope and in the elevator effectiveness.

2. Leading-edge roughness caused a sizable reduction in the variation of elevator hinge-moment coefficient with elevator deflection.

Results of tests made to evaluate the effect of unsealing the elevator-nose gap indicated that:

1. Unsealing the elevator-nose gap had no important effect on the lift-curve slope, but reduced the elevator effectiveness.

2. Little change in the elevator hinge-moment coefficients resulted from unsealing the elevator-nose gap.

Comparison of the effects of Mach number on the aerodynamic characteristics of the horizontal tail tested in this investigation and of a horizontal tail with 35° of sweepback which had the same aspect ratio, taper ratio, and airfoil section indicated that:

1. The Mach number at which abrupt decrease in the lift-curve slope occurred was approximately 0.08 greater for the swept-back horizontal tail.

2. The elevator effectiveness began to decrease at about the same Mach number for both horizontal tails, but the decrease was much less rapid for the swept-back horizontal tail.

3. The Mach number at which abrupt change in the elevator hinge-moment coefficient occurred was greater for the swept-back horizontal tail.

Ames Aeronautical Laboratory,
National Advisory Committee for Aeronautics,
Moffett Field, Calif.

APPENDIX

The following tables have been included to provide a convenient index to the data of this report.

FORCE AND MOMENT CHARACTERISTICS

Reynolds number primary variable
 $[\delta_t = 0^\circ]$

Results presented	R	M	α , deg	δ_e , deg	Figure number
C_L vs α	2,000,000 to 11,000,000	0.21	-10 to 20	0, -10, -20	3(a)
C_{he} vs α	↓	↓	↓	↓	3(b)
C_L vs C_m	↓	↓	↓	↓	3(c)
C_L vs C_D	↓	↓	↓	↓	3(d)
C_L vs α	1,000,000 and 2,000,000	0.60, 0.80, 0.88		0	4(a)
C_{he} vs α	↓	↓	↓	↓	4(b)
C_L vs C_m	↓	↓	↓	↓	4(c)
C_L vs C_D	↓	↓	↓	↓	4(d)

Mach Number Primary Variable
[R=2,000,000]

Results presented	M	α , deg	δ_e , deg	δ_t , deg	Figure number	
C_L vs α	0.21	-10 to 20	4 to -25	0	5(a)	
	0.60	↓	4 to -20		5(b)	
	0.75	↓	↓		5(c)	
	0.80	↓	↓		5(d)	
	0.85	-10 to 16	↓		5(e)	
	0.88	-10 to 14	4 to -15		5(f)	
C_{he} vs α	0.21	-10 to 20	4 to -25		0 to 15	6(a)
	0.60	↓	4 to -20			6(b)
	0.75	↓	↓			6(c)
	0.80	↓	↓			6(d)
	0.85	-10 to 16	4 to -15			6(e)
	0.88	-10 to 14	4 to -15			6(f)
C_{he} vs δ_e	0.21	0, 4	4 to -25	0 to 15		7(a)
	0.60	↓	4 to -20			7(b)
	0.75	↓	↓			7(c)
	0.80	↓	↓			7(d)
	0.85	↓	4 to -15			7(e)
	0.88	↓	4 to -15			7(f)
C_{ht} vs δ_e	0.21, 0.60	↓	4 to -25		0	8(a)
	0.75	↓	4 to -20			8(b)
	0.80, 0.85	↓	4 to -20			↓
	0.88	↓	4 to -25			9(a)
	0.21	-8 to 20	4 to -20			9(b)
	0.60	↓	4 to -20			9(c)
$\Delta p/q$ vs δ_e	0.75	↓	↓	9(d)		
	0.80	↓	↓	9(e)		
	0.85	-8 to 12	4 to -15	9(f)		
	0.88	-8 to 12	4 to -25	0		
	0.21	-10 to 20	4 to -20			10(a)
	0.60	↓	4 to -20			10(b)
0.75	↓	↓	10(c)			
0.80	↓	↓	10(d)			
0.85	-10 to 16	↓	10(e)			
C_L vs C_m	0.88	-10 to 14	4 to -15	0	10(f)	
	0.21	-10 to 20	4 to -25		11(a)	
	0.60	↓	0 to -20		11(b)	
	0.75	↓	0 to -20		11(c)	
	0.80	↓	↓		11(d)	
	0.85	-10 to 16	-2 to -20		11(e)	
C_L vs C_D	0.88	-10 to 14	0 to -15		11(f)	

CHORDWISE DISTRIBUTION OF STATIC PRESSURE AT THE MIDSEMI SPAN
 [R=2,000,000; $\delta_t = 0^\circ$]

Results presented	M	α , deg	δ_e , deg	Figure number	
P vs percent chord ↓	0.21	0, 4, 8	0, -4, -10, -15, -20	12(a)	
	0.21	12, 16, 20	↓	12(b)	
	0.60	0, 4, 8		12(c)	
	0.60	12, 16, 20		12(d)	
	0.75	0, 4, 8		12(e)	
	0.75	12, 16, 20		12(f)	
	0.80	0, 4, 8		12(g)	
	0.80	12, 16, 20		12(h)	
	0.85	0, 4, 8		-4, -10, -15, -20	12(i)
	0.88	0, 4, 8		0, -4, -10, -15	12(j)

SEPARATE EFFECTS OF LEADING-EDGE ROUGHNESS AND OF
REMOVAL OF ELEVATOR-NOSE SEAL

[$R=2,000,000$; $\delta_e = 4^\circ, 0^\circ, -15^\circ$; $\delta_t = 0^\circ$]

Results presented	M	α , deg	Figure number
C_L vs α ↓	0.21	-10 to 20	13(a)
	0.80	-10 to 20	13(b)
	0.88	-10 to 12	13(c)
C_{h_e} vs α ↓	0.21	-10 to 20	14(a)
	0.80	-10 to 20	14(b)
	0.88	-10 to 12	14(c)
C_L vs C_m ↓	0.21	-10 to 20	15(a)
	0.80	-10 to 20	15(b)
	0.88	-10 to 12	15(c)
C_L vs C_D ↓	0.21	-10 to 20	16(a)
	0.80	-10 to 20	16(b)
	0.88	-10 to 12	16(c)



SUMMARY FIGURES
[R=2,000,000; M=0.21 to 0.94]

Results presented	α , deg	δ_e , deg	δ_t , deg	Figure number
C_L vs δ_e	0	4 to -25	0 to 15	17
$C_{L\alpha}$, $C_{L\delta_e}$, and $\alpha\delta_e$ vs M	---	---	0	18
C_{he} vs M	-8 to 20	0	0	19(a)
C_{he} vs M	0	4 to -20	0	19(b)
ΔC_{he} vs M	0	0, -6, -10	5, 10, 15	20
¹ C_{he} vs δ_e , C_{he} vs α	-10 to 20	4 to -25	0	21
² $C_{L\alpha}$, $C_{L\delta_e}$, and $\alpha\delta_e$ vs M	---	---	0	22
² C_{he} vs M	0, 4, 8	0, -2, -6, -10	0	23
² Aerodynamic center location (for $C_L=0$ at $\delta_e=0$) vs M	---	0	0	24
² Maximum L/D, C_L for maximum L/D, and minimum C_D vs M	---	0	0	25

¹Shows computed effect of a sealed internal aerodynamic balance on the elevator hinge-moment coefficients.

²Presents data for two horizontal tails; one with the hinge line normal to the plane of symmetry and one with the quarter-chord line swept back 35°.



REFERENCES

1. Dods, Jules B., Jr.: Wind-Tunnel Investigation of Horizontal Tails. I - Unswept and 35° Swept-Back Plan Forms of Aspect Ratio 3. NACA RM A7K24, 1948.
2. Dods, Jules B., Jr.: Wind-Tunnel Investigation of Horizontal Tails. II - Unswept and 35° Swept-Back Plan Forms of Aspect Ratio 4.5. NACA RM A8B11, 1948.
3. Dods, Jules B., Jr.: Wind-Tunnel Investigation of Horizontal Tails. III - Unswept and 35° Swept-Back Plan Forms of Aspect Ratio 6. NACA RM A8H30, 1948.
4. Dods, Jules B., Jr.: Wind-Tunnel Investigation of Horizontal Tails. IV - Unswept Plan Form of Aspect Ratio 2 and a Two-Dimensional Model. NACA RM A8J21, 1948.
5. Dods, Jules B., Jr.: Wind-Tunnel Investigation of Horizontal Tails. V - 45° Swept-Back Plan Form of Aspect Ratio 2. NACA RM A9D05, 1949.
6. Tinling, Bruce E., and Dickson, Jerald K.: Tests of a Model Horizontal Tail of Aspect Ratio 4.5 in the Ames 12-Foot Pressure Wind Tunnel. I - Quarter-Chord Line Swept Back 35° . NACA RM A9G13, 1949.
7. Sivells, James C., and Deters, Owen J.: Jet-Boundary and Plan Form Corrections for Partial-Span Models with Reflection Plane, End Plate, or No End Plate, in a Closed Circular Wind Tunnel. NACA Rep. 843, 1946.
8. DeYoung, John: Theoretical Additional Span Loading Characteristics of Wings with Arbitrary Sweep, Aspect Ratio, and Taper Ratio. NACA TN 1491, 1947.
9. Herriot, John G.: Blockage Corrections for Three-Dimensional-Flow Closed-Throat Wind Tunnels with Consideration of the Effect of Compressibility. NACA RM A7B28, 1947.
10. Abbott, Ira H., von Doenhoff, Albert E., and Stivers, Louis S. Jr.: Summary of Airfoil Data. NACA Rep. 824, 1945.

TABLE I.— COORDINATES FOR THE NACA 64A010 AIRFOIL SECTION
 [All dimensions in percent of wing chord]

Upper and Lower Surfaces

Station	Ordinate
0.	0.
.50	.804
.75	.969
1.25	1.225
2.50	1.688
5.00	2.327
7.50	2.805
10.00	3.199
15.00	3.813
20.00	4.272
25.00	4.606
30.00	4.837
35.00	4.968
40.00	4.995
45.00	4.894
50.00	4.684
55.00	4.388
60.00	4.021
65.00	3.597
70.00	3.127
75.00	2.623
80.00	2.103
85.00	1.582
90.00	1.062
95.00	.541
100.00	.021
L.E. radius 0.687	T.E. radius 0.023

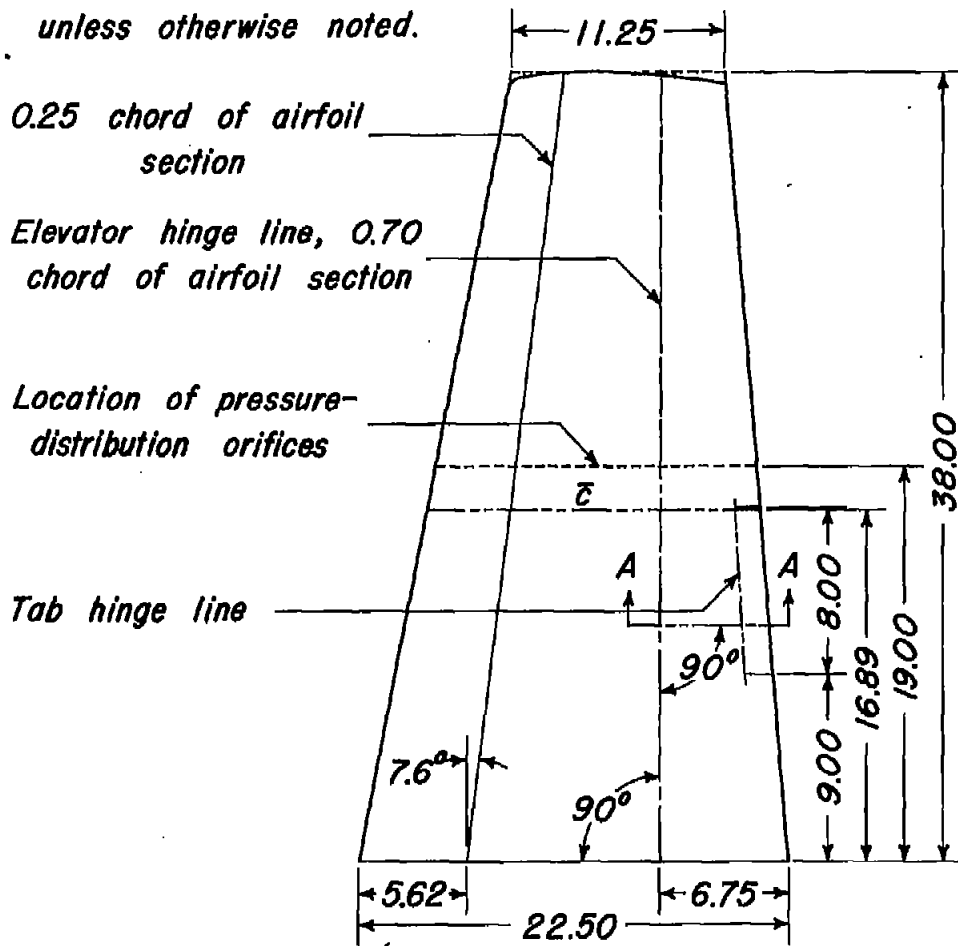


1
2
3

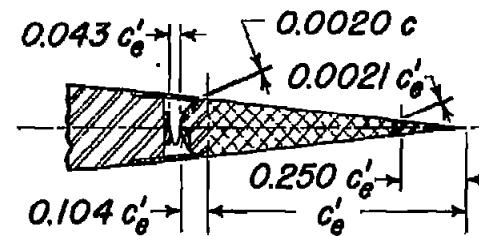
4
5
6

7
8
9

Dimensions shown in inches unless otherwise noted.



Aspect ratio	4.5
Taper ratio	0.5
Area, semispan	4.438 ft ²
Elevator area	1.327 ft ²
Tab area	0.0777 ft ²
\bar{c}	1.458 ft
Sections	NACA 64A010 parallel to the plane of symmetry



Section A - A



Figure 1.- The geometry of the horizontal-tail model with the hinge line normal to the plane of symmetry.

1
2
3

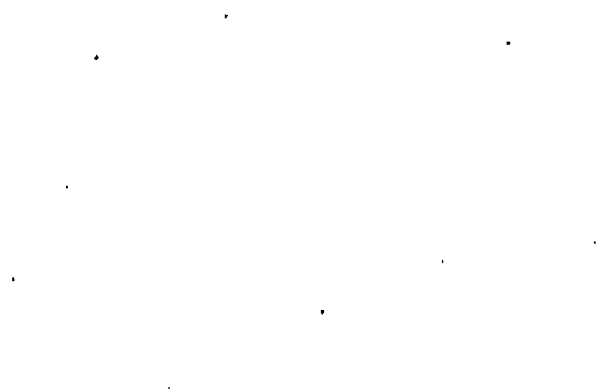
4
5
6

7
8
9



Figure 2.- Semispan horizontal-tail model mounted in the Ames 12-foot pressure wind tunnel.

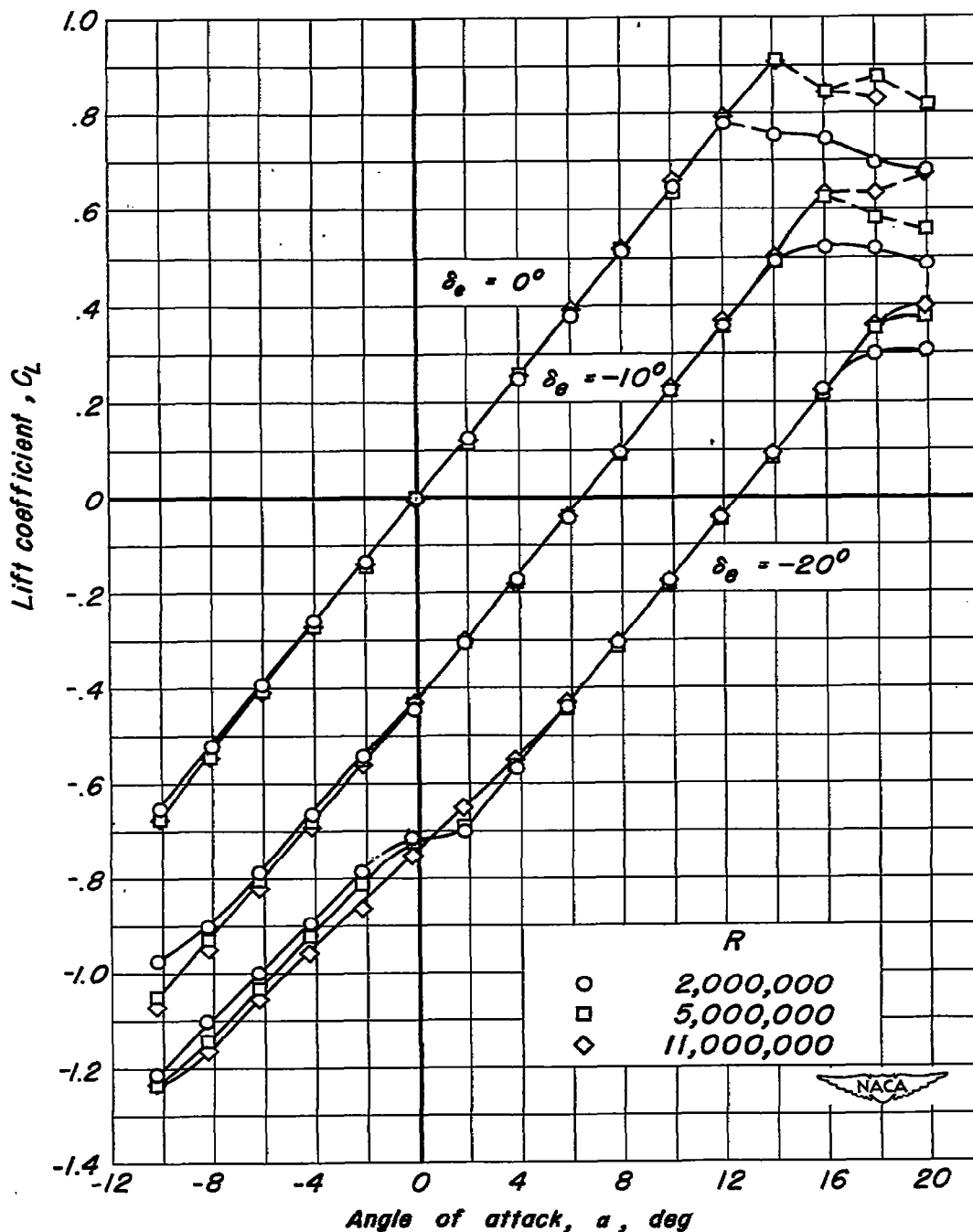
•
•
•
•



•
•
•
•

•

•
•
•
•



(a) C_L vs a .

Figure 3.— The effect of Reynolds number on the low-speed aerodynamic characteristics. $M, 0.21$; $\delta_f, 0^\circ$.

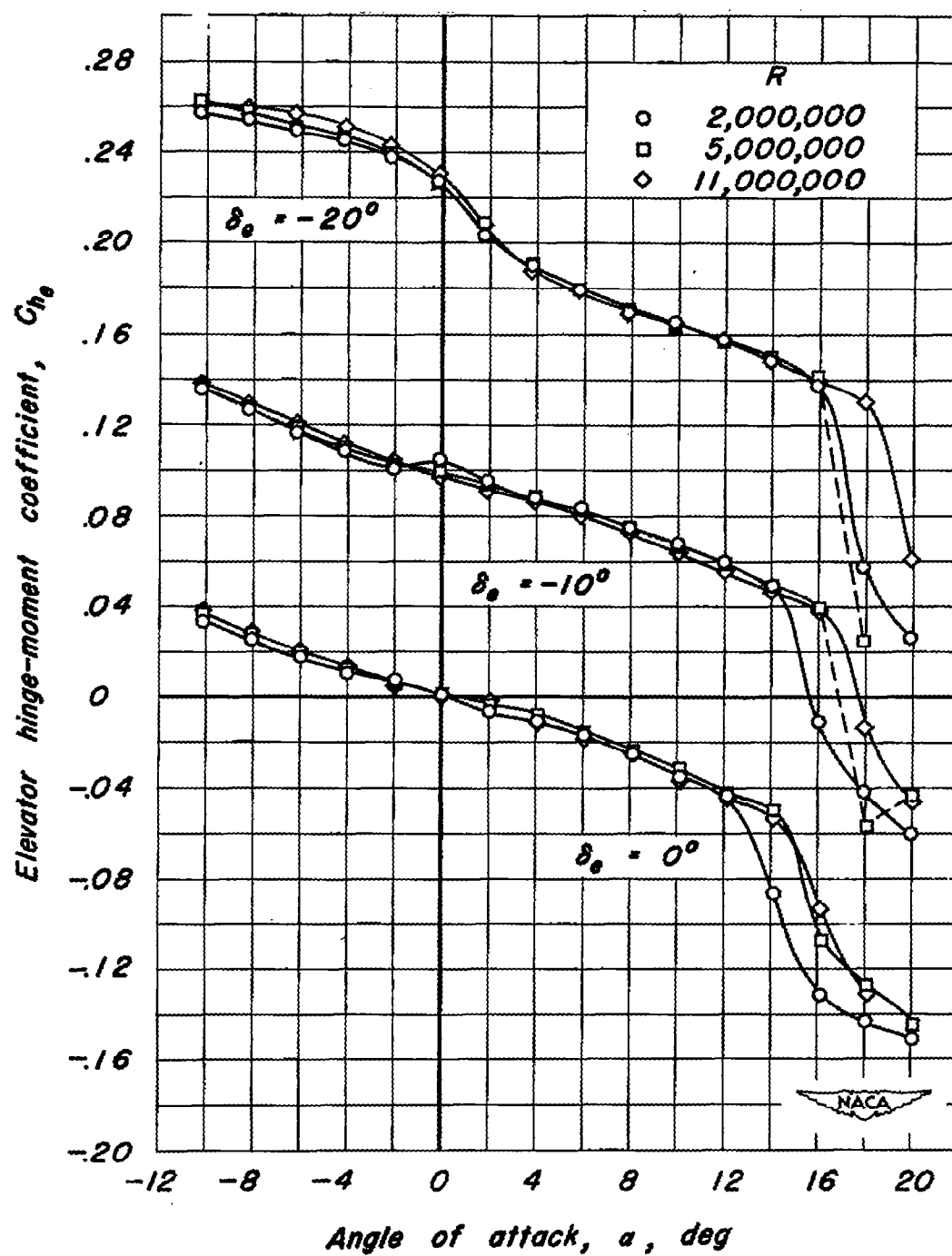
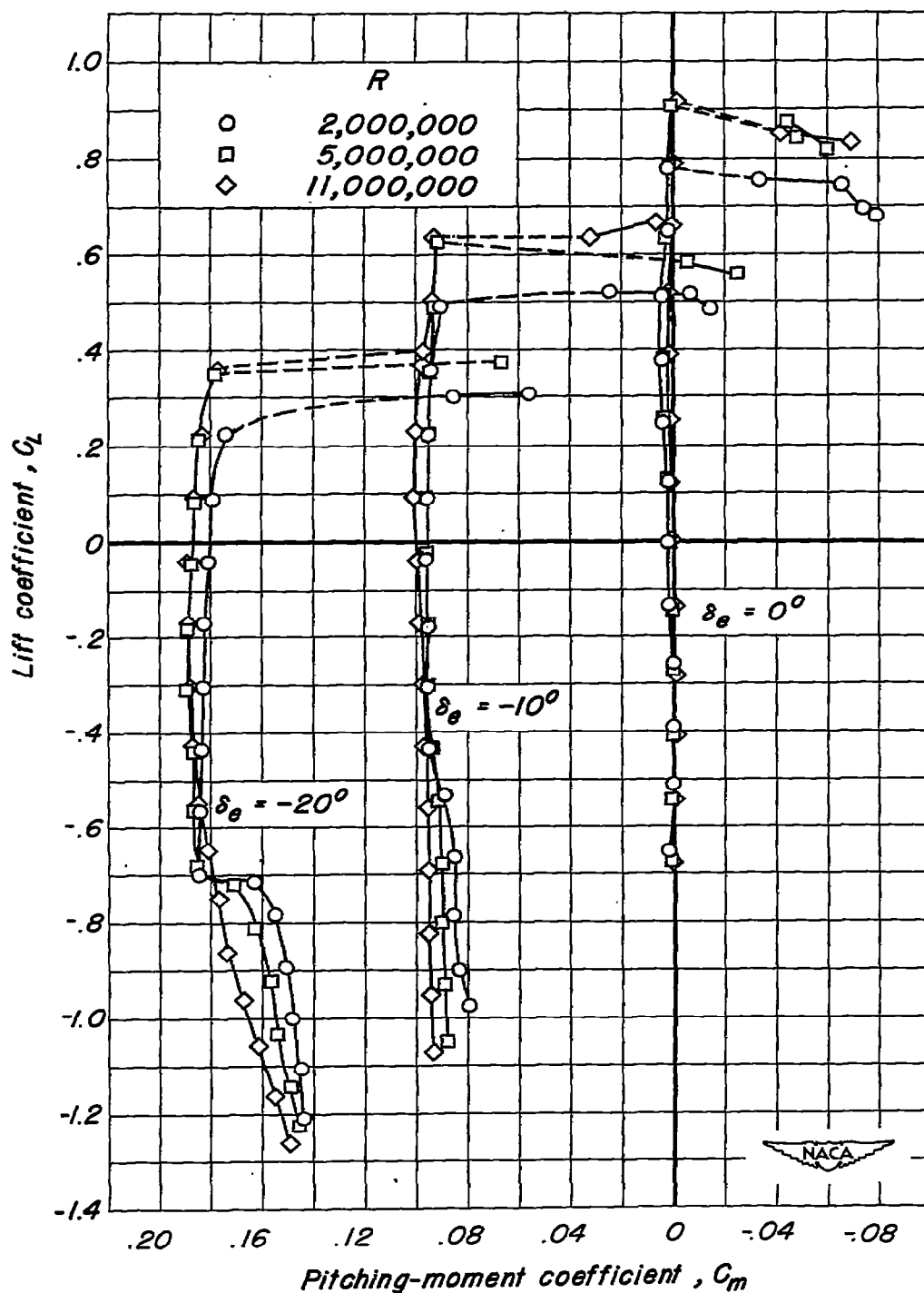
(b) C_{h_e} vs α .

Figure 3.— Continued.



(c) C_L vs C_m .

Figure 3. - Continued.

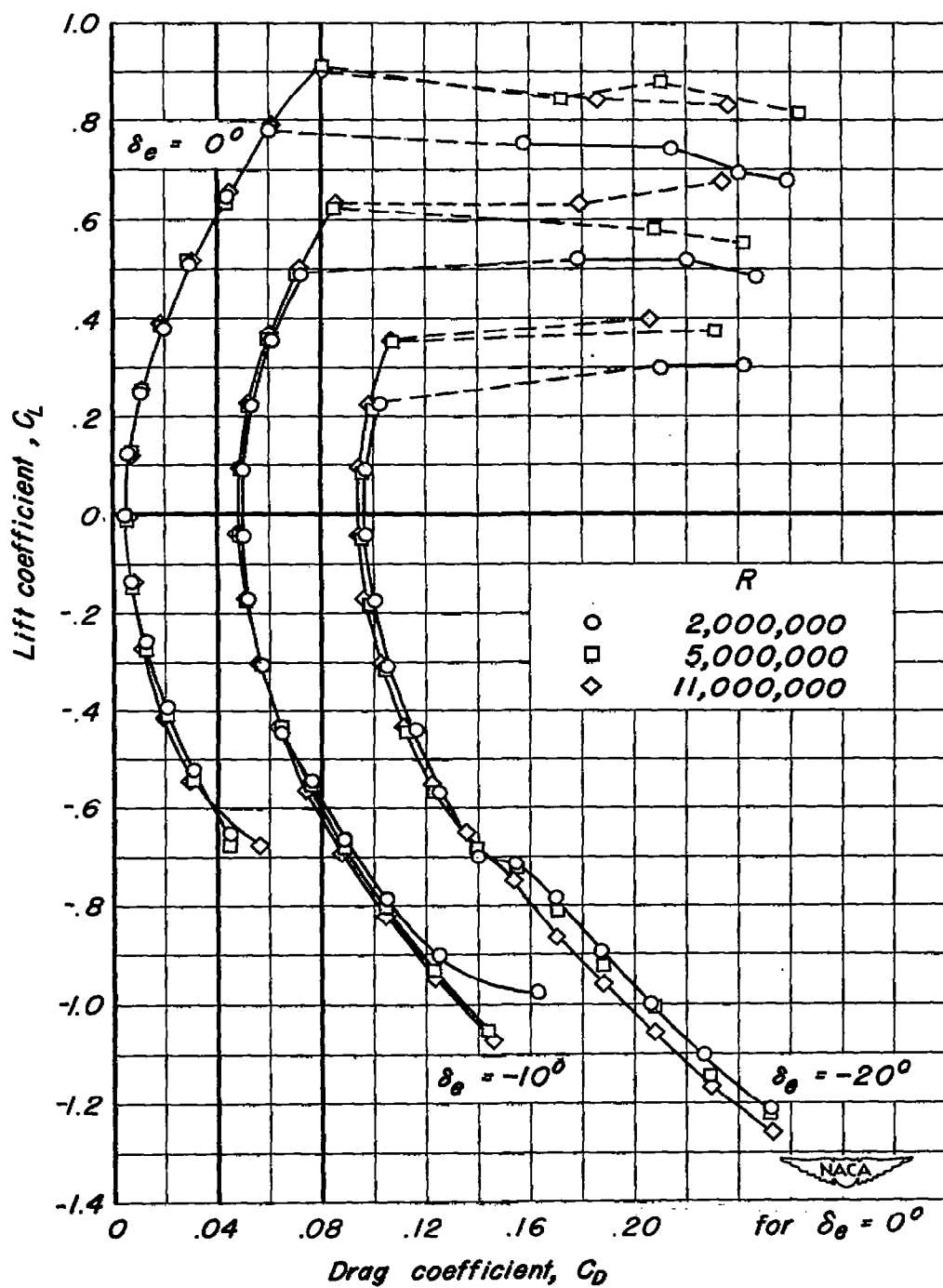
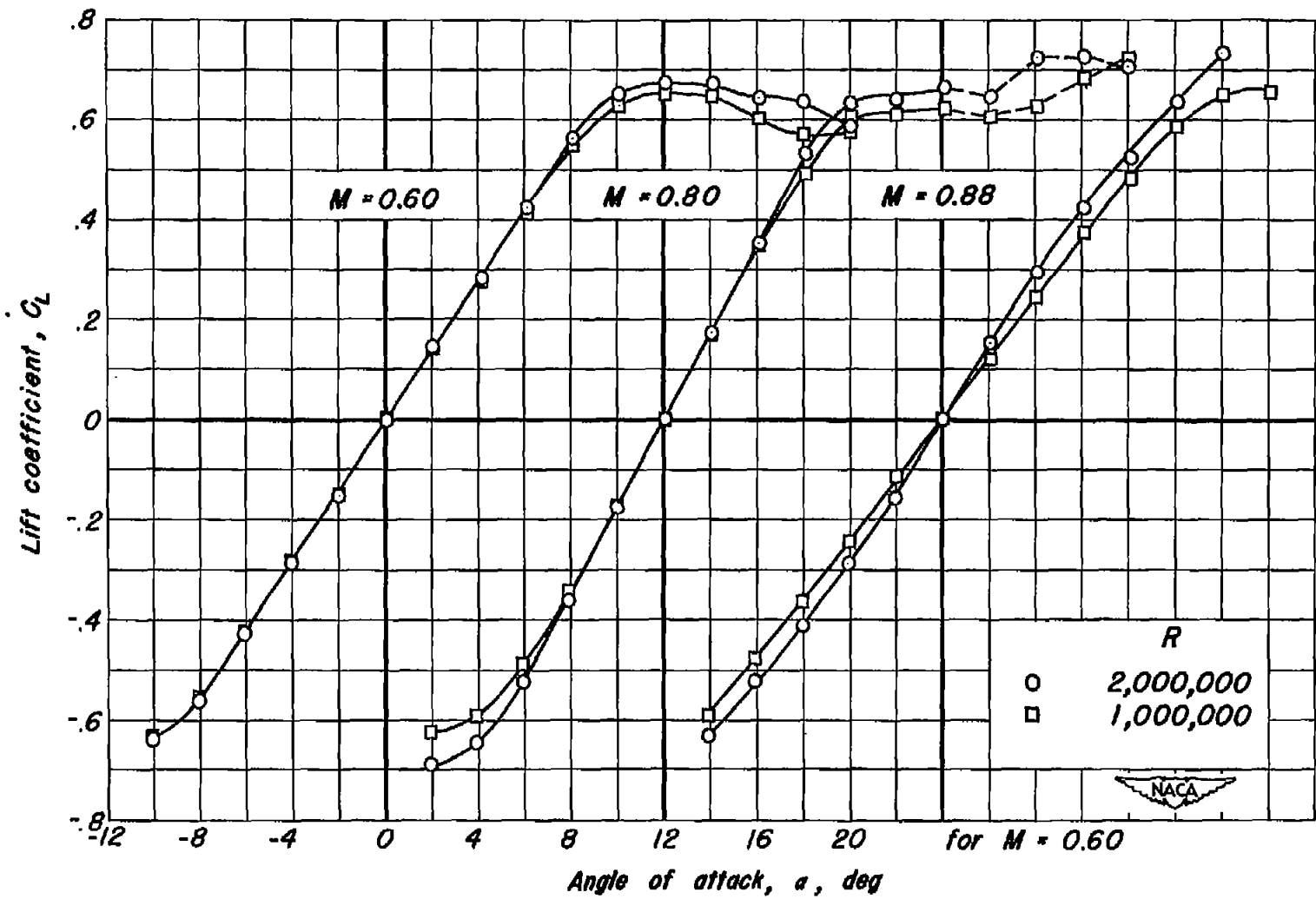
(d) C_L vs C_D .

Figure 3. - Concluded.



(a) C_L vs α .

Figure 4.—The effect of Reynolds number on the high-speed aerodynamic characteristics. $\delta_e, 0^\circ$; $\delta_f, 0^\circ$.

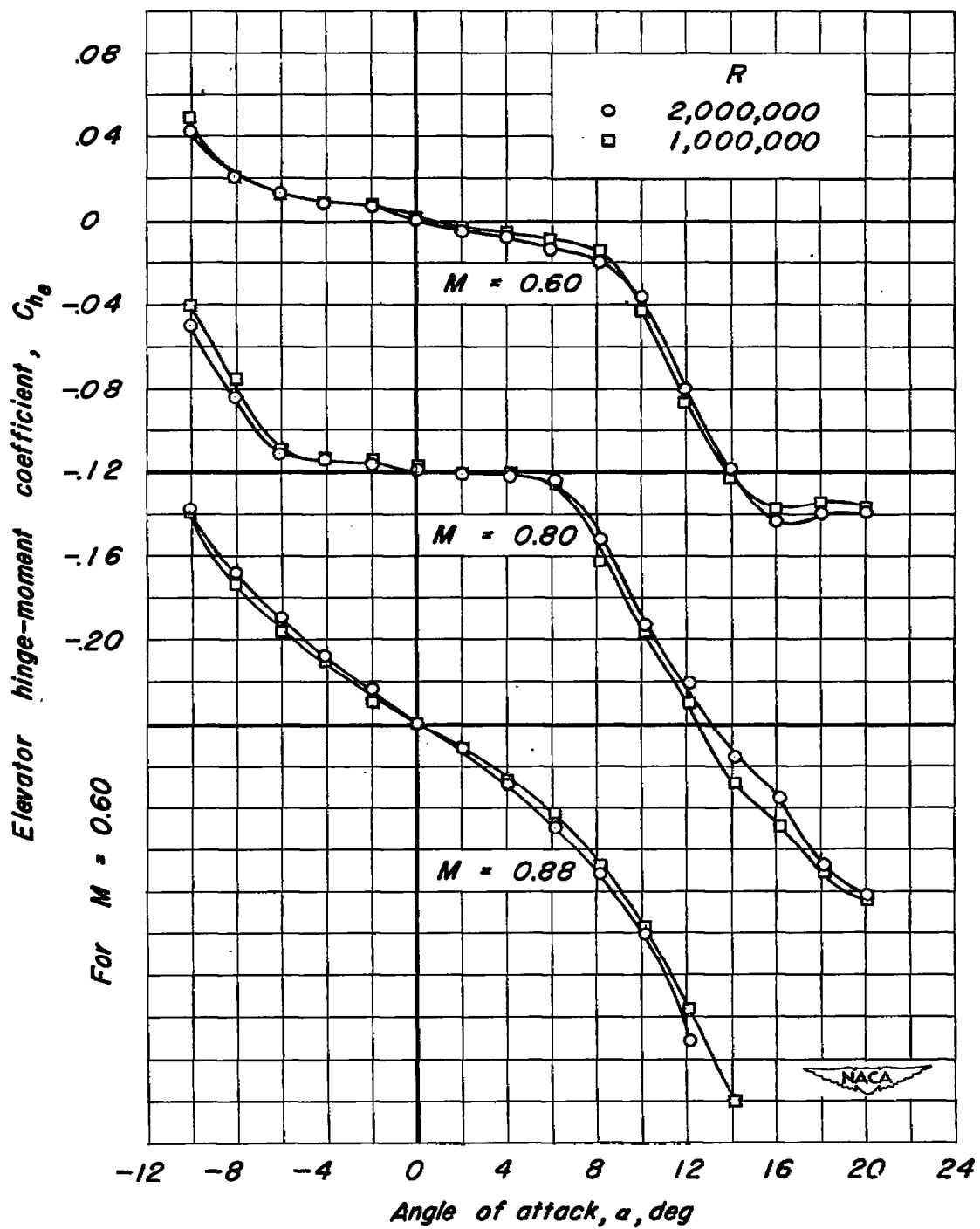
(b) C_{h0} vs α .

Figure 4. — Continued.

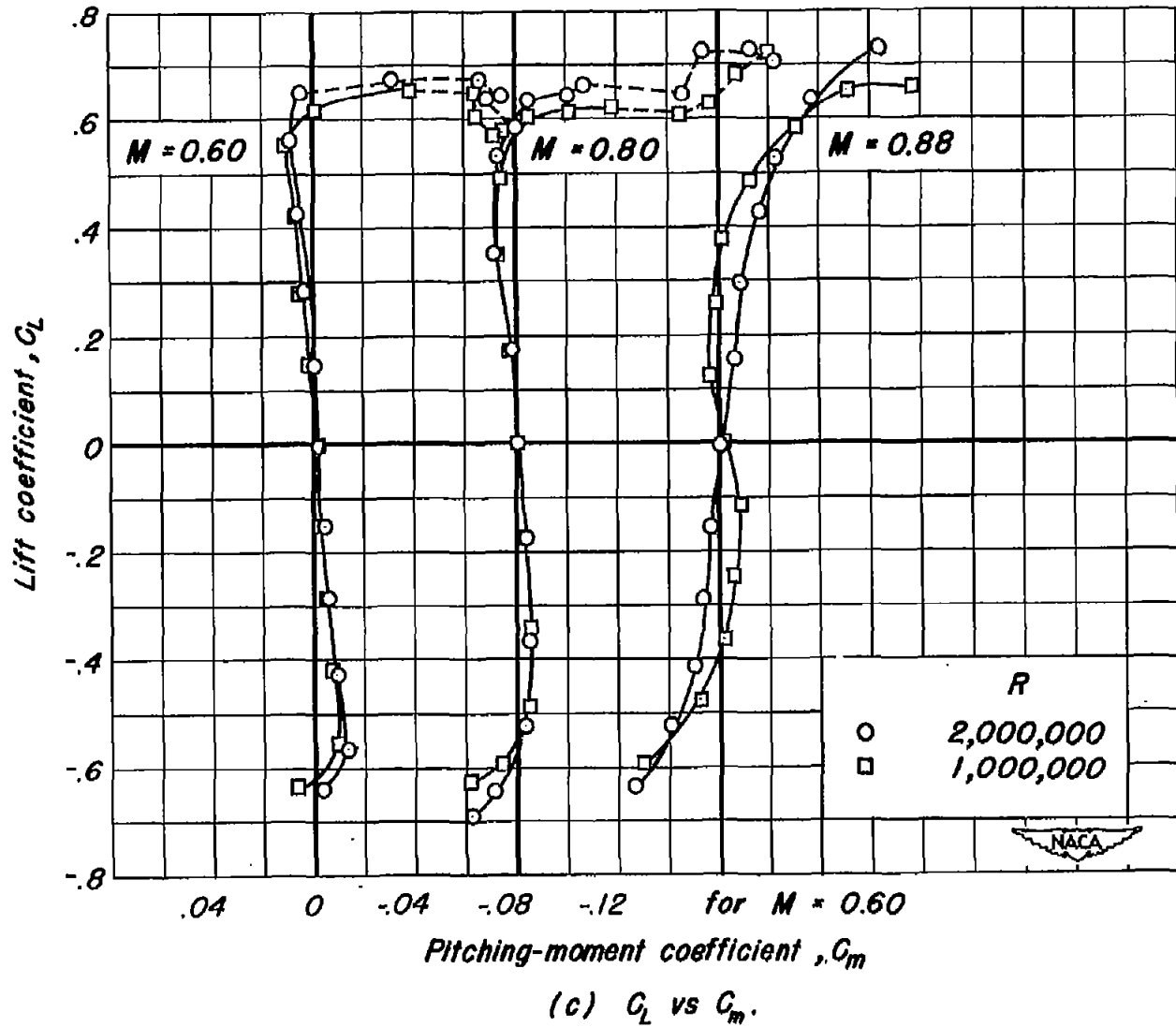


Figure 4. — Continued.

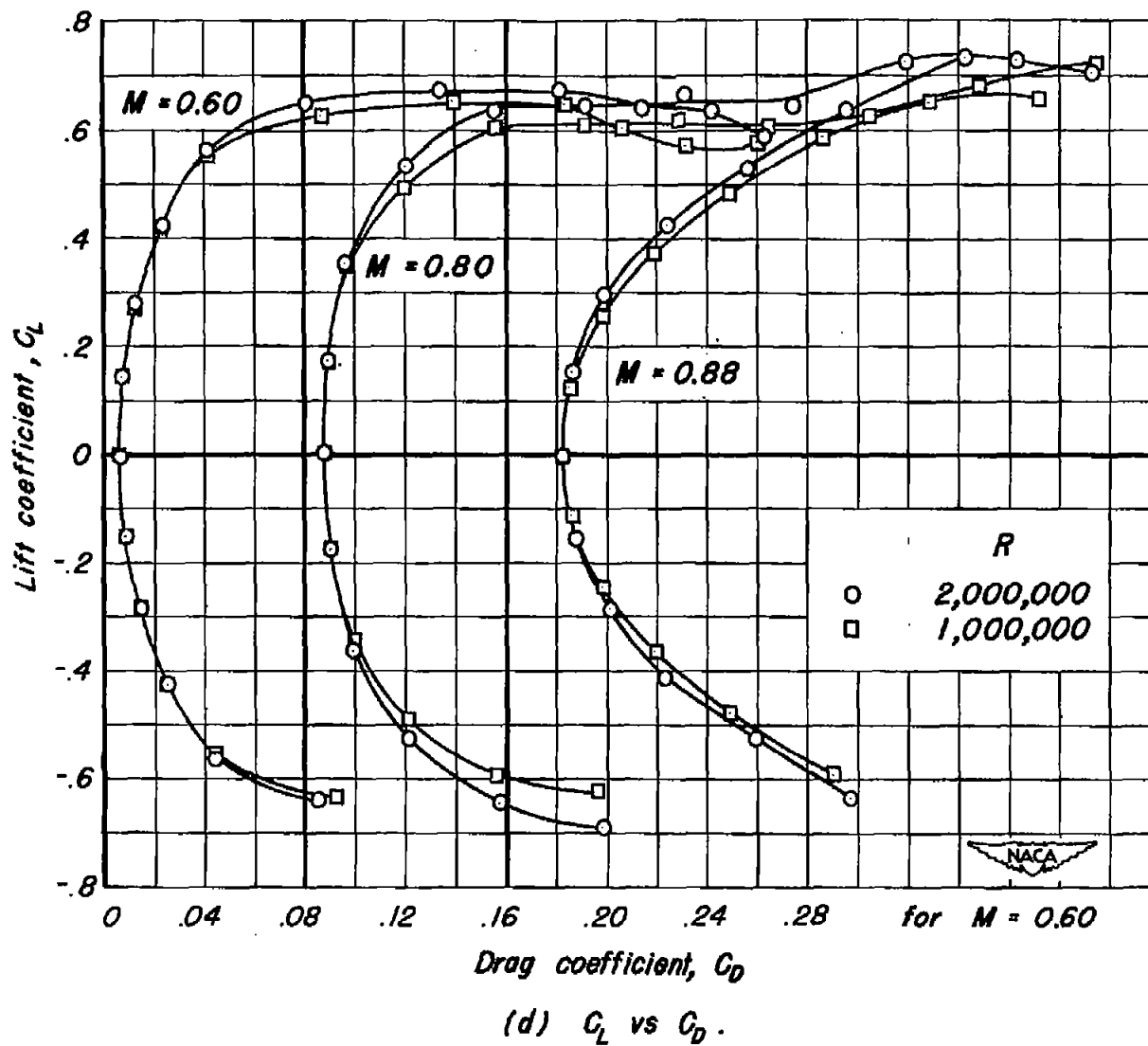
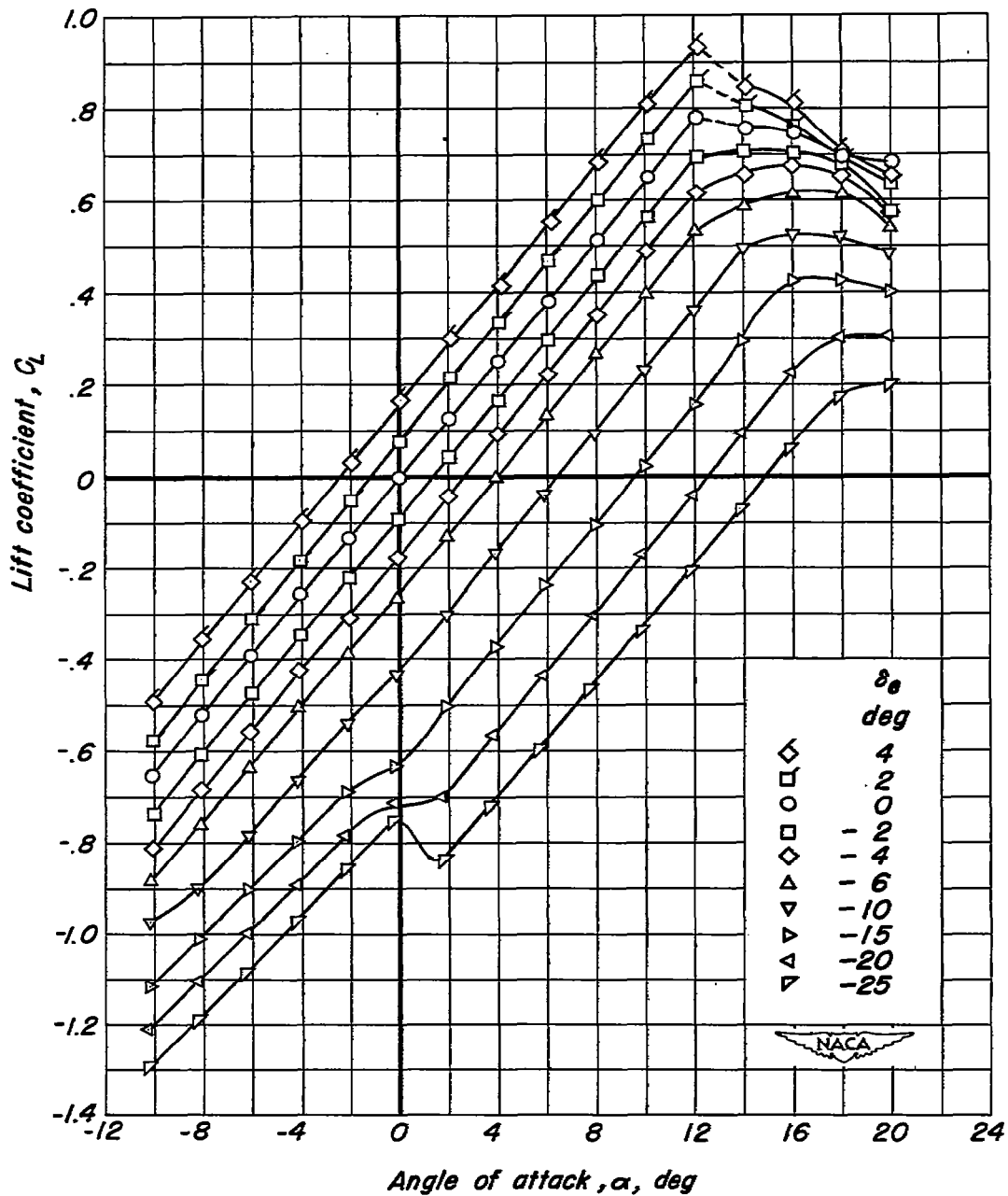


Figure 4.— Concluded.



(a) $M, 0.21.$

Figure 5.— The variation of lift coefficient with angle of attack. $\delta_f, 0^\circ$;
 $R, 2,000,000.$

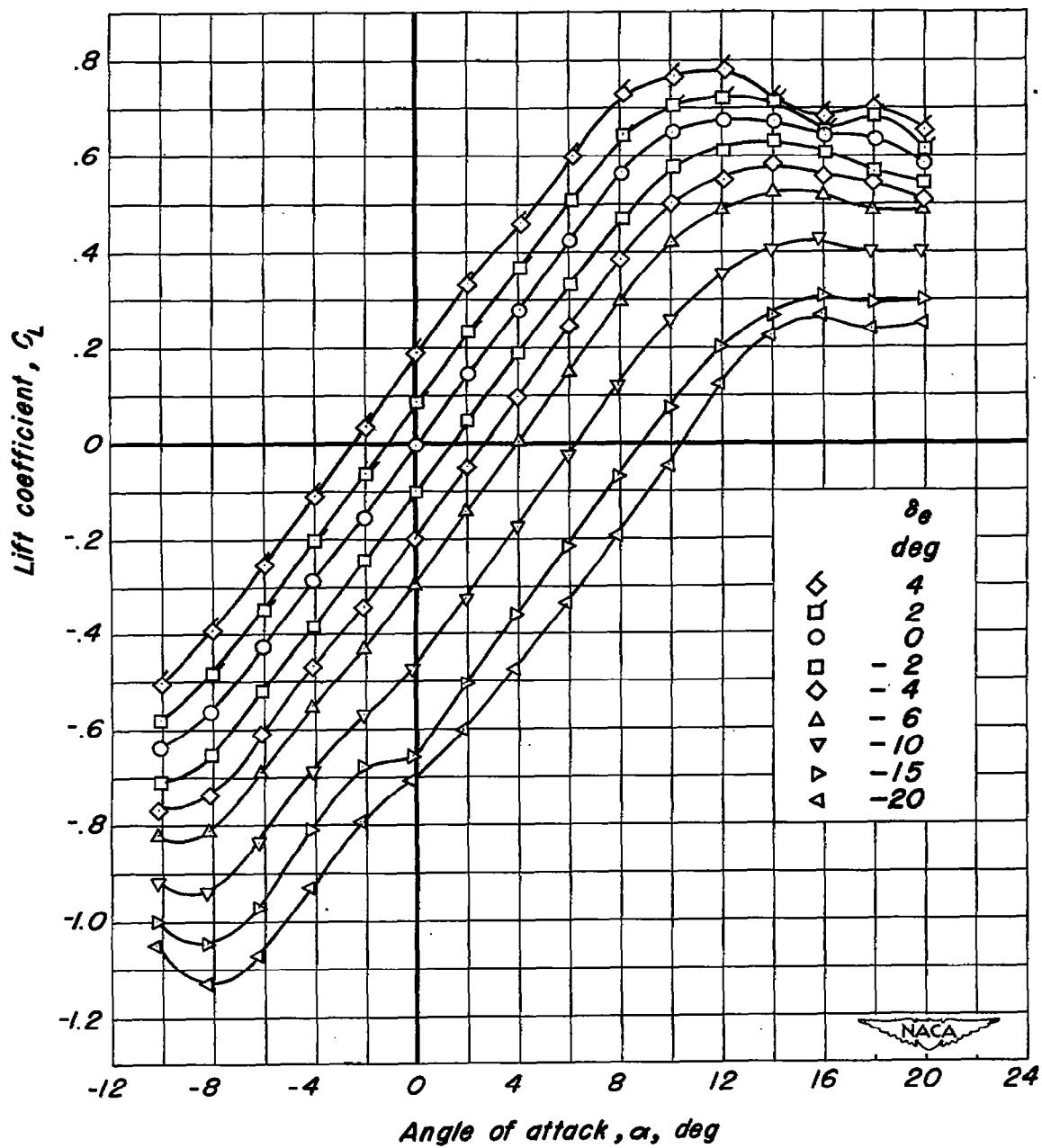
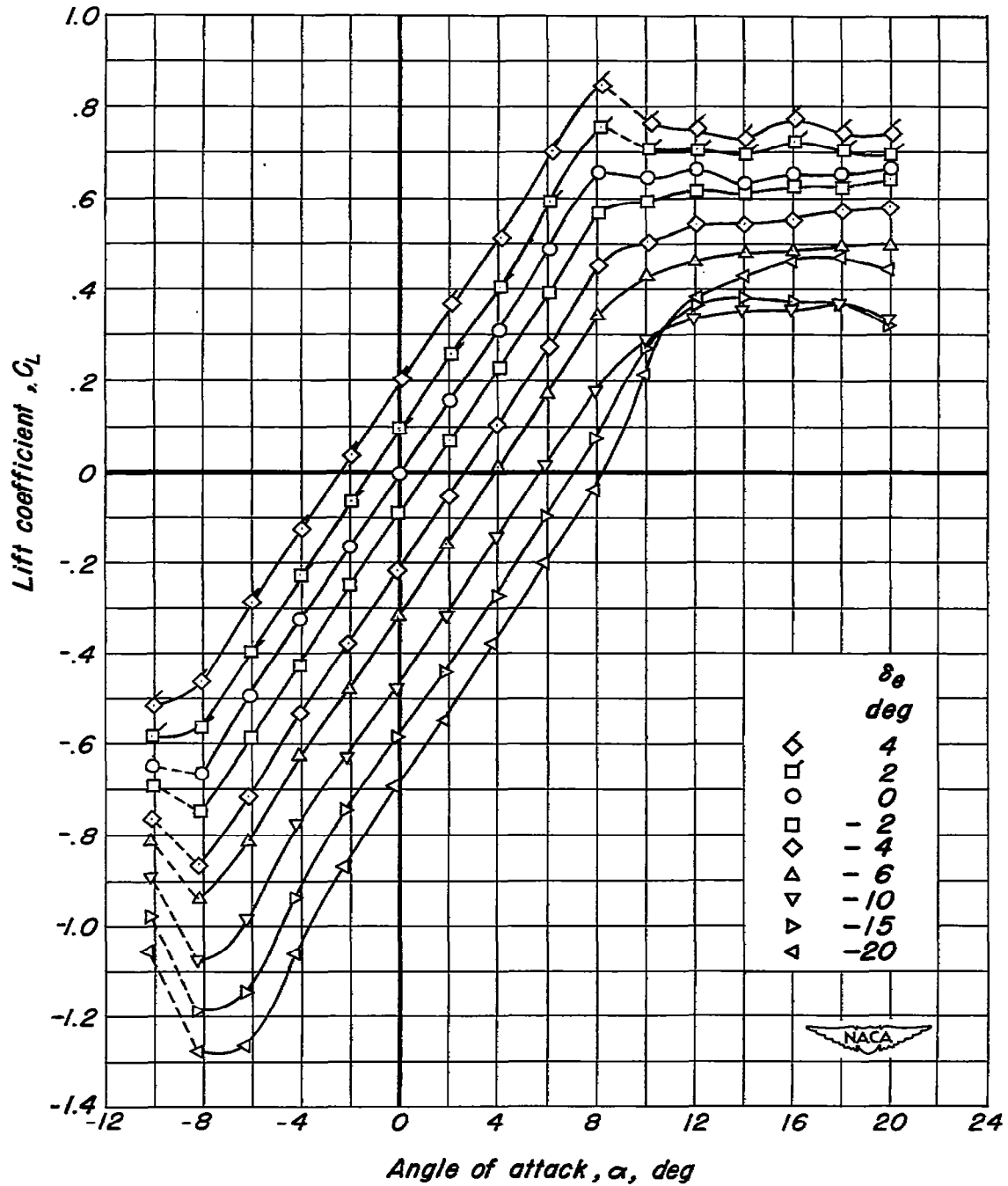
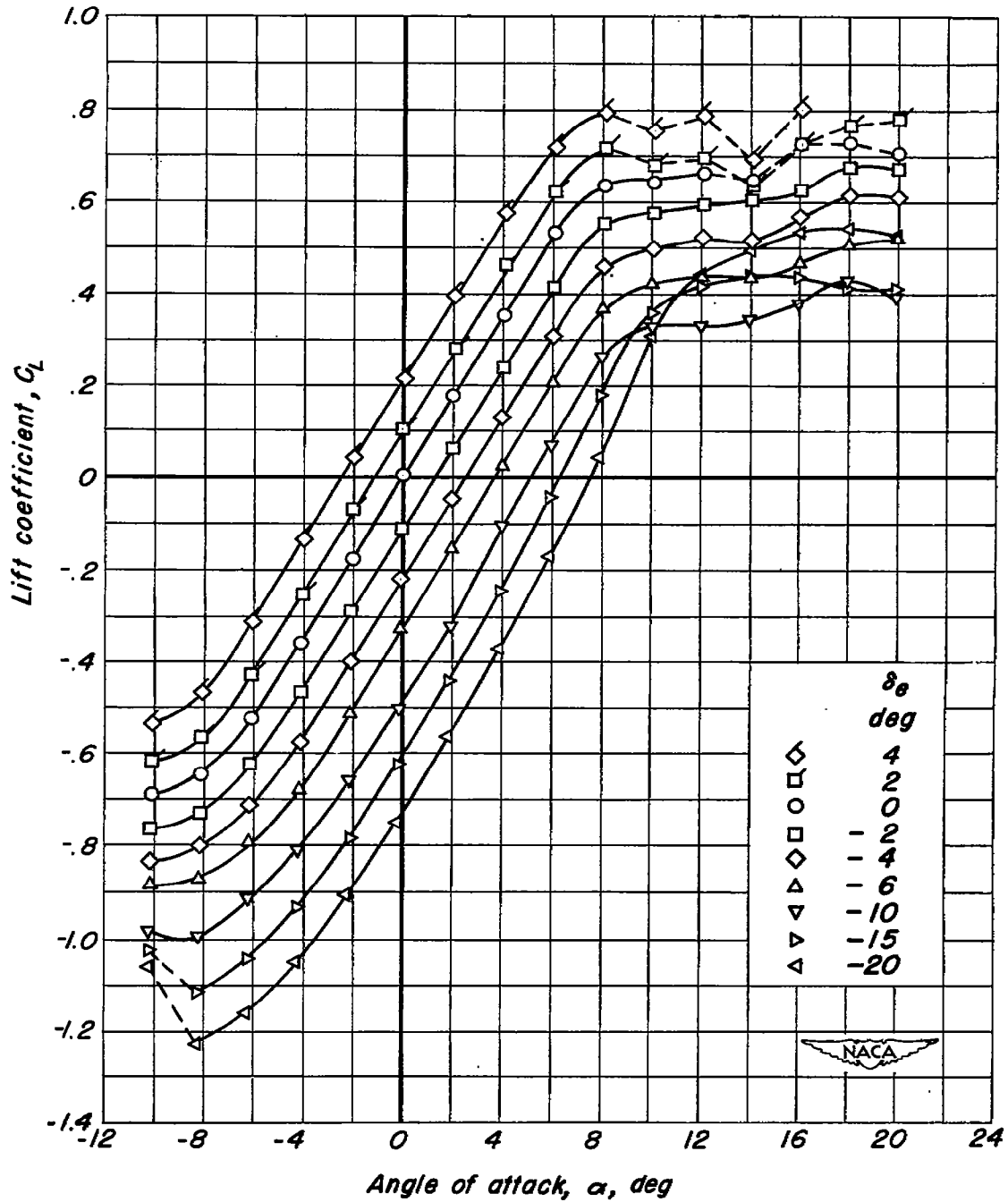
(b) $M, 0.60.$

Figure 5.— Continued.



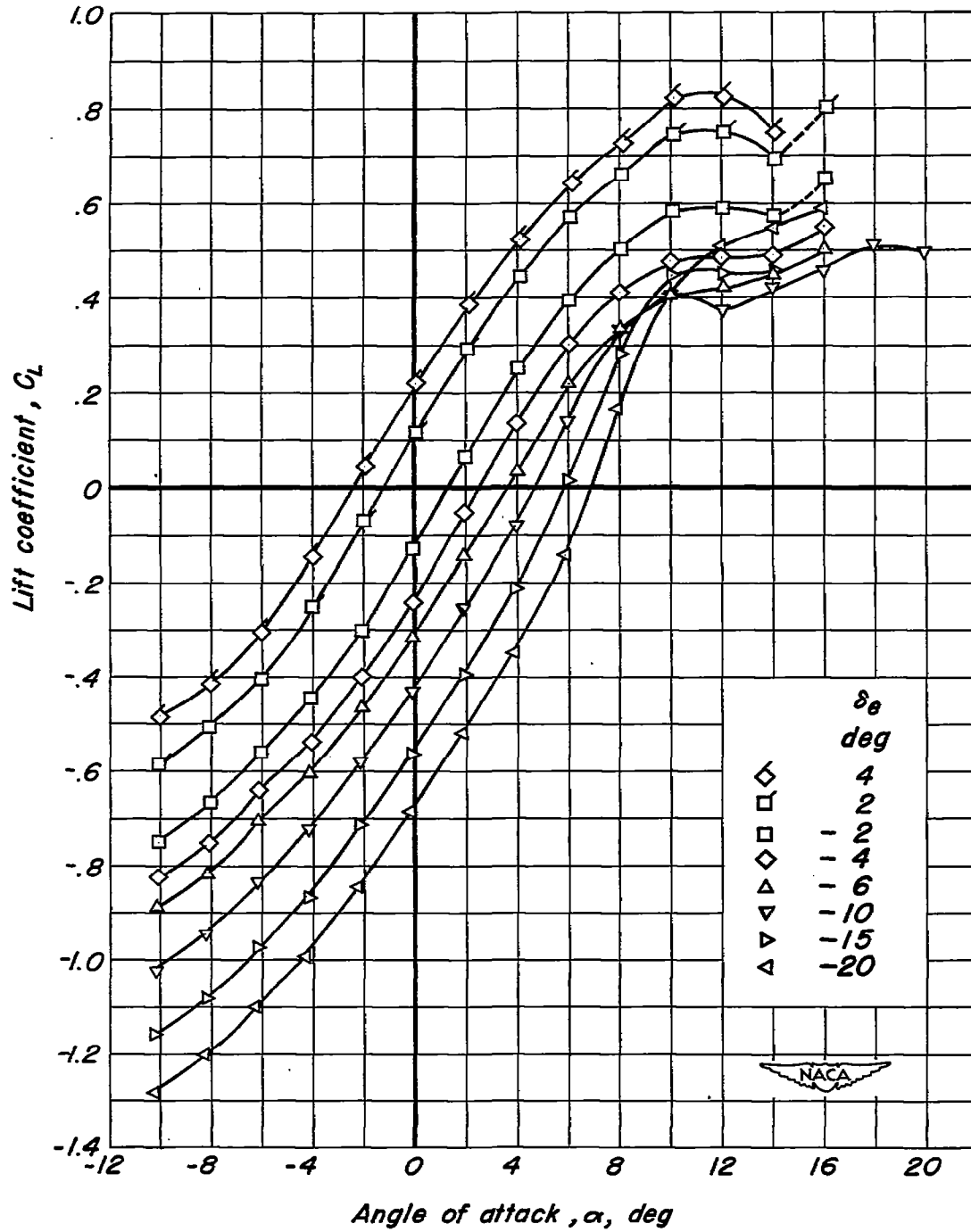
(c) $M, 0.75.$

Figure 5. — Continued.



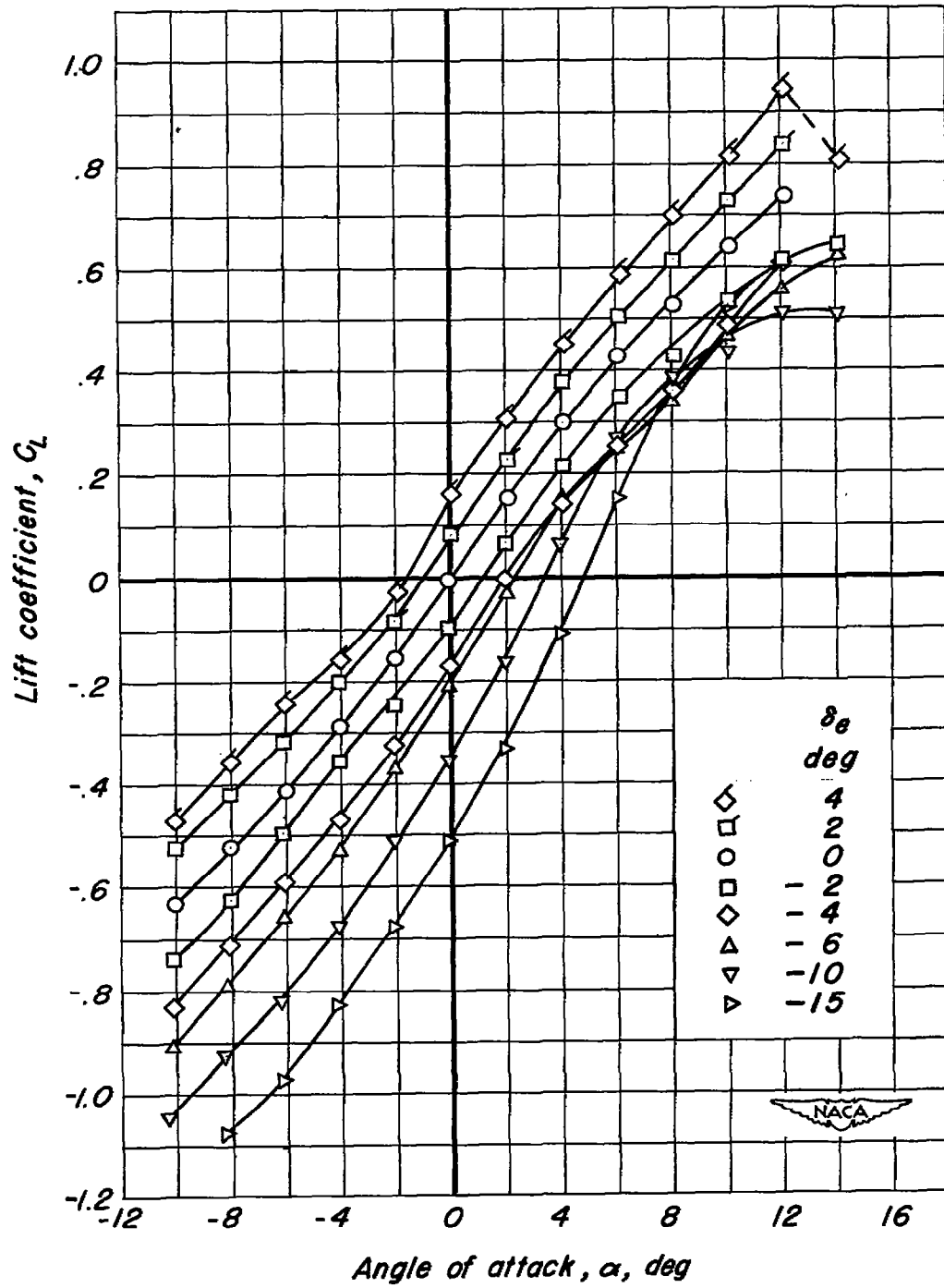
(d) $M, 0.80.$

Figure 5.— Continued.



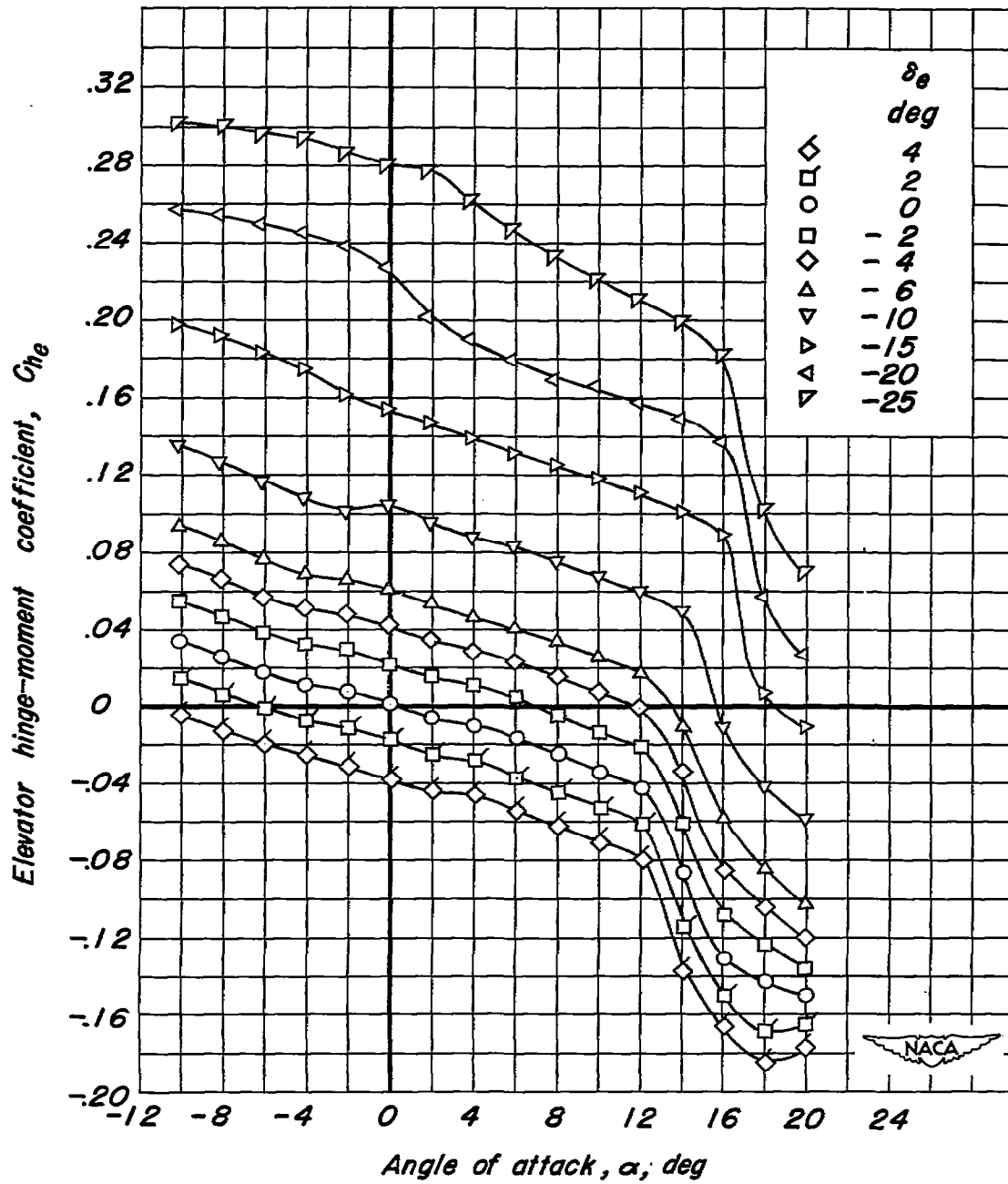
(e) $M, 0.85.$

Figure 5.— Continued.



(f) $M, 0.88.$

Figure 5. — Concluded.



(a) $M, 0.21.$

Figure 6.- The variation of elevator hinge-moment coefficient with angle of attack. $\delta_t, 0^\circ; R, 2,000,000.$

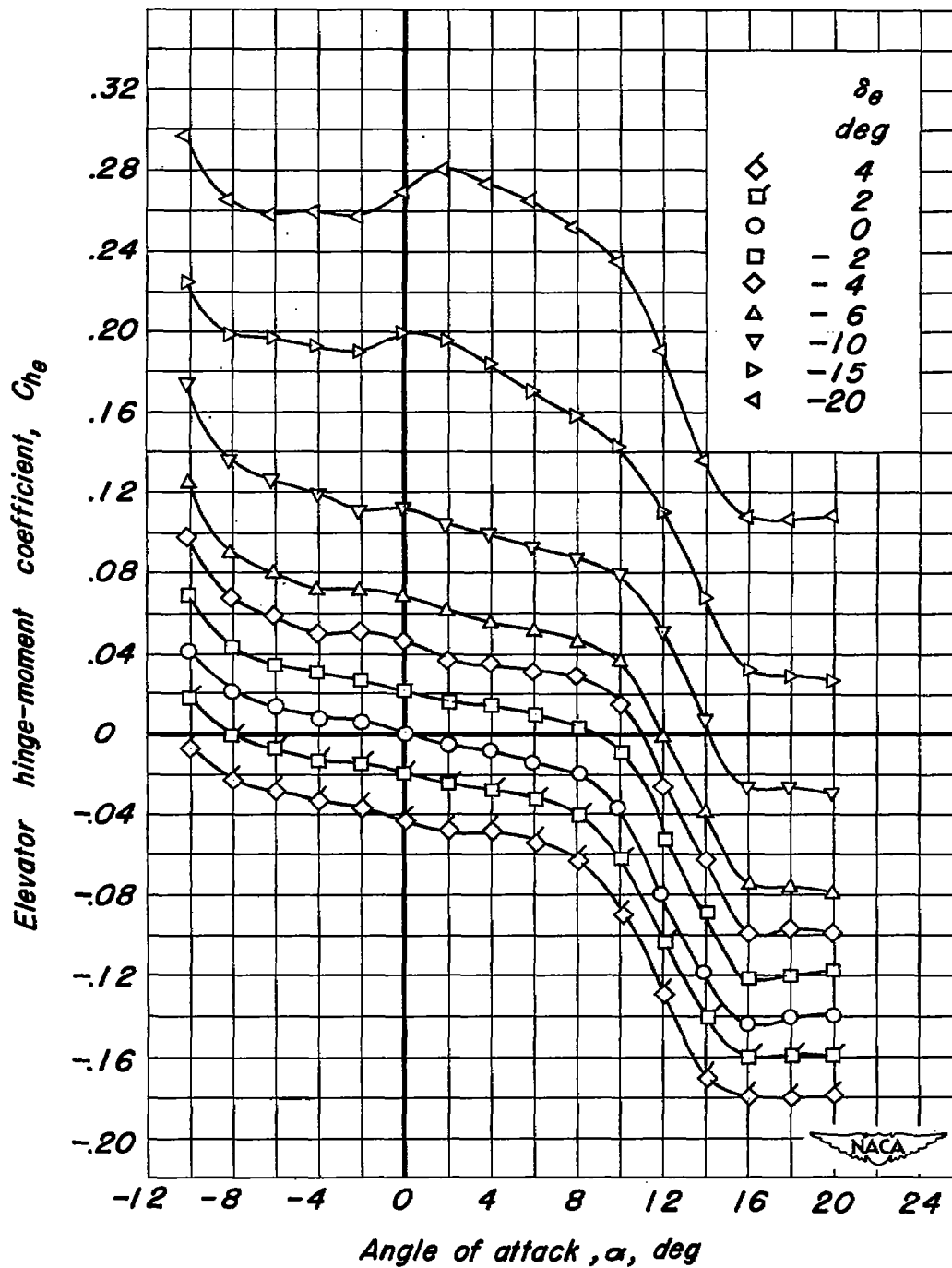
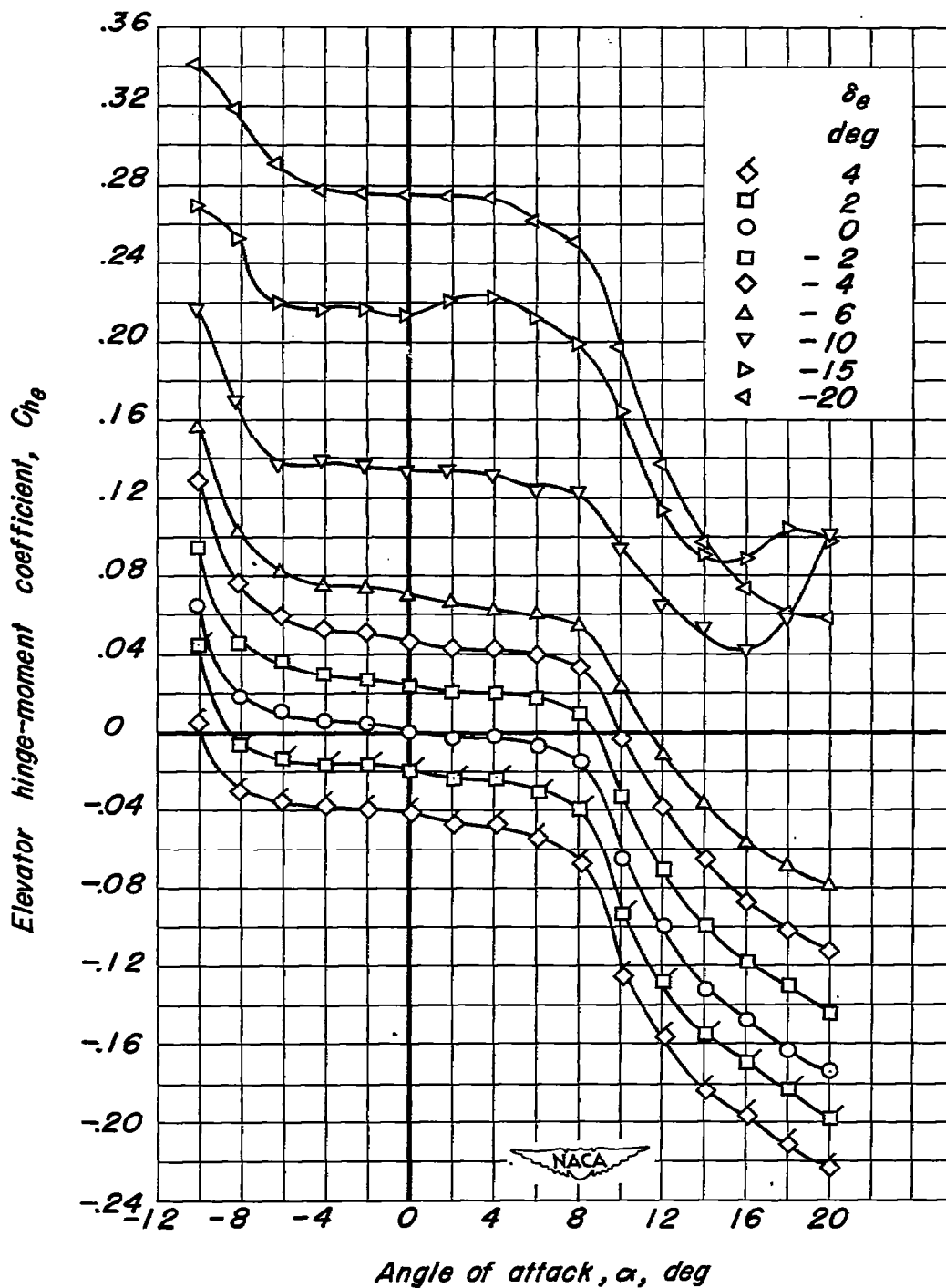
(b) $M, 0.60$.

Figure 6. — Continued.



(c) $M, 0.75.$

Figure 6. - Continued.

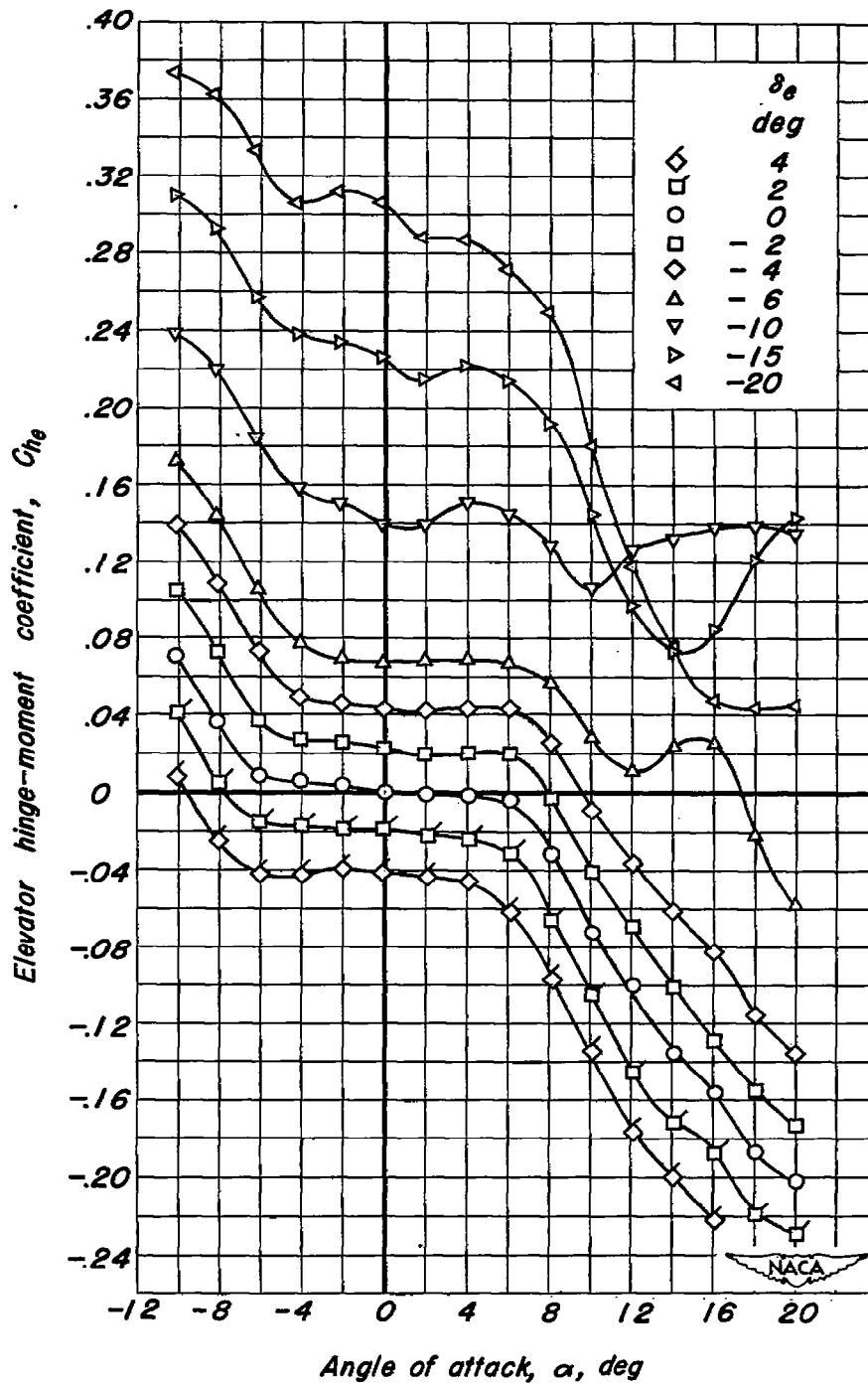
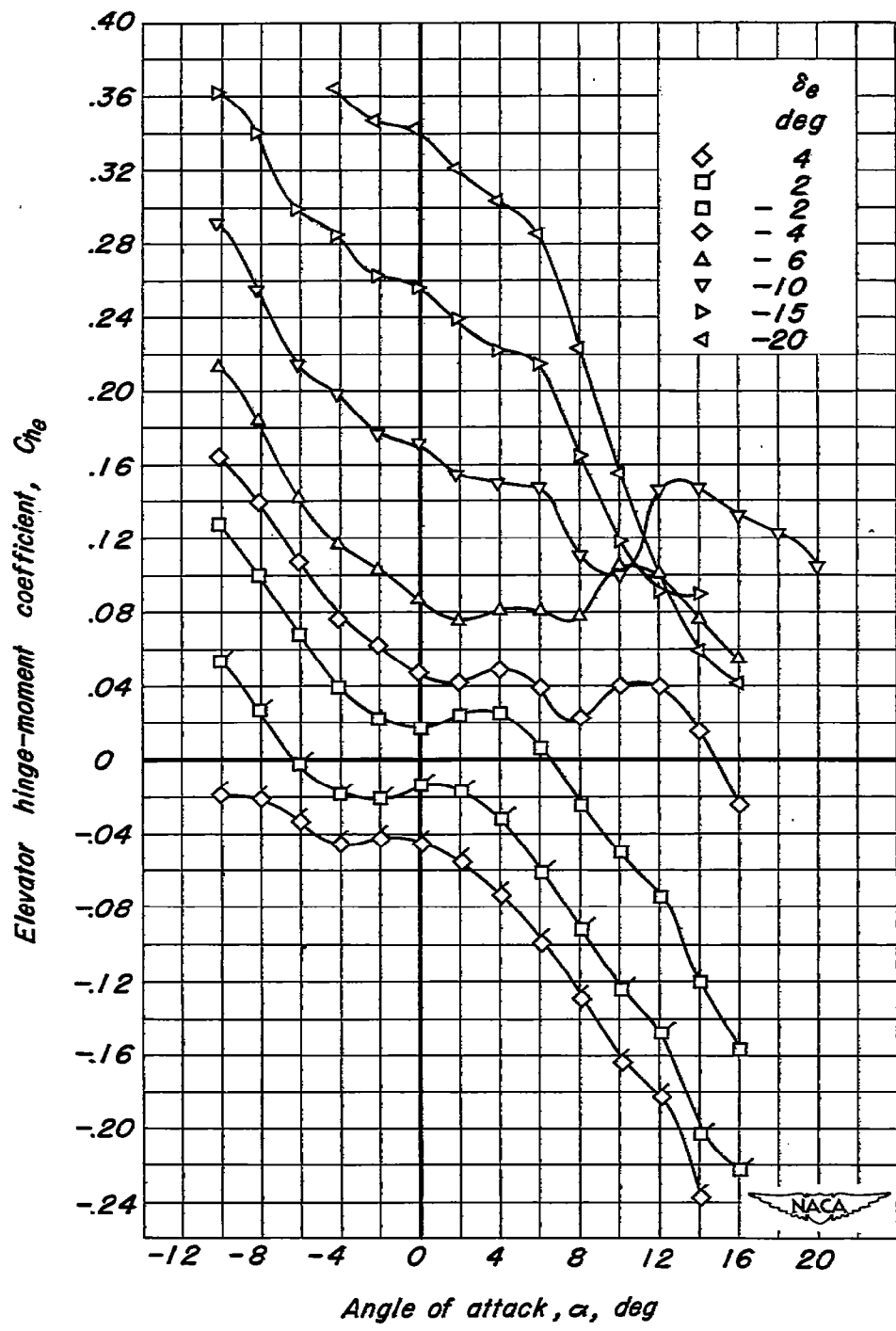
(d) $M, 0.80$.

Figure 6. - Continued.



(e) $M, 0.85.$

Figure 6. - Continued.

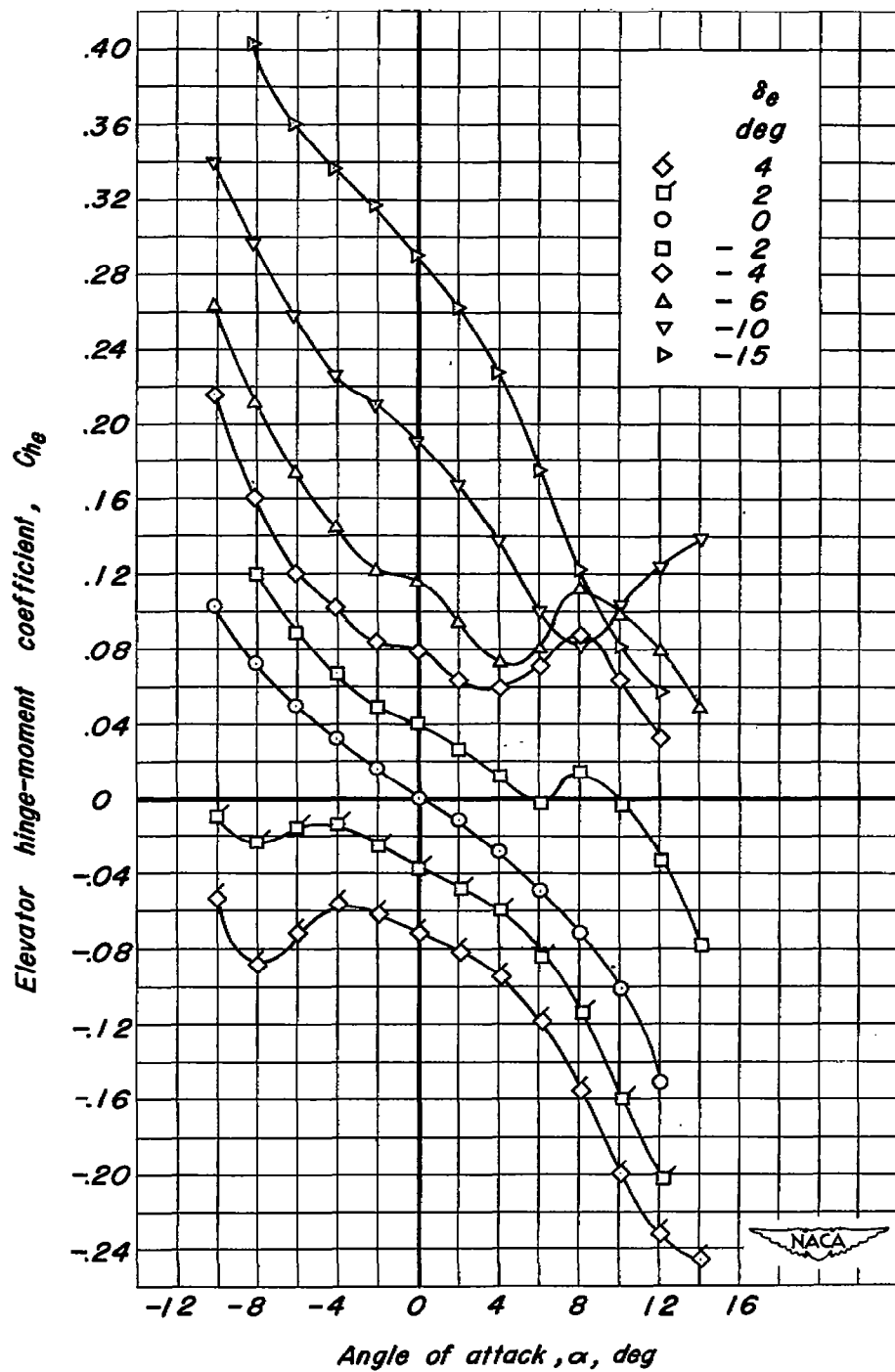
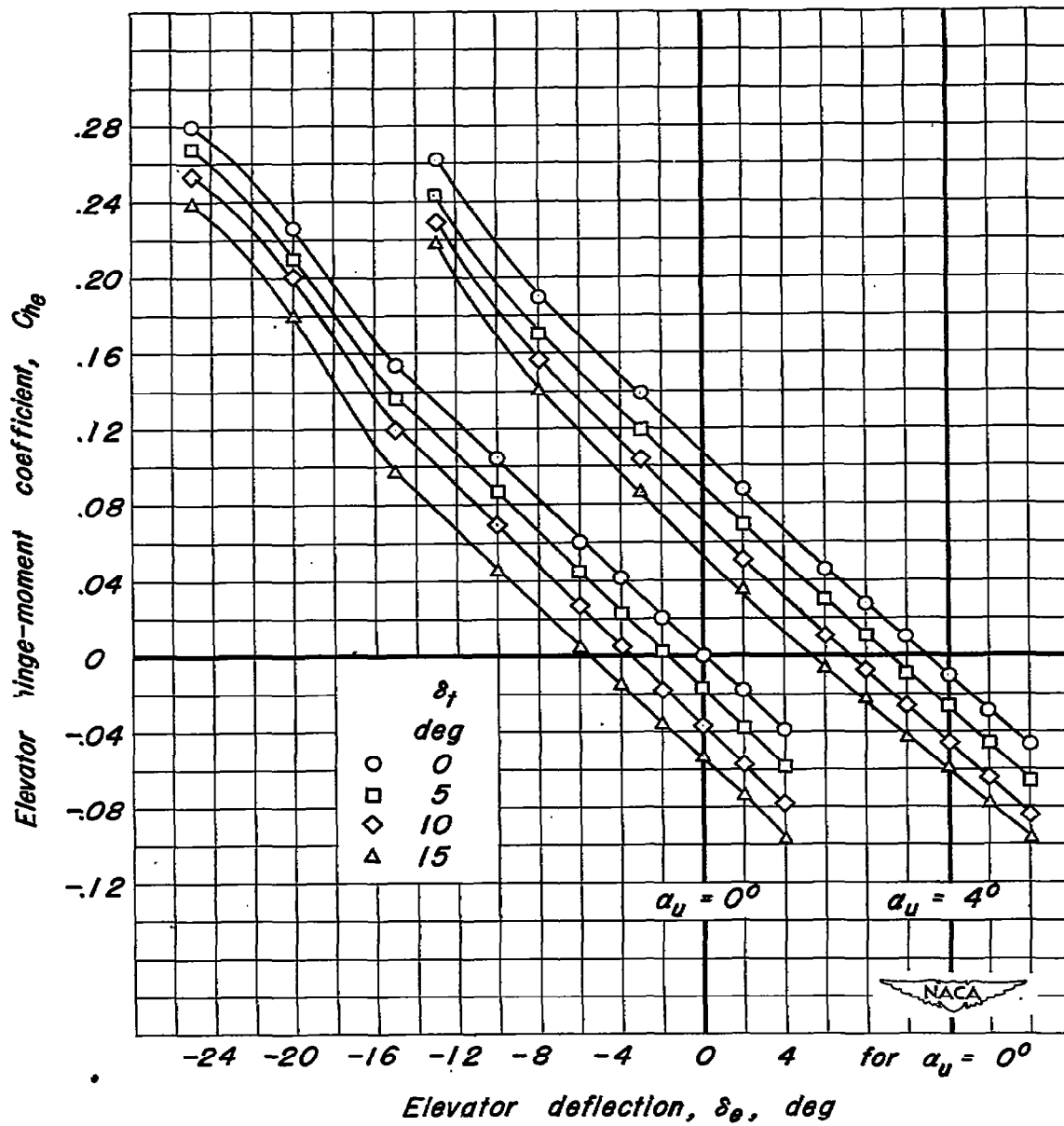
(f) $M, 0.88$.

Figure 6. - Concluded.



(a) $M, 0.21.$

Figure 7.— The variation of elevator hinge-moment coefficient with elevator deflection. $R, 2,000,000.$

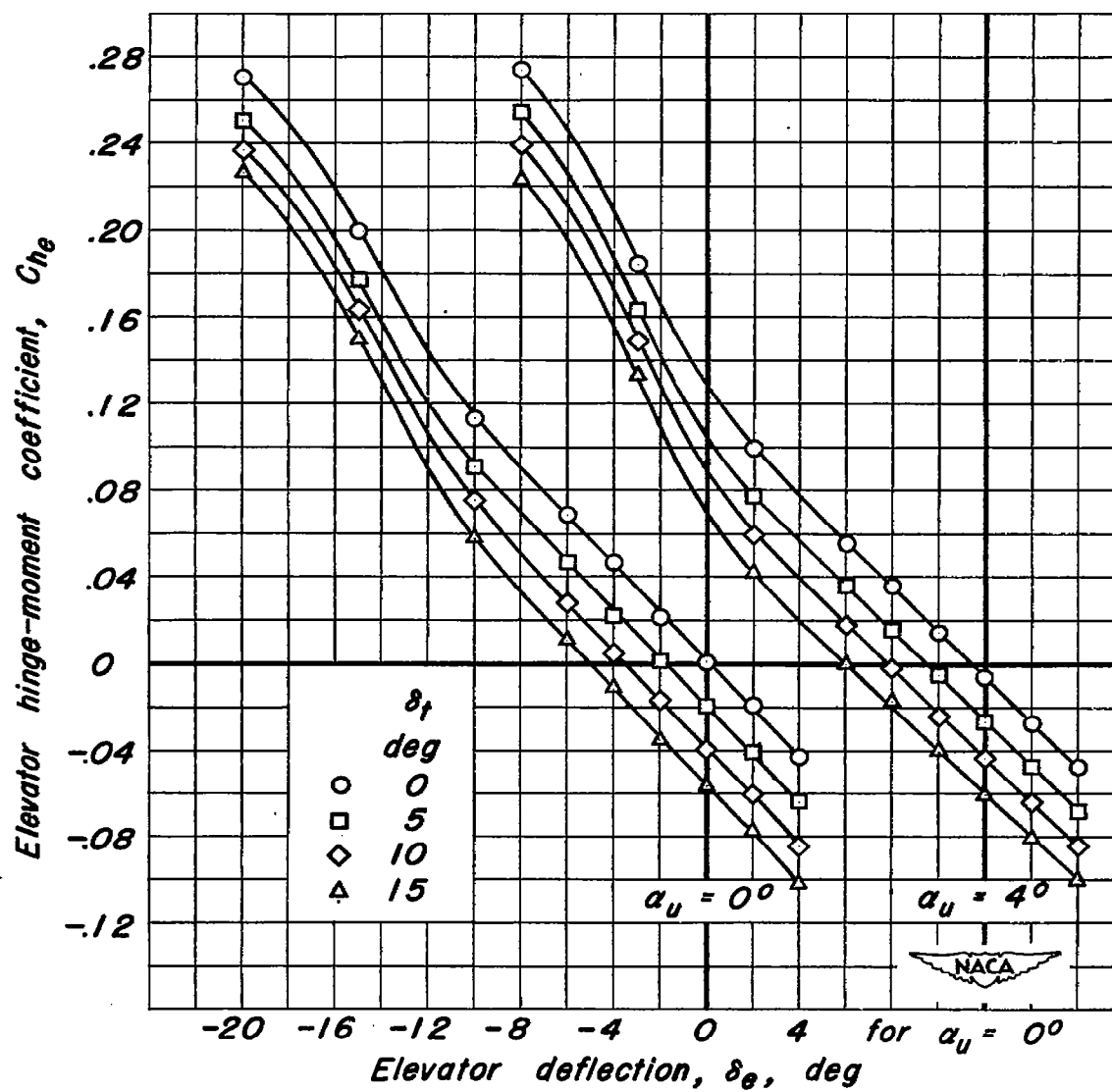
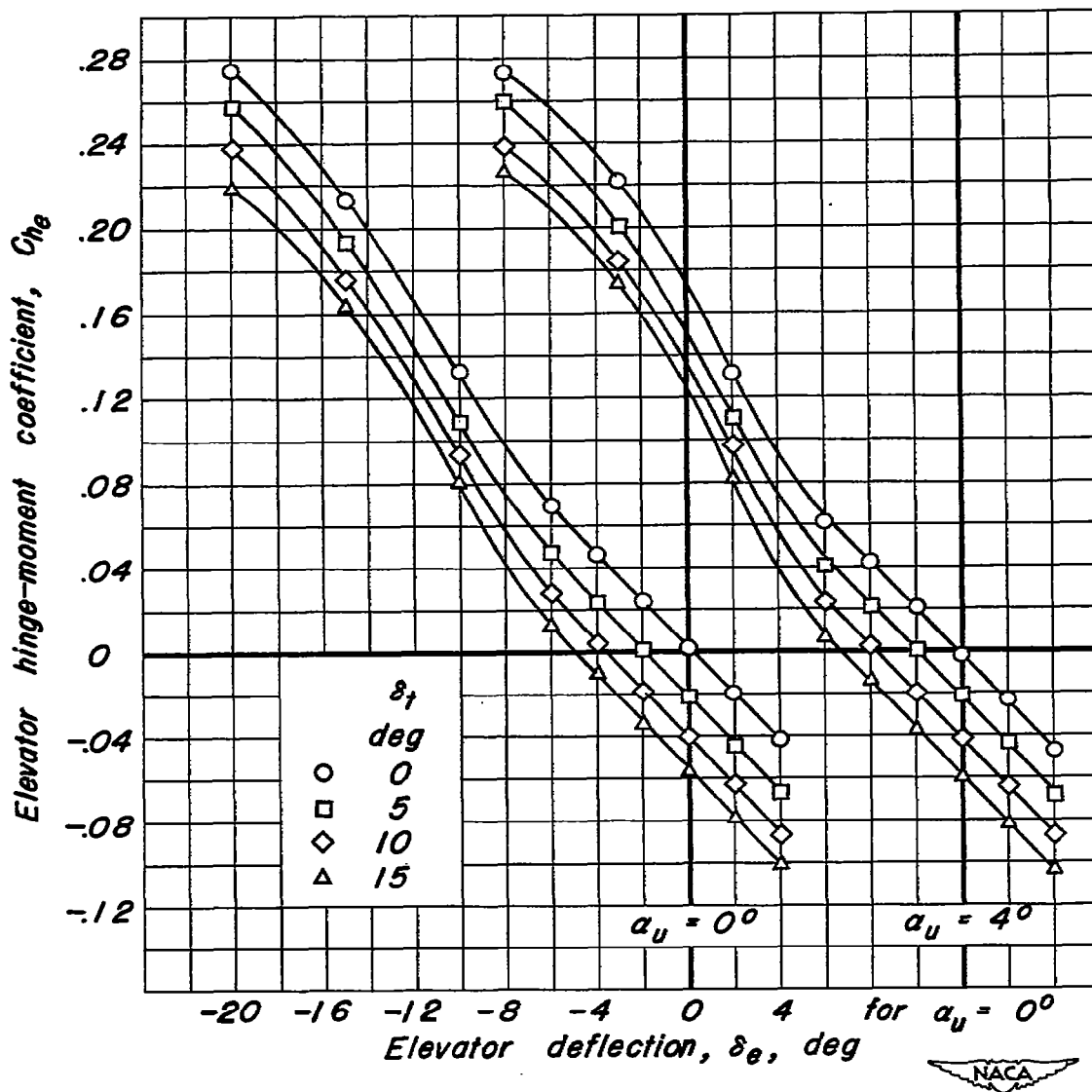
(b) $M, 0.60$.

Figure 7. — Continued.



(c) $M, 0.75.$

Figure 7. - Continued.

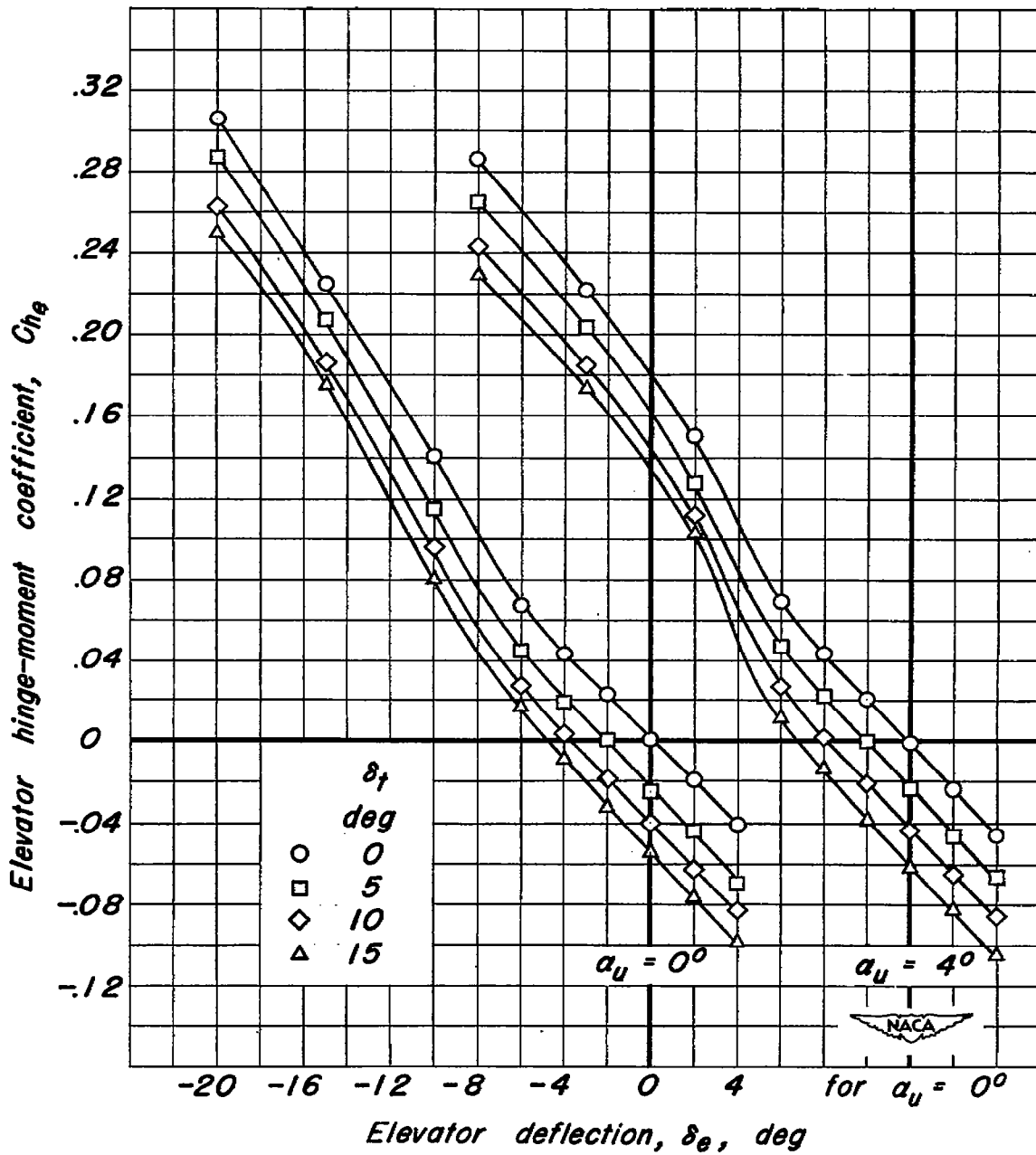
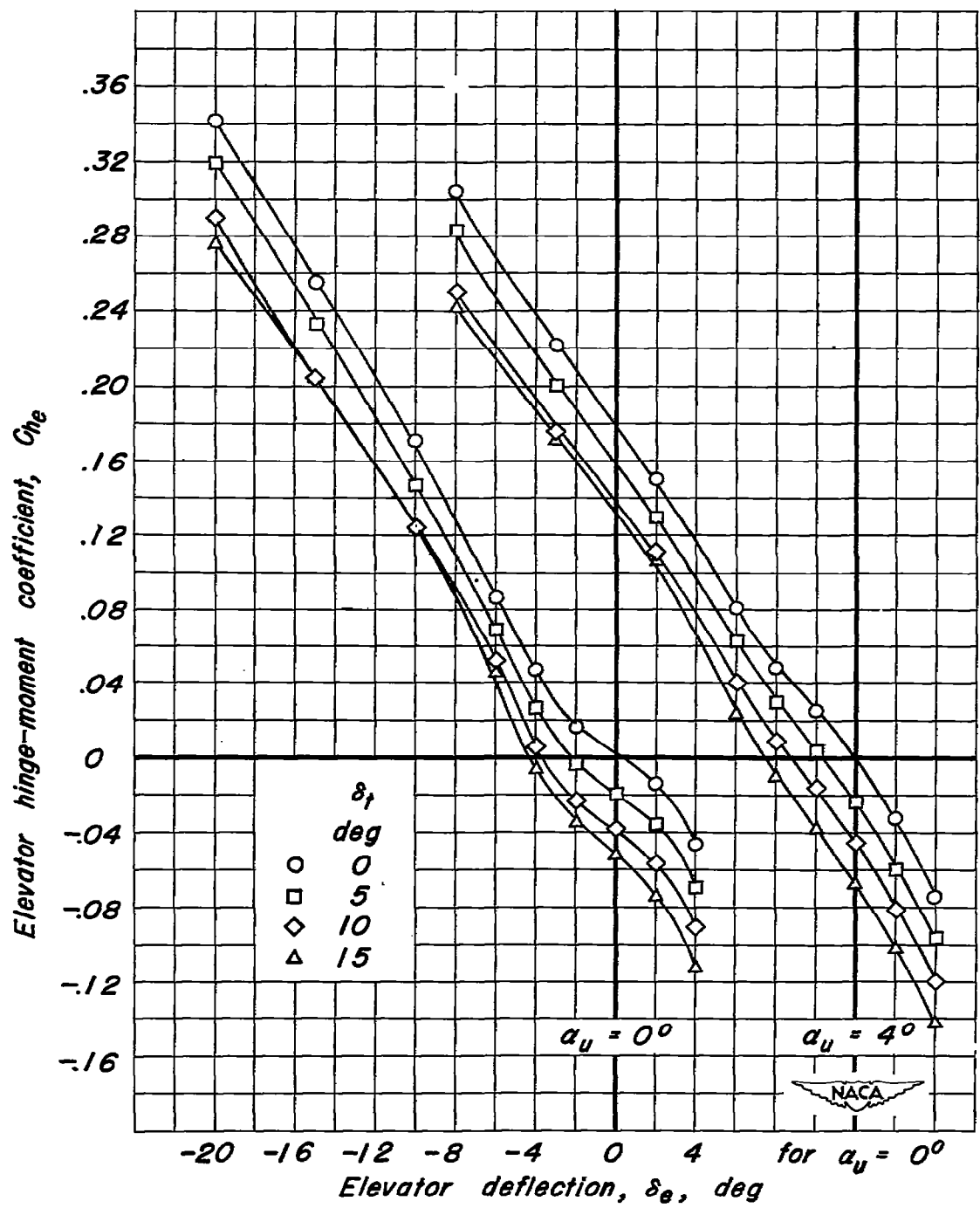
(d) $M, 0.80$.

Figure 7. - Continued.



(e) $M, 0.85.$

Figure 7. — Continued.

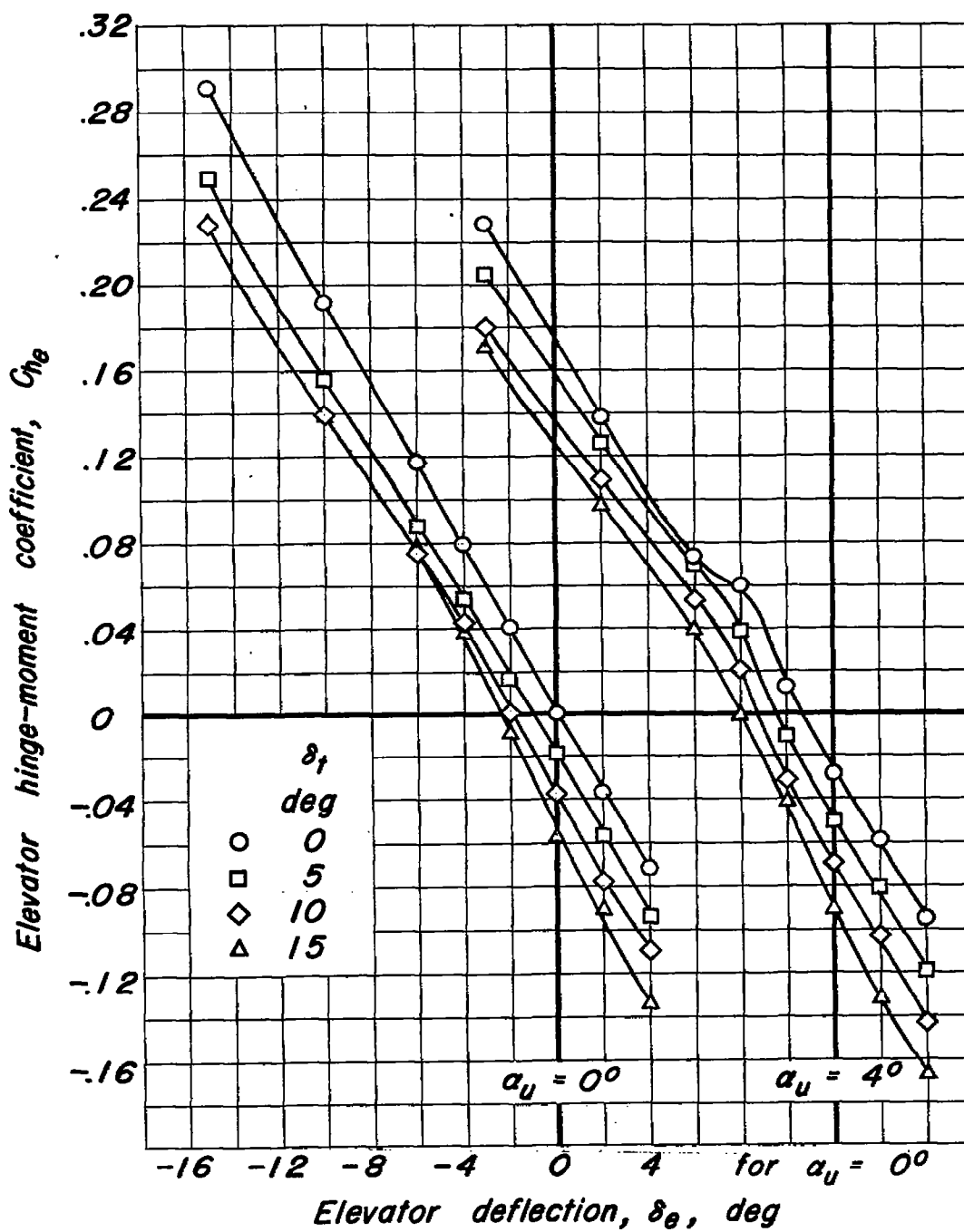
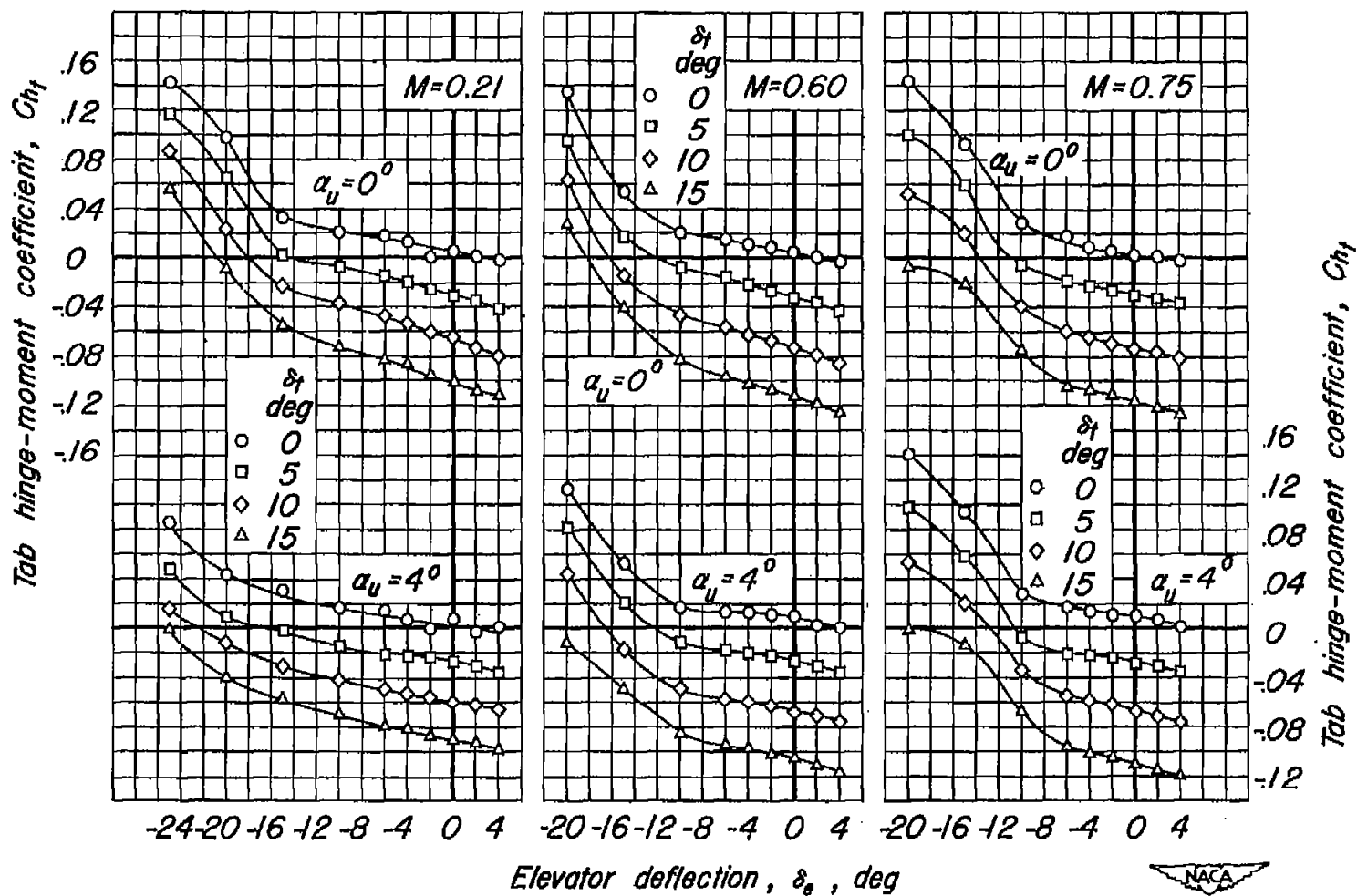
(f) $M, 0.88.$

Figure 7. - Concluded.



(a) M ; 0.21, 0.60, and 0.75.

Figure 8.— The variation of tab hinge-moment coefficient with elevator deflection. R , 2,000,000.

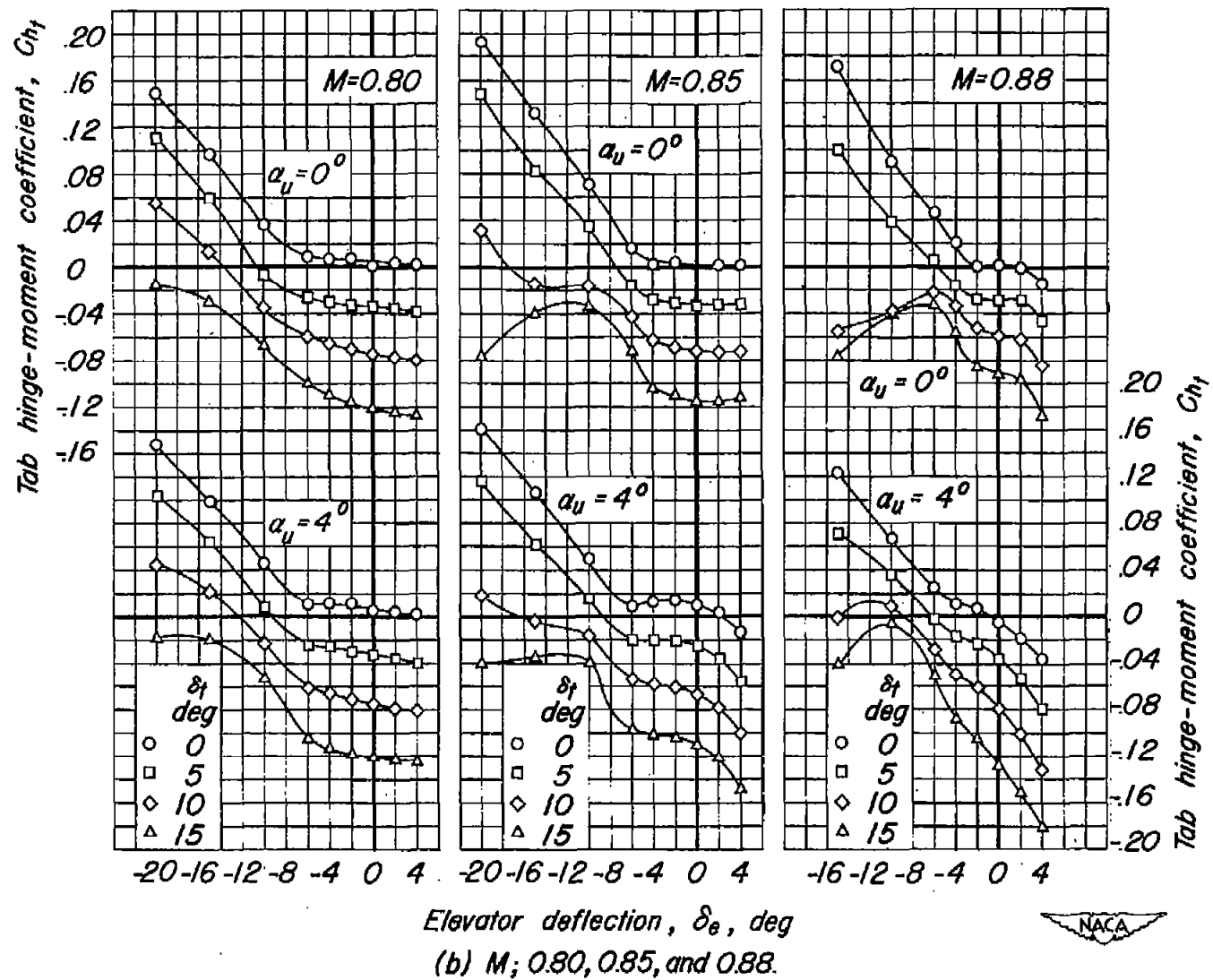


Figure 8.— Concluded.

(b) M ; 0.80, 0.85, and 0.88.

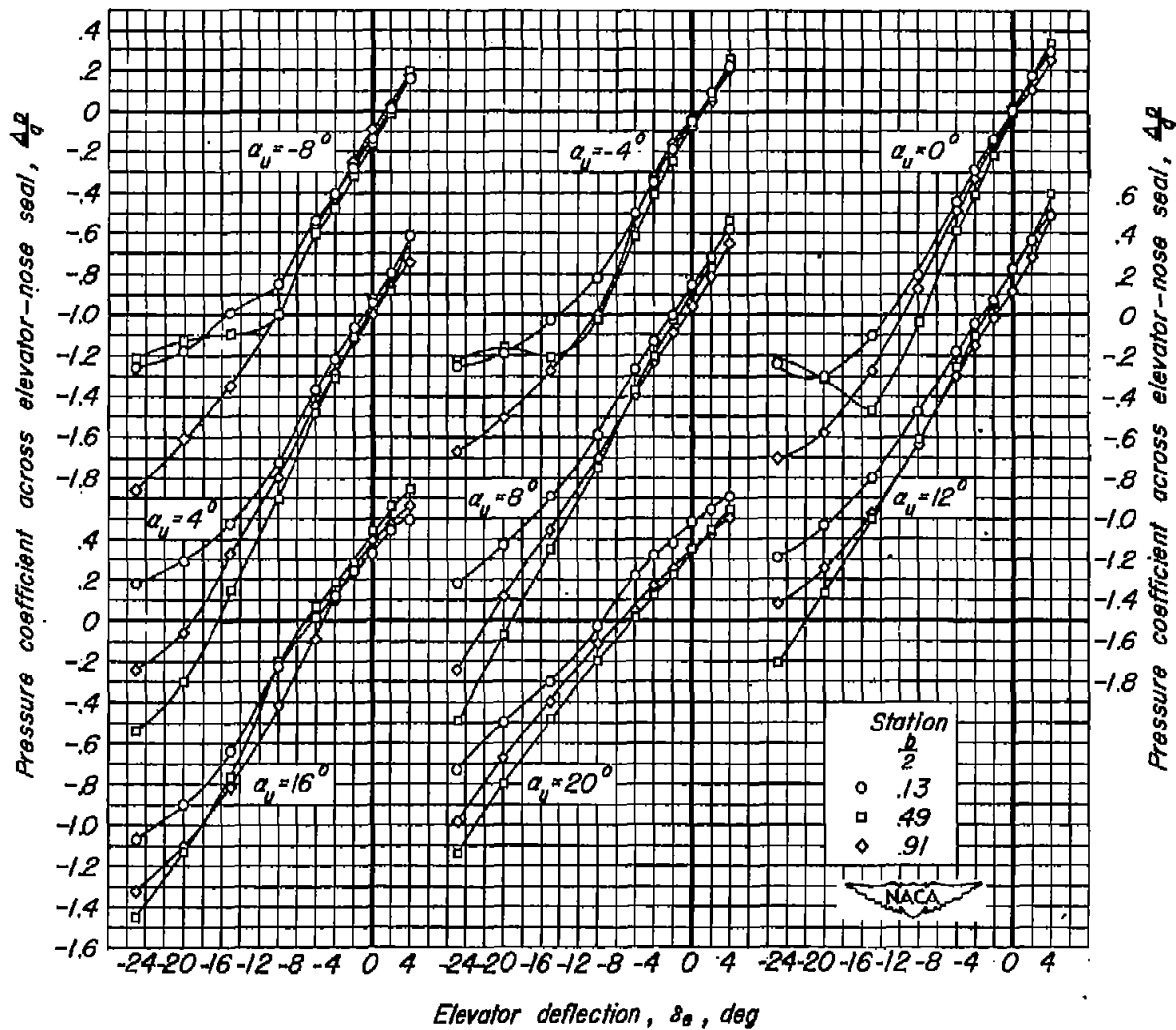
(a) $M_\infty 0.21$.

Figure 9.— The variation of pressure coefficient across the elevator-nose seal with elevator deflection. $\delta_y, 0^\circ$; $R, 2,000,000$.

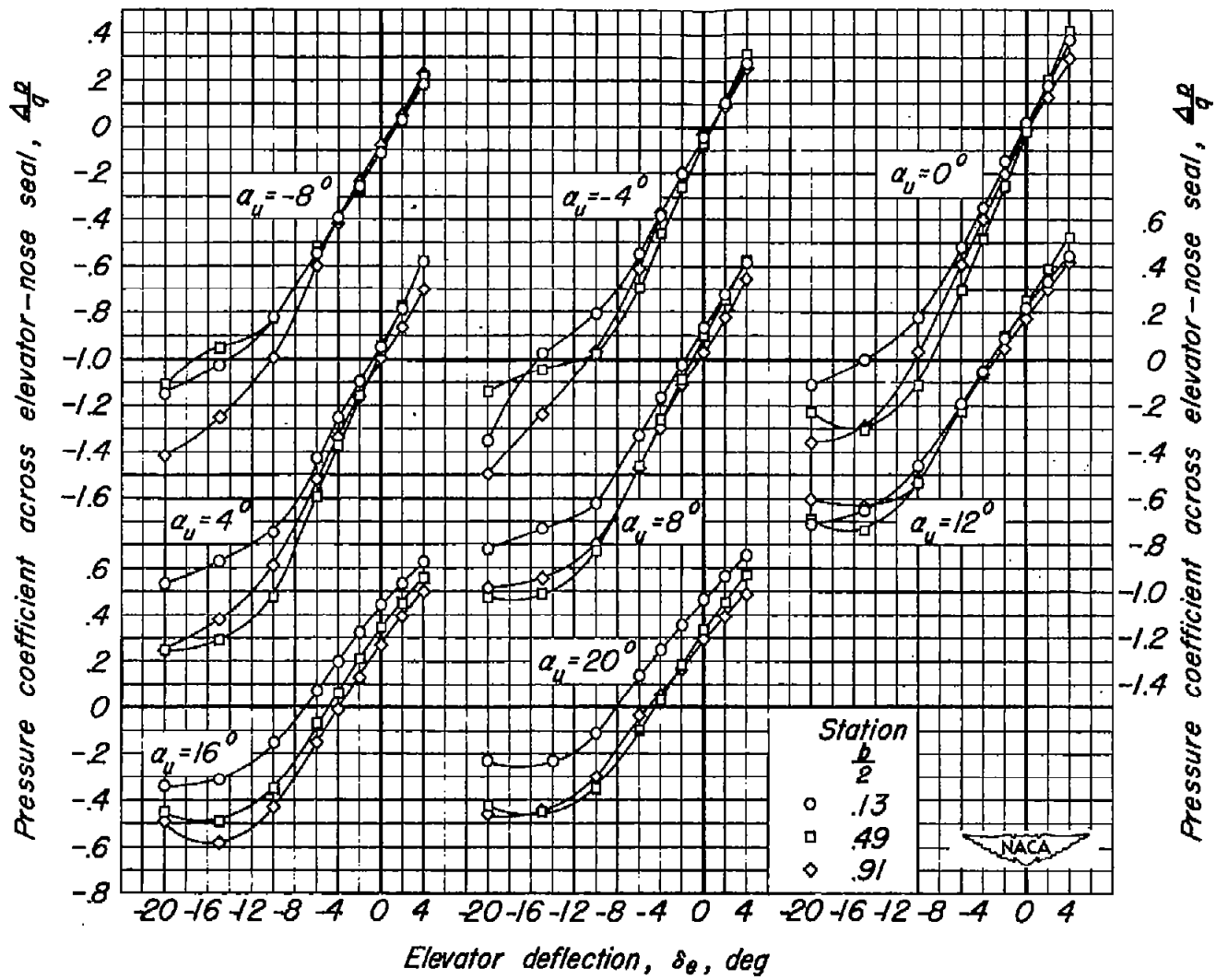


Figure 9. — Continued.

(b) $M, 0.60$.

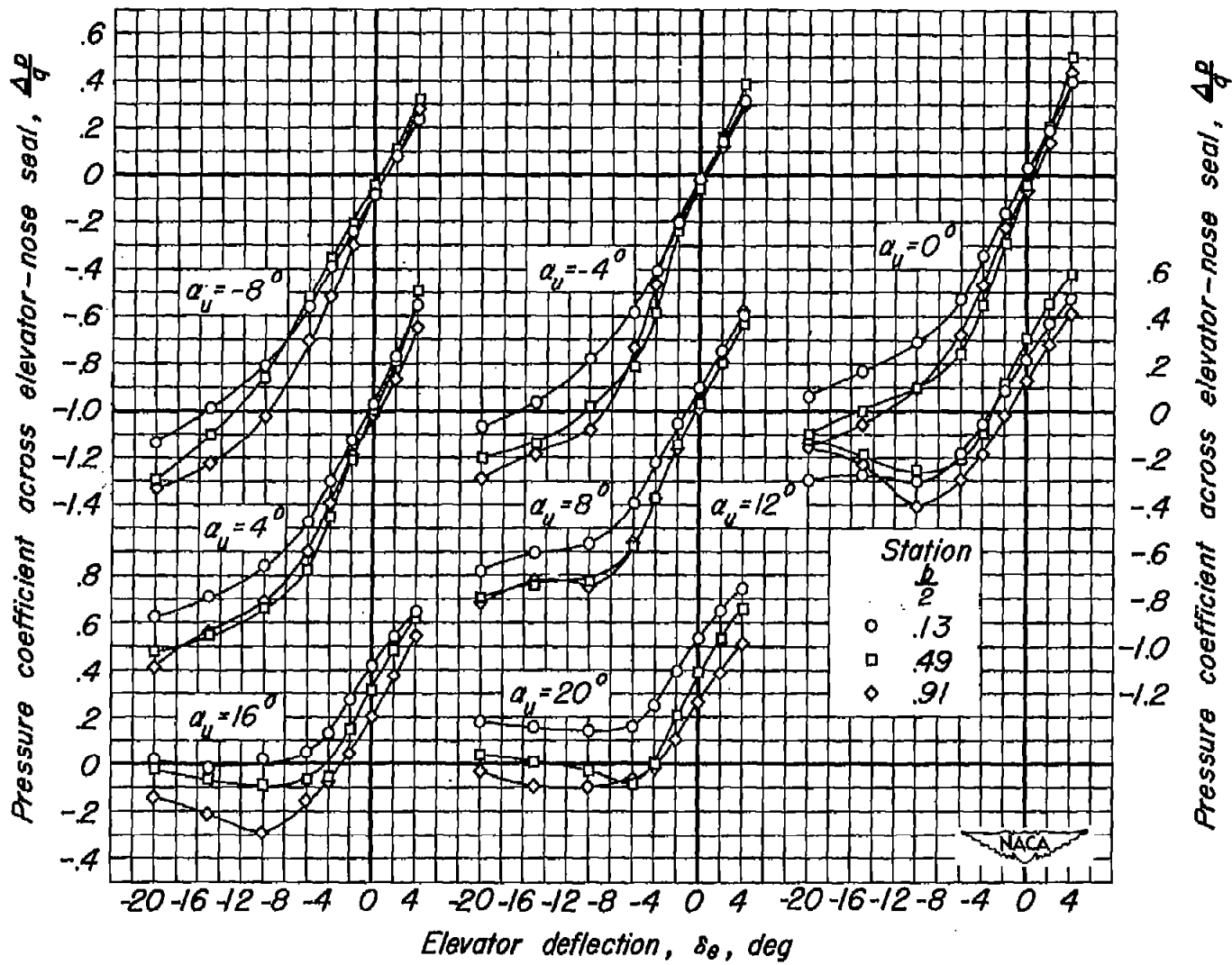


Figure 9.— Continued.

(c) $M, 0.75.$

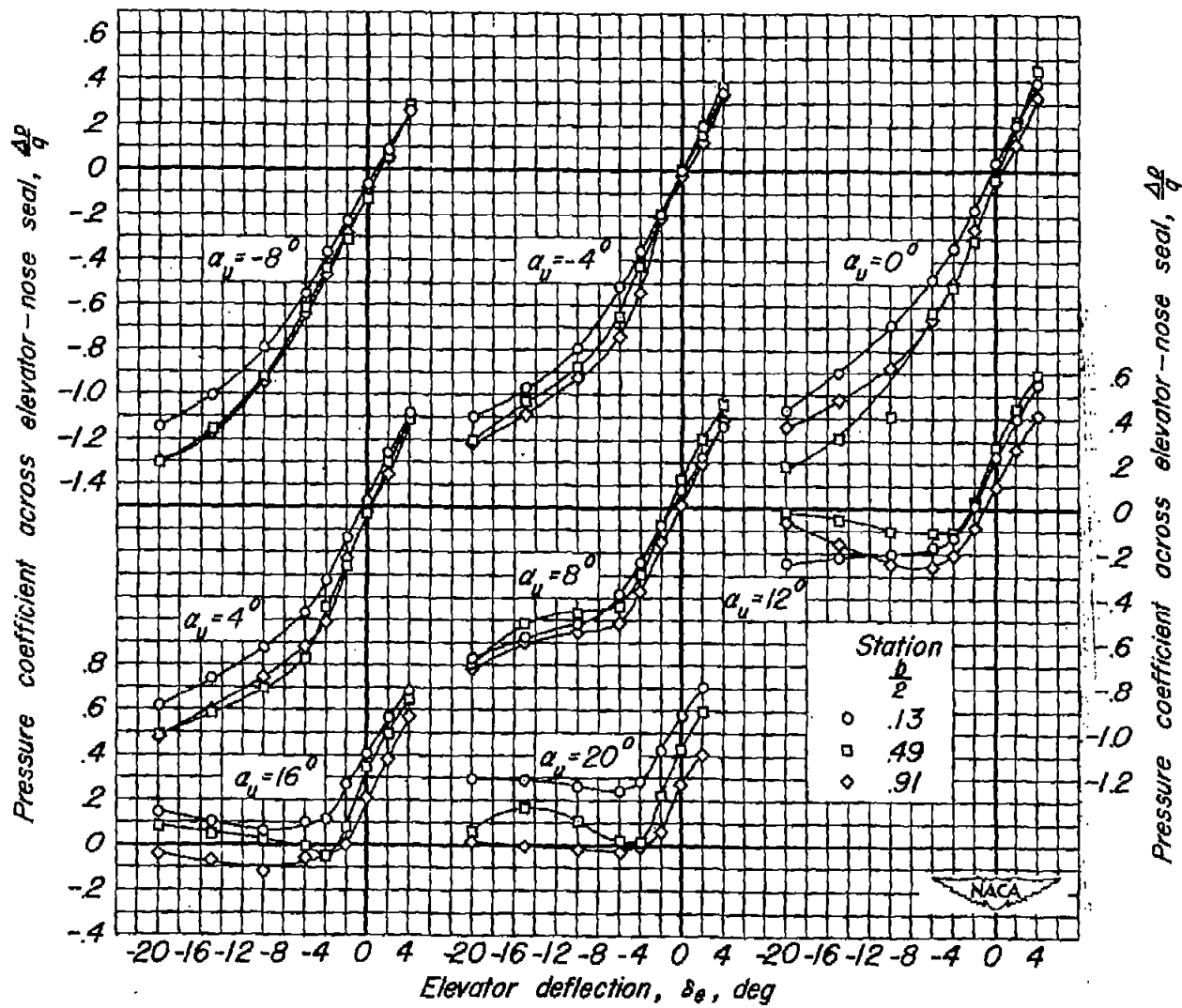
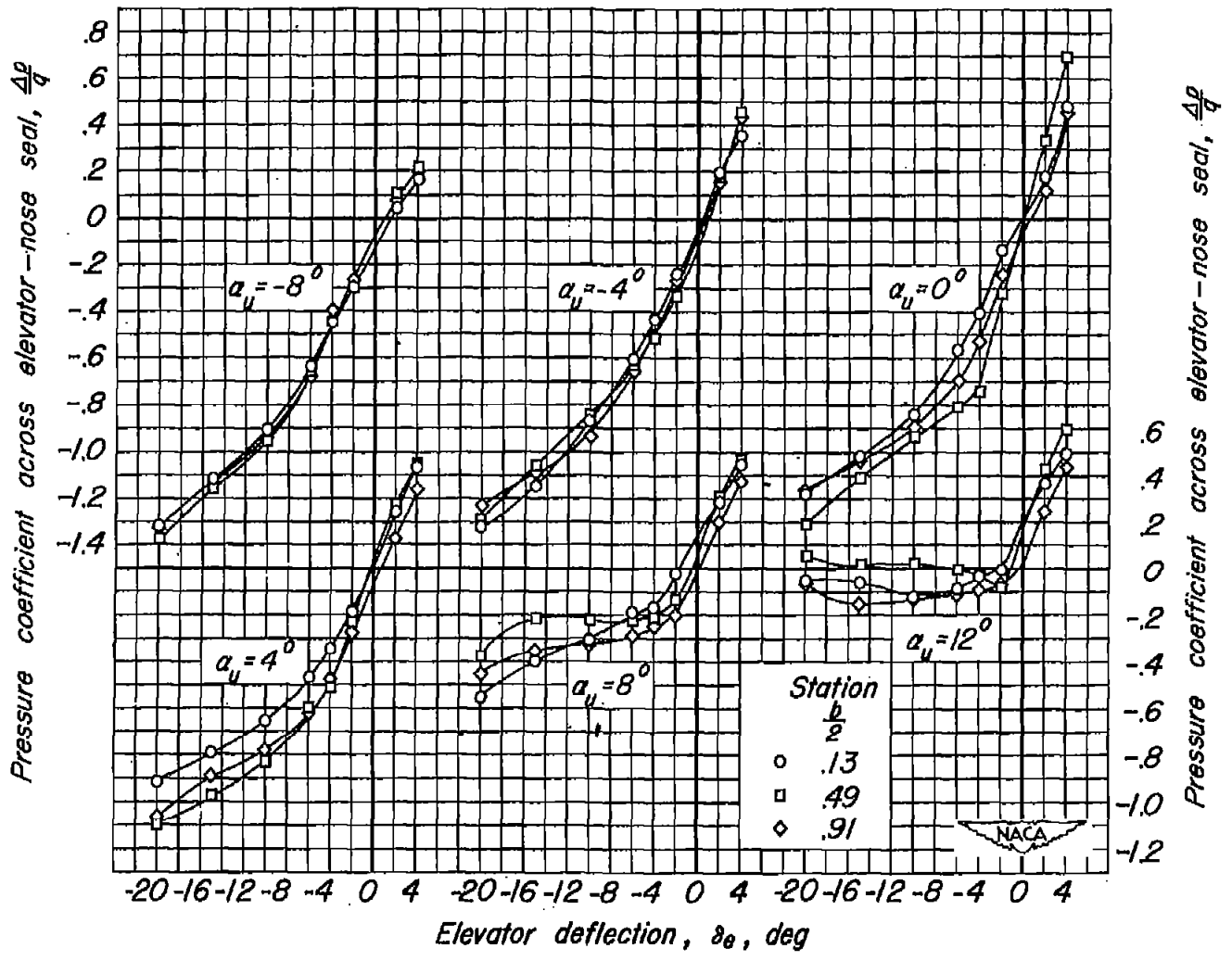


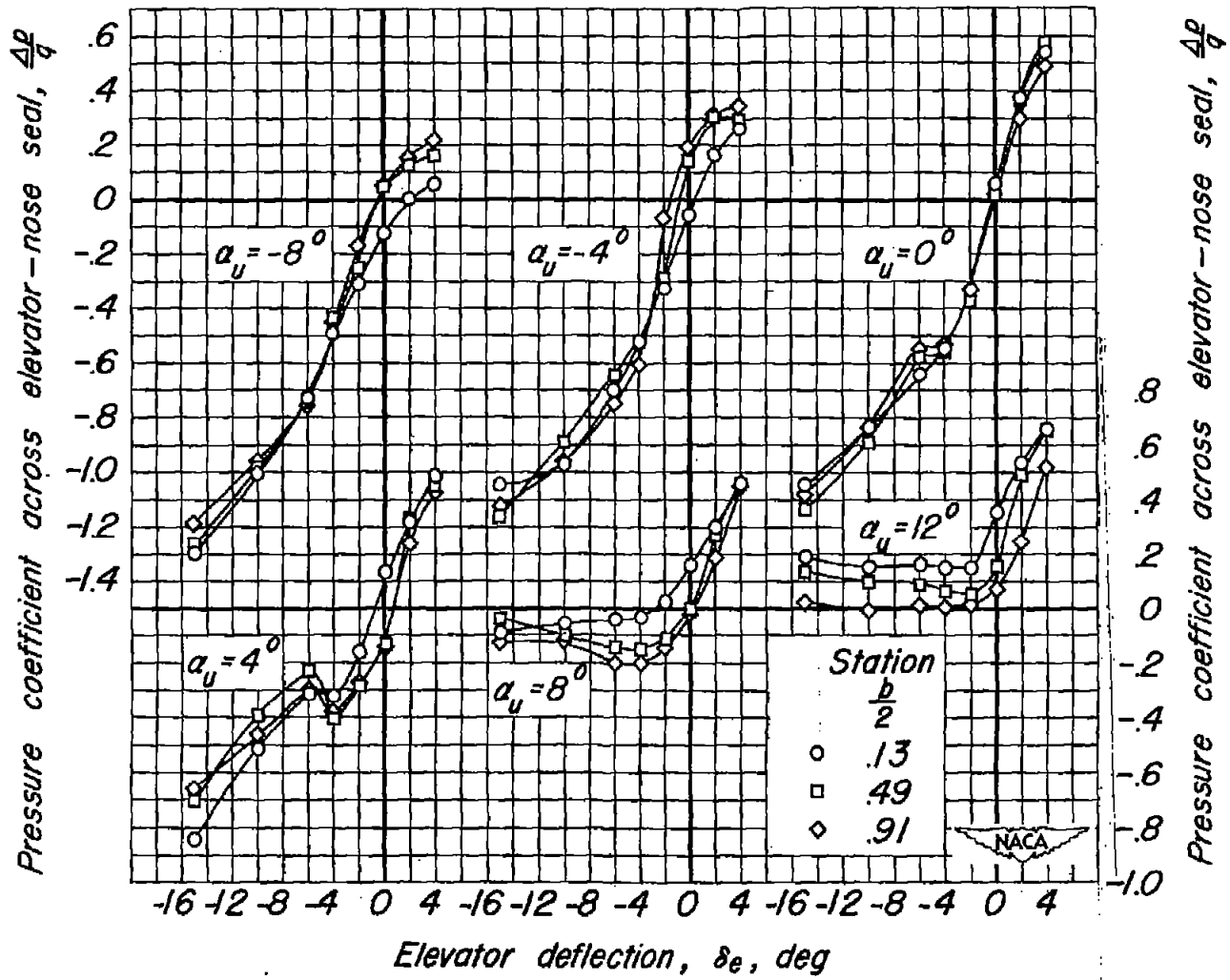
Figure 9. — Continued.

(d) $M, 0.80$.



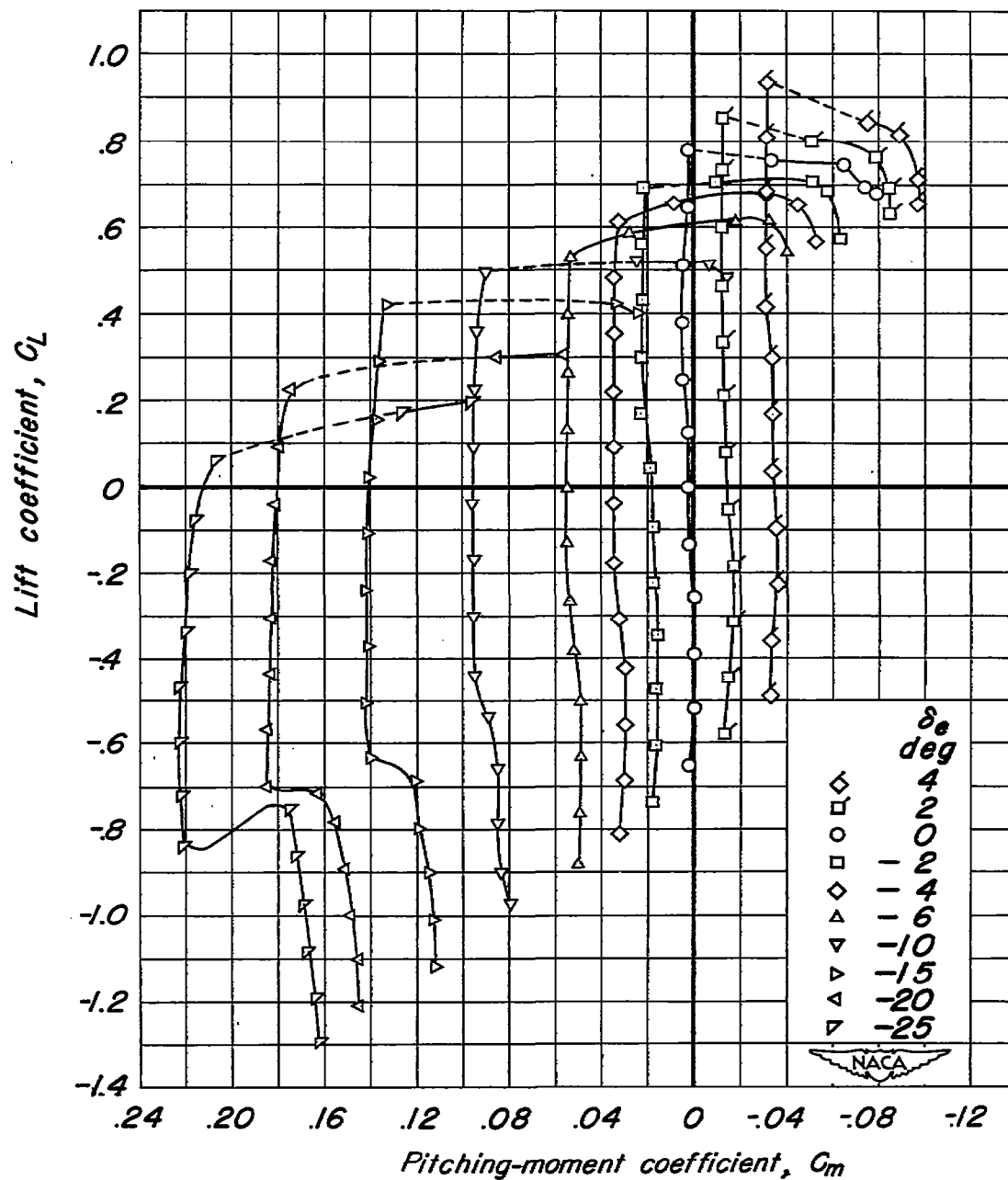
(e) M, 0.85.

Figure 9.— Continued.



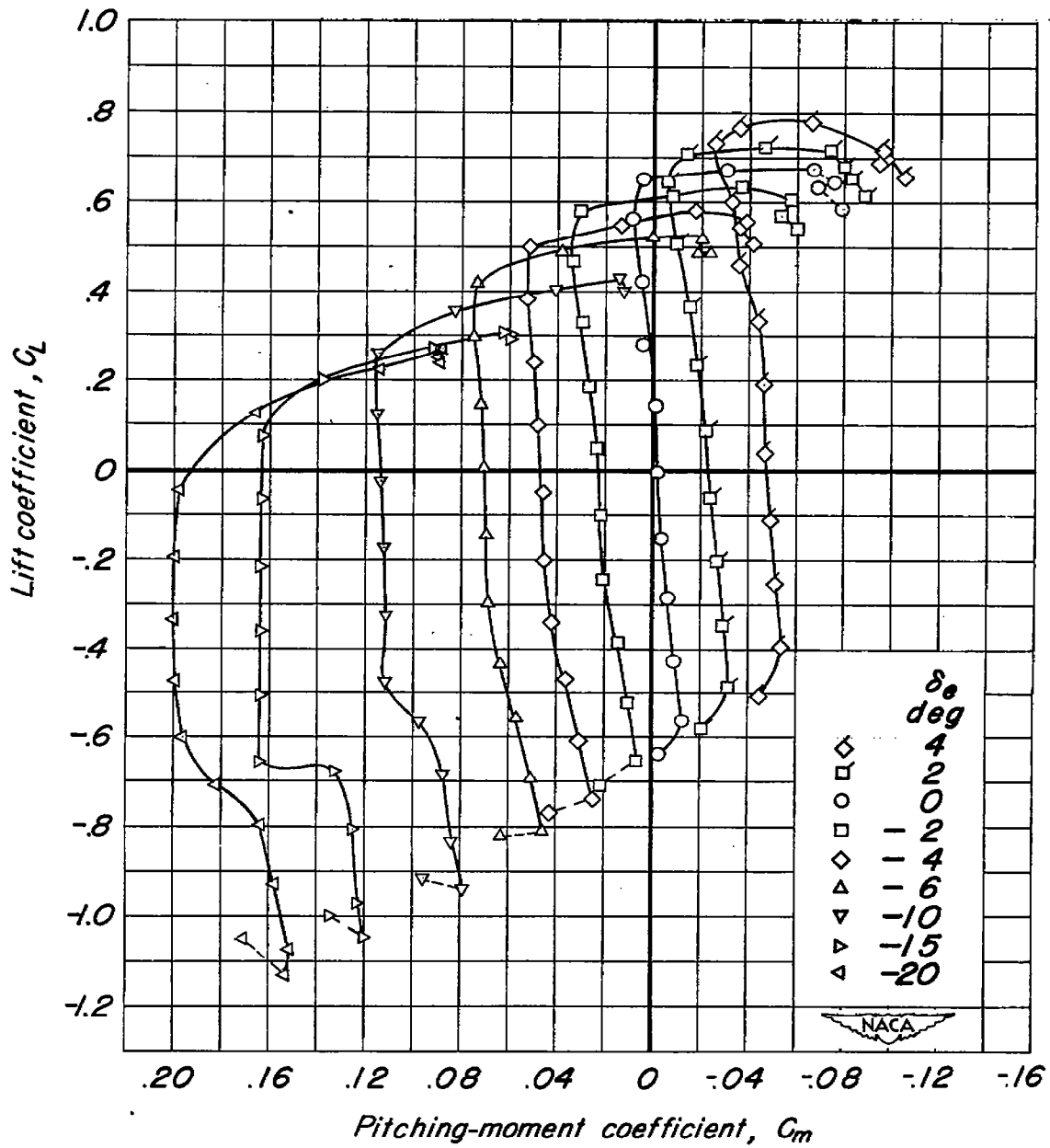
(f) $M, 0.88.$

Figure 9. — Concluded.



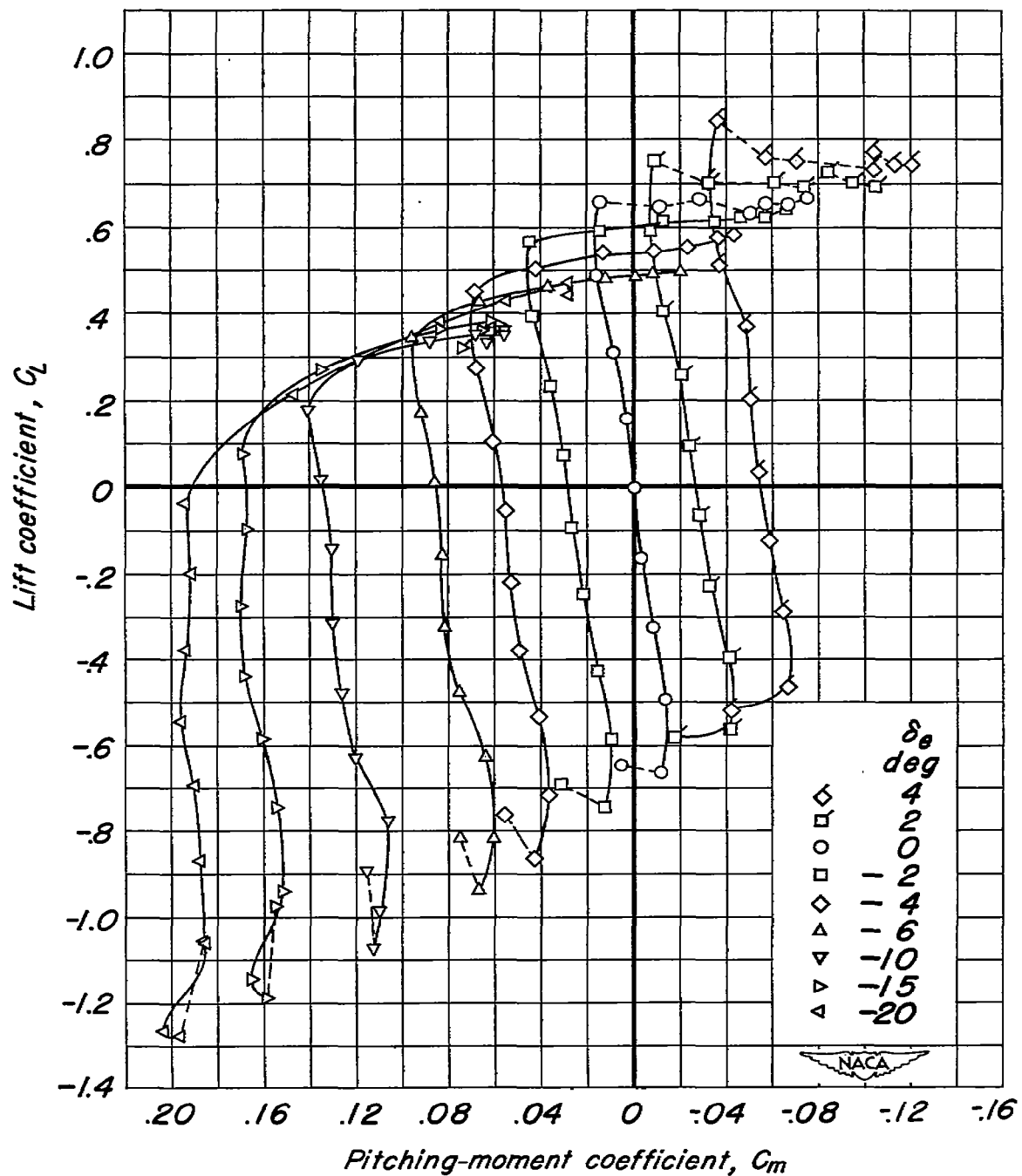
(a) $M, 0.21.$

Figure 10.— The variation of lift coefficient with pitching-moment coefficient. $\delta_t, 0^\circ; R, 2,000,000.$



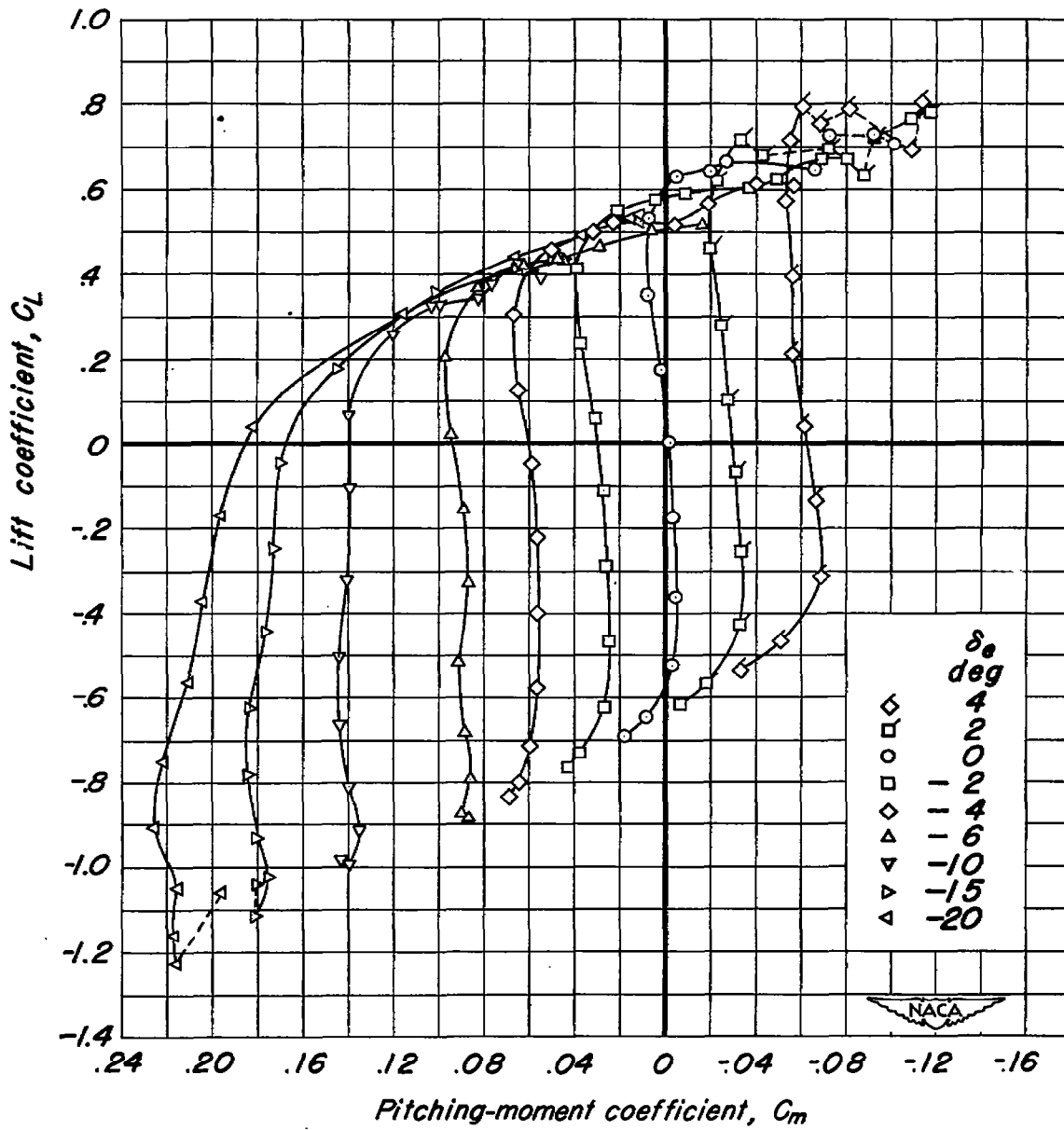
(b) $M, 0.60.$

Figure 10. — Continued.



(c) $M, 0.75.$

Figure 10. — Continued.



(d) M , 0.80.

Figure 10. — Continued.

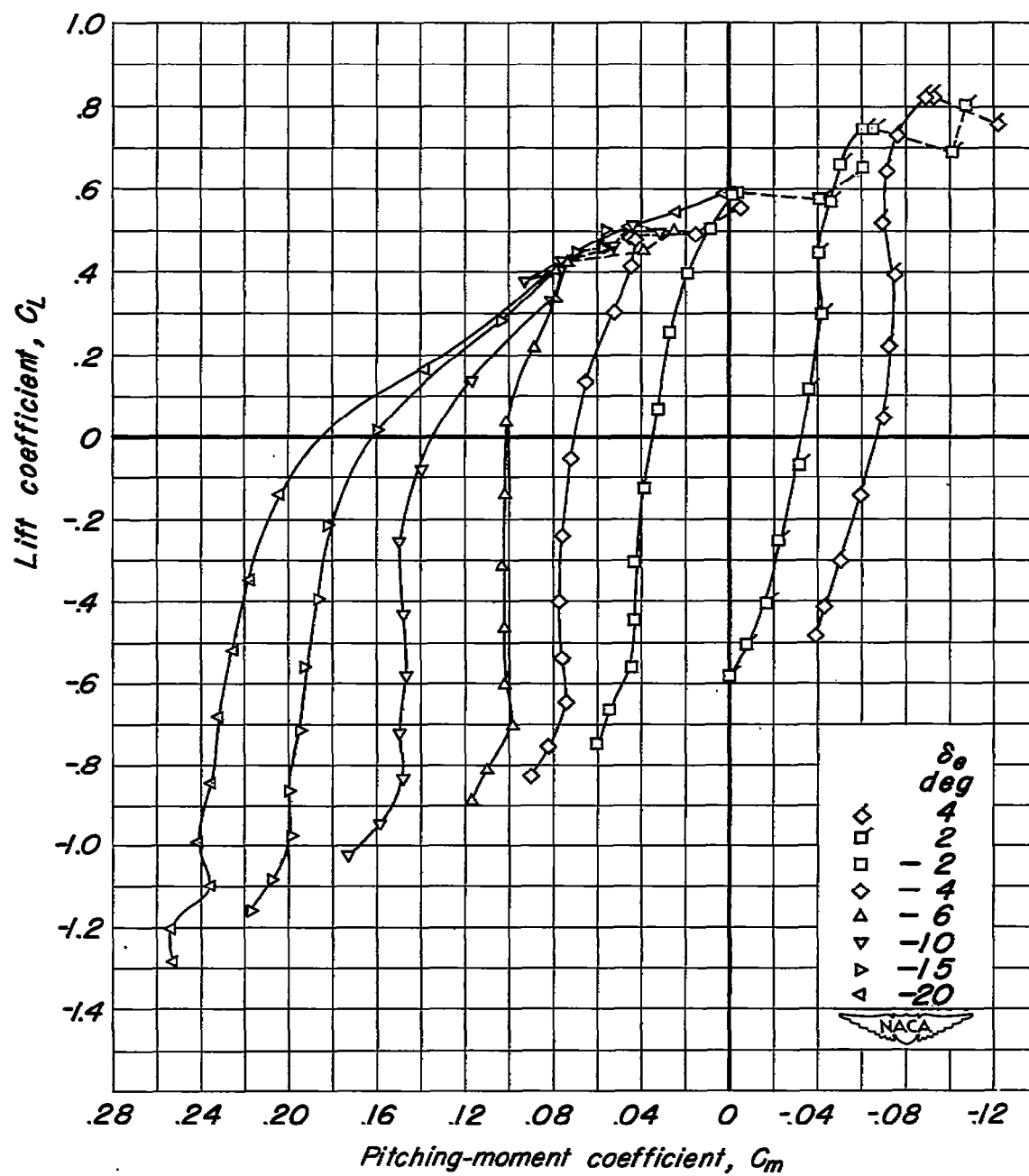
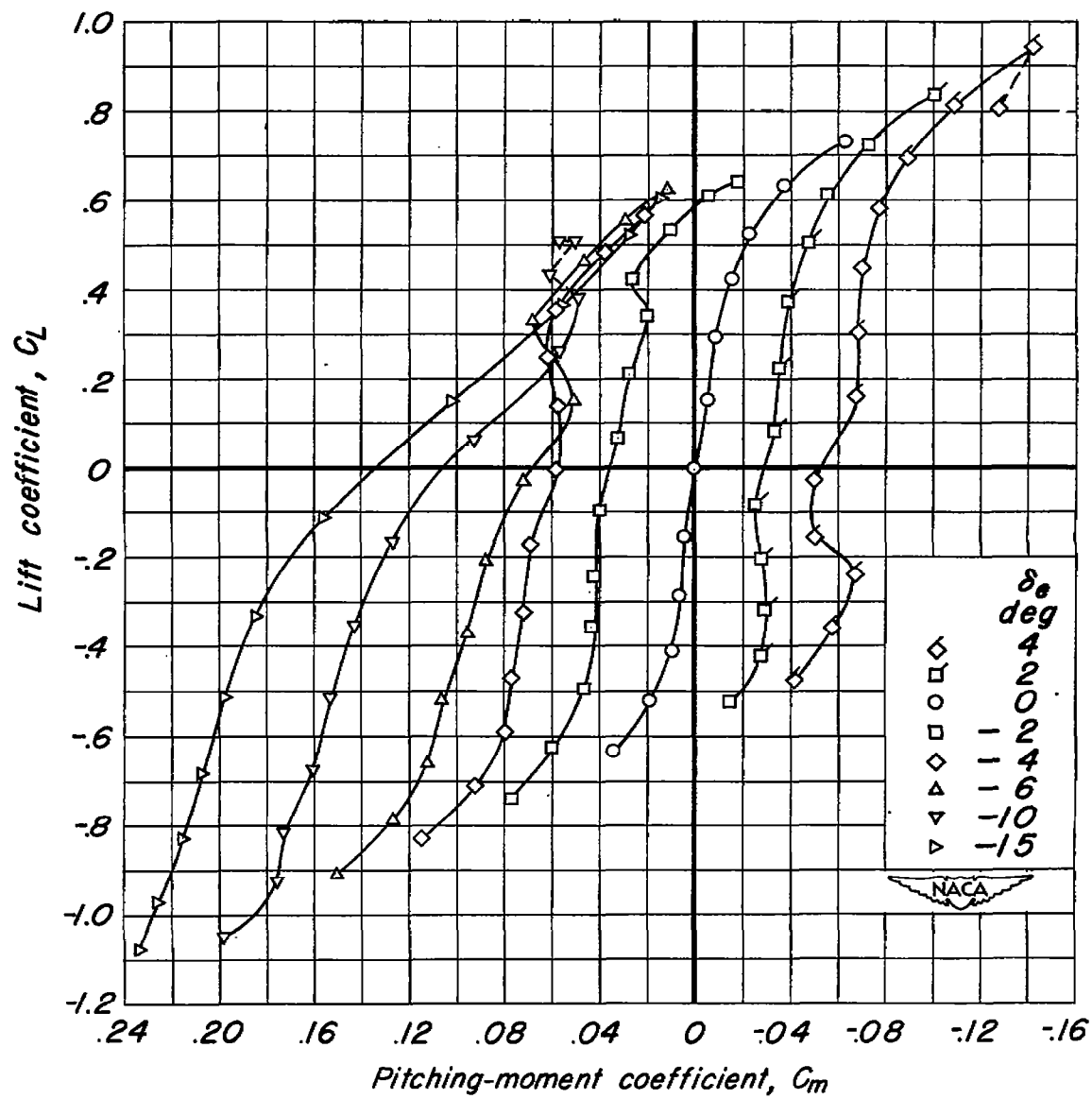
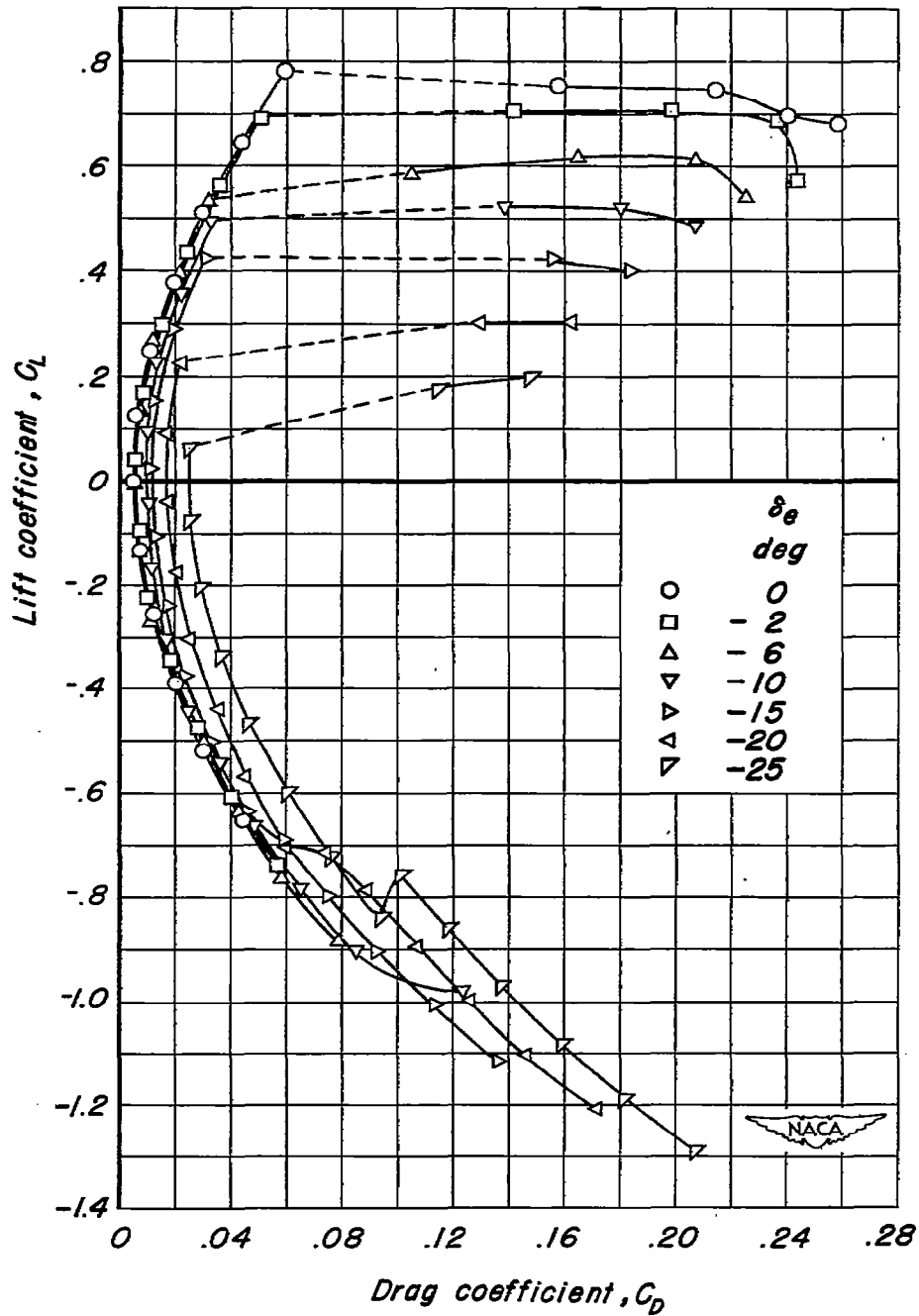
(e) $M, 0.85.$

Figure 10. — Continued.



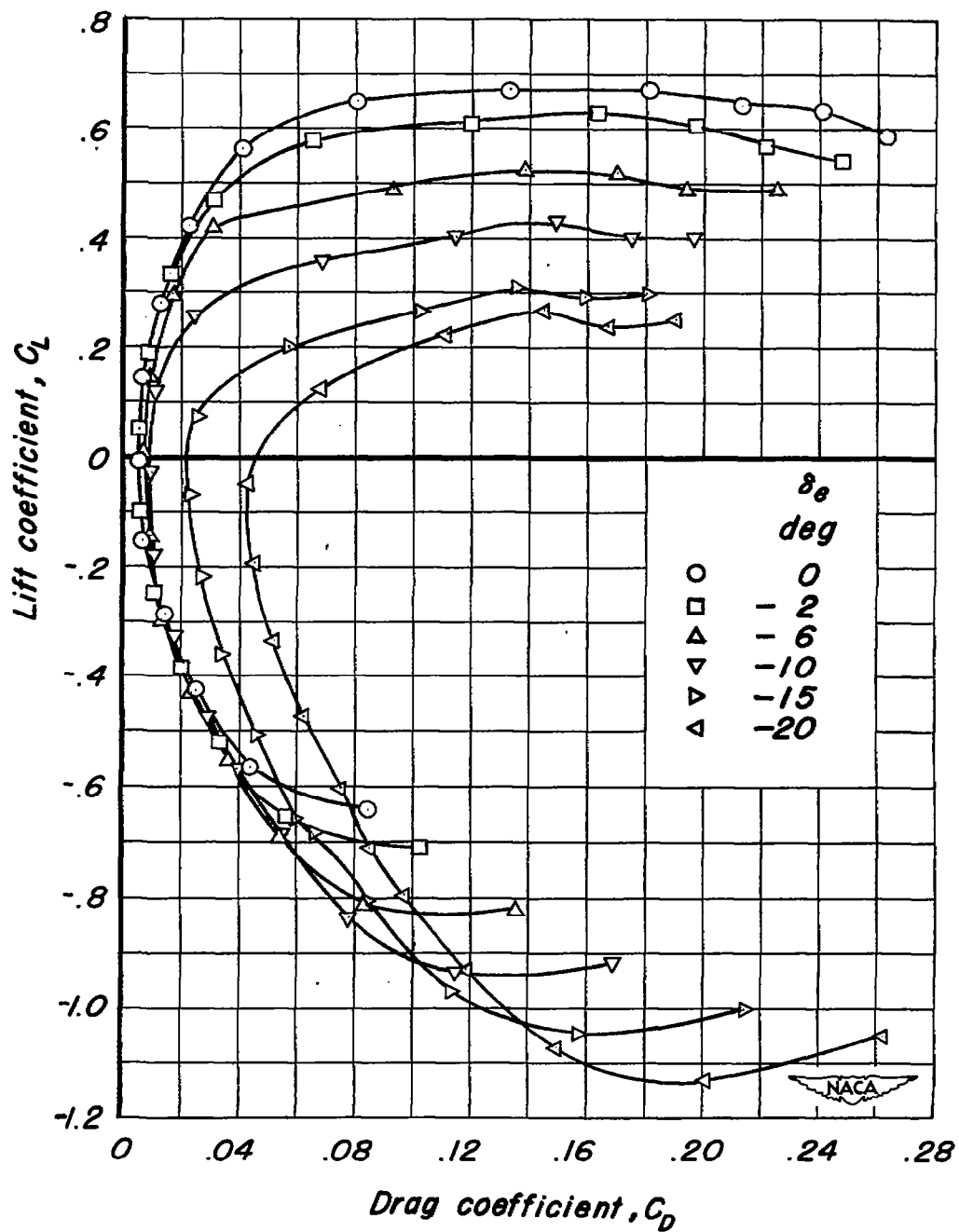
(f) $M, 0.88.$

Figure 10. — Concluded.



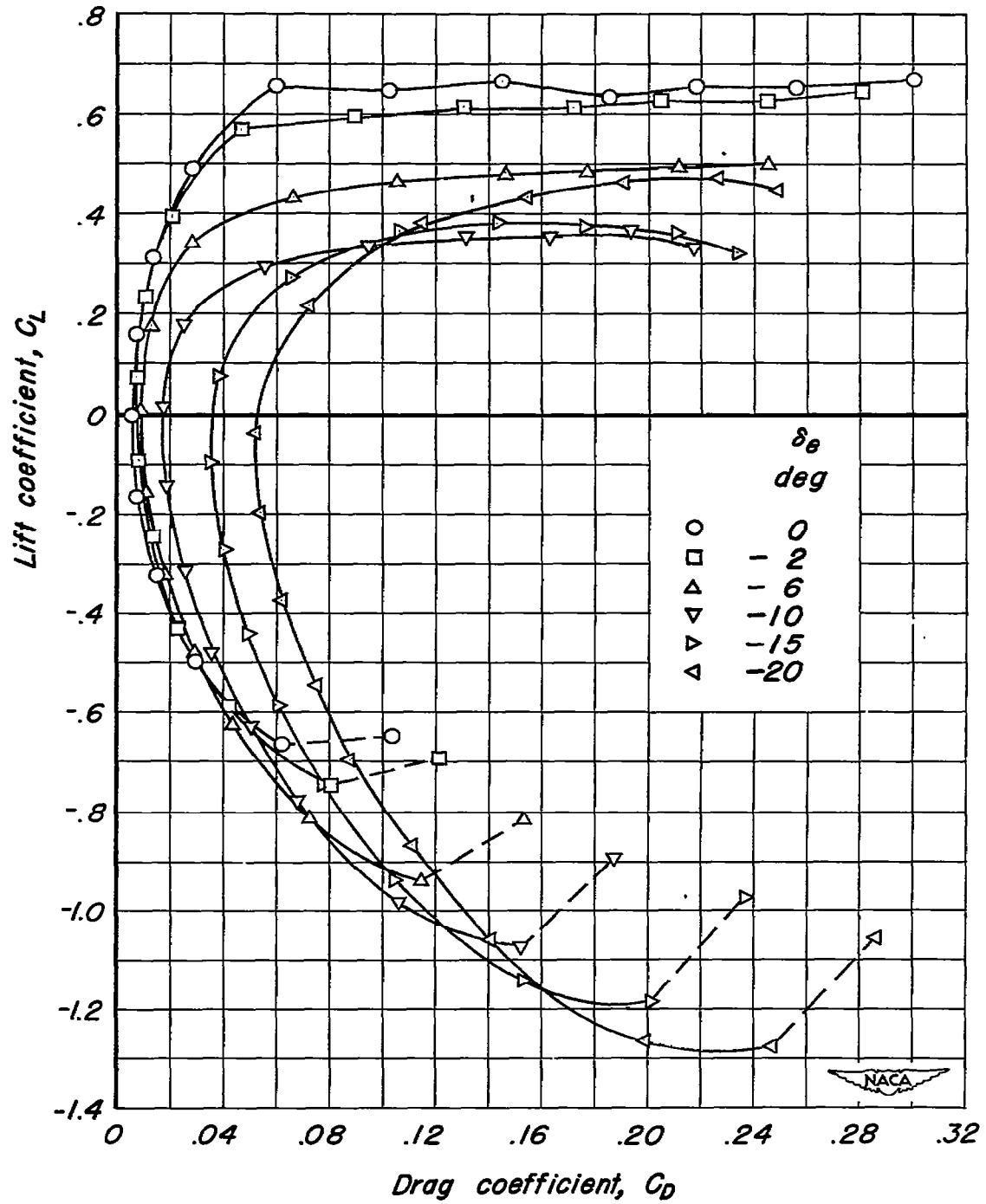
(a) $M, 0.21$.

Figure 11.— The variation of lift coefficient with drag coefficient. $\delta_T, 0^\circ$; $R, 2,000,000$.



(b) $M, 0.60.$

Figure 11. - Continued.



(c) $M, 0.75.$

Figure 11. - Continued.

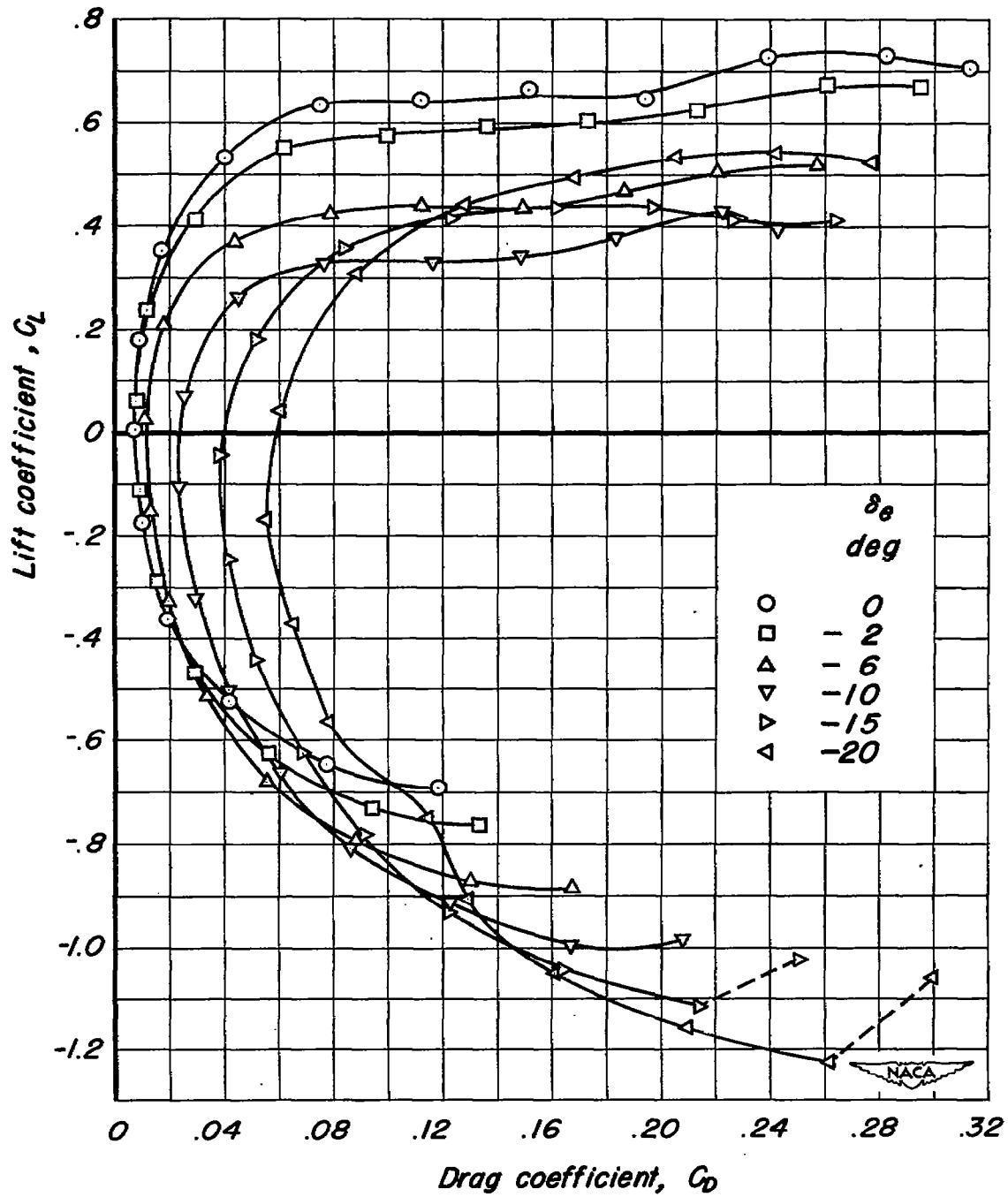
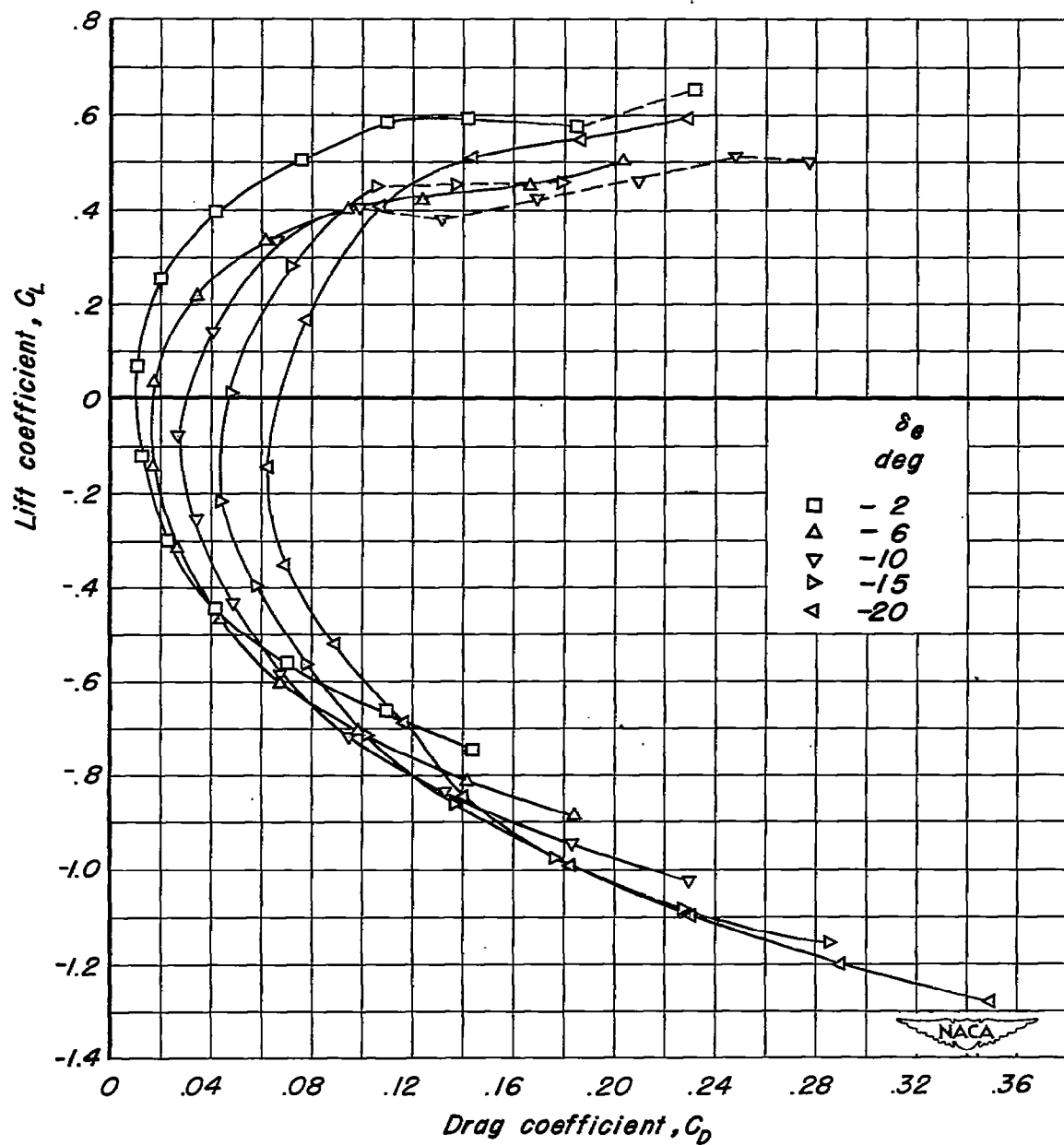
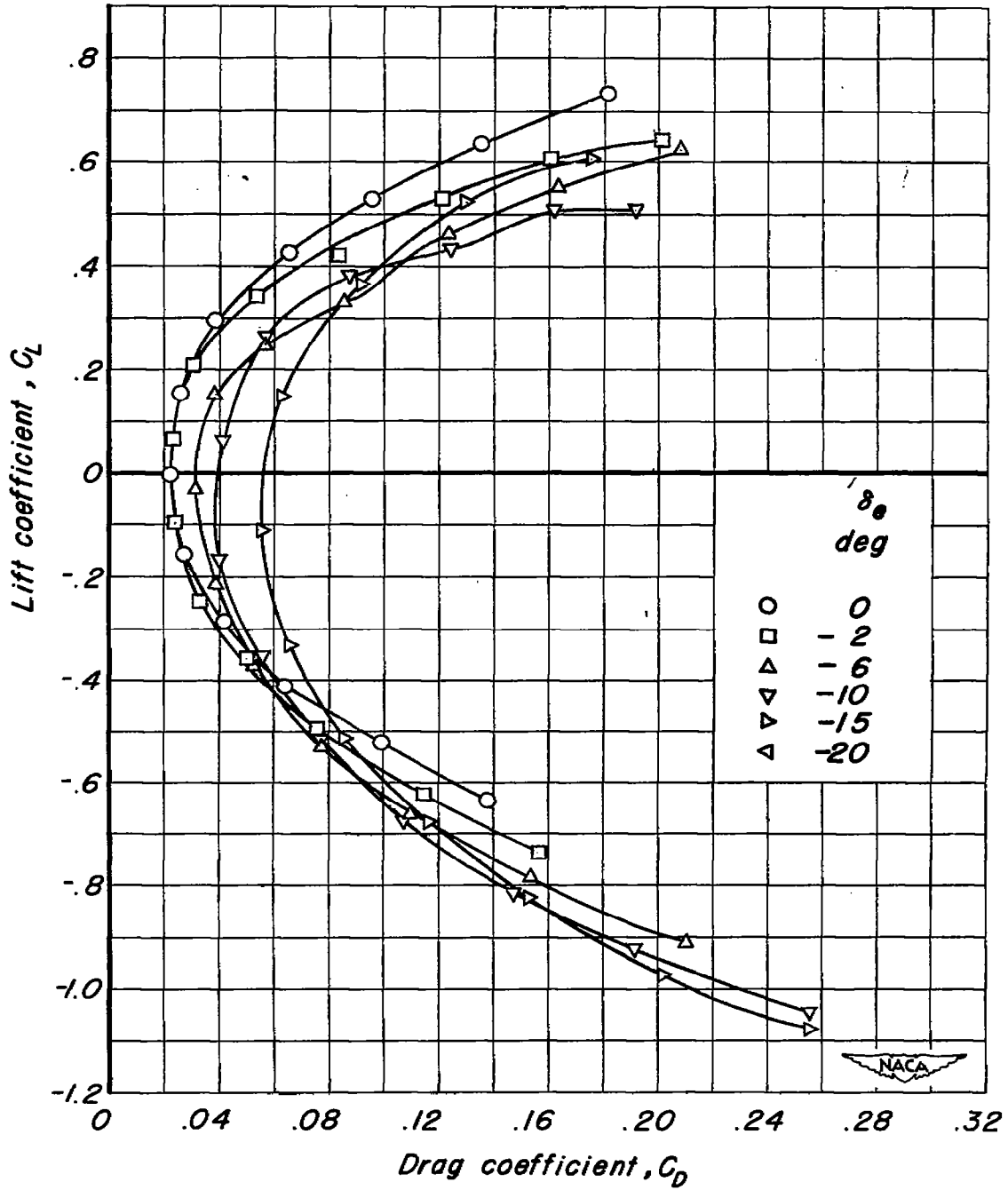
(d) $M, 0.80$.

Figure 11. — Continued.



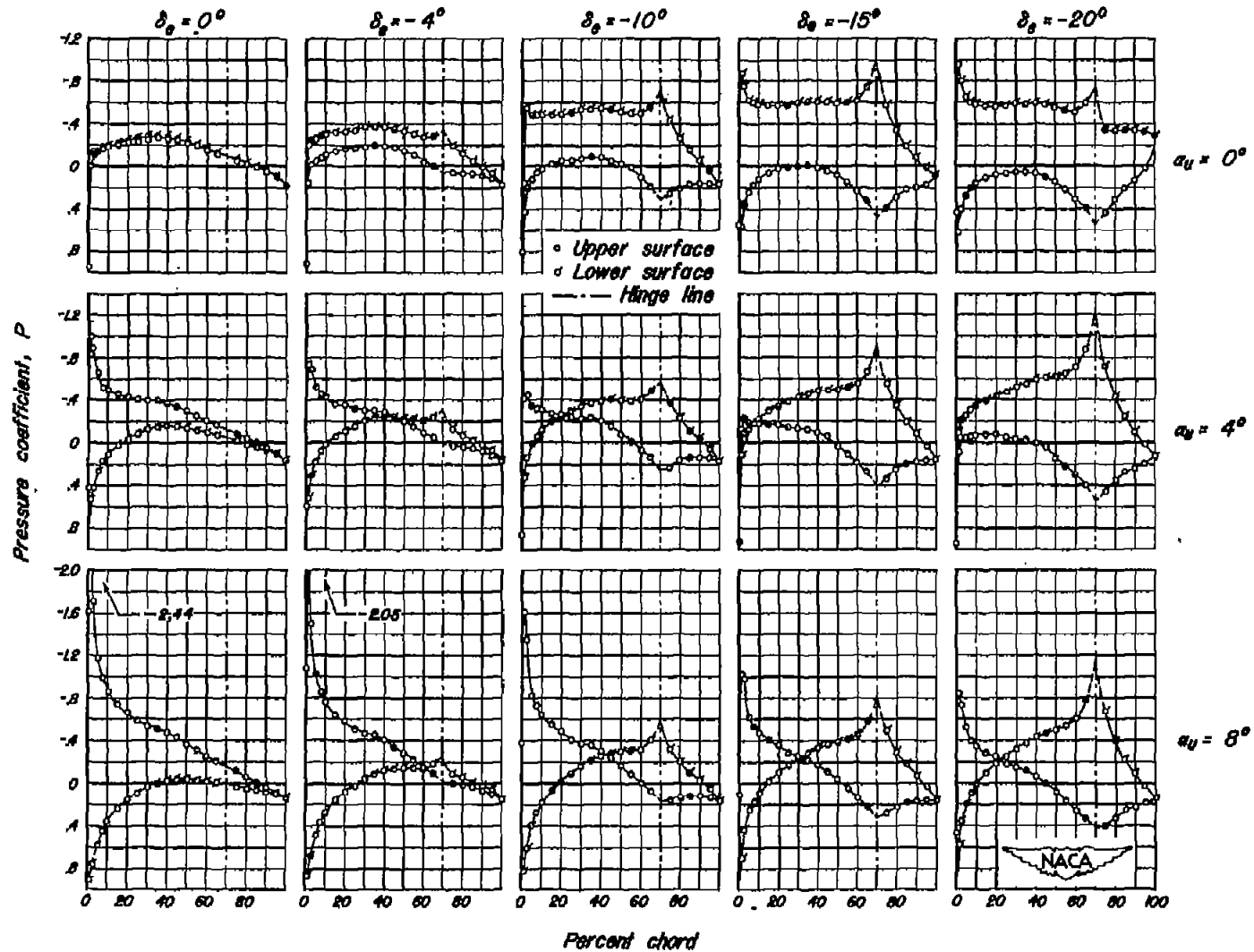
(e) $M, 0.85.$

Figure 11. - Continued.



(f) $M, 0.88.$

Figure 11. — Concluded.



(a) $M, 0.21.$

Figure 12.— The chordwise distribution of pressure coefficient at 50 percent of the semispan. $\alpha, 0^\circ; R, 2,000,000.$

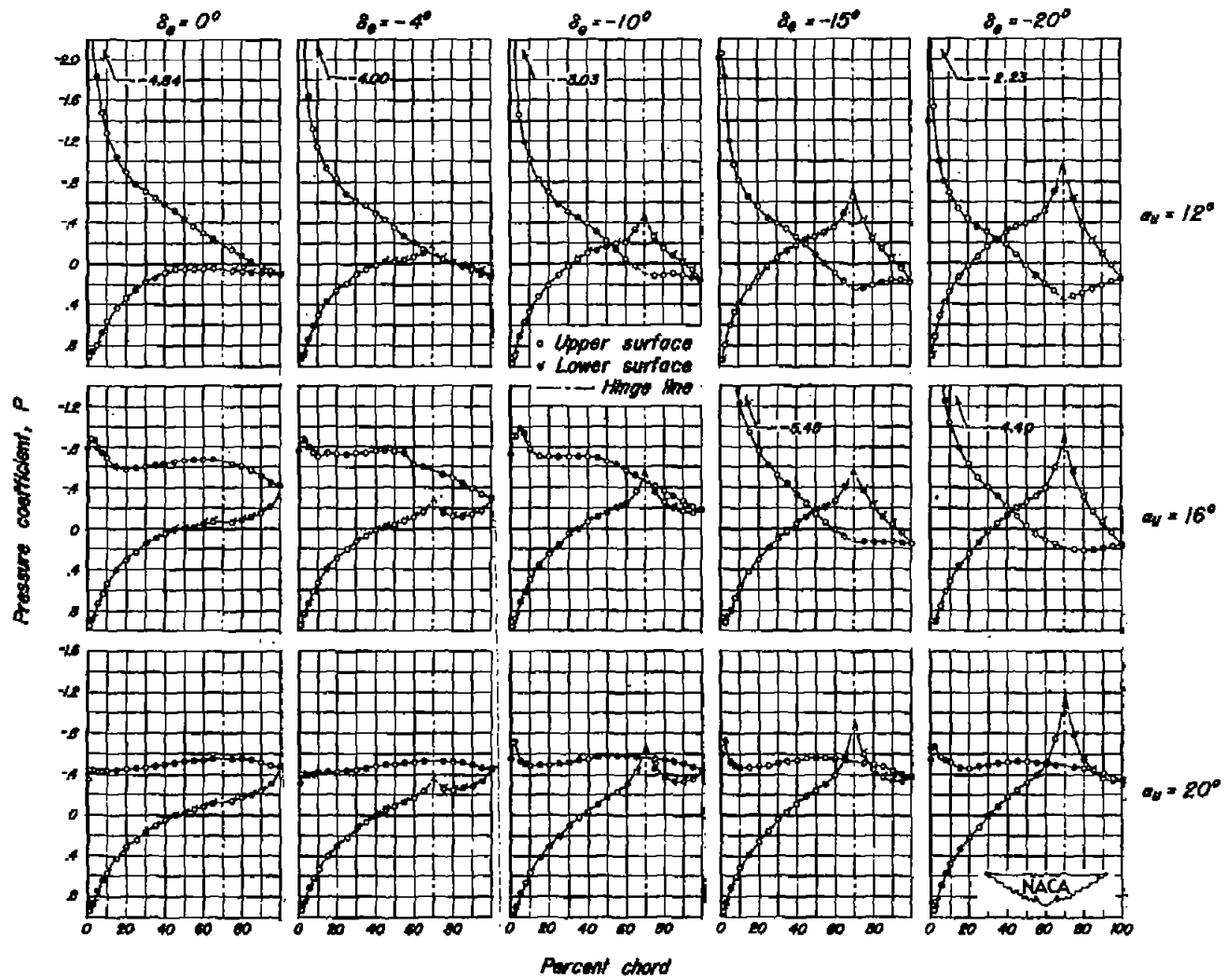
(b) $M_\infty = 0.21$, concluded.

Figure 12.— Continued.

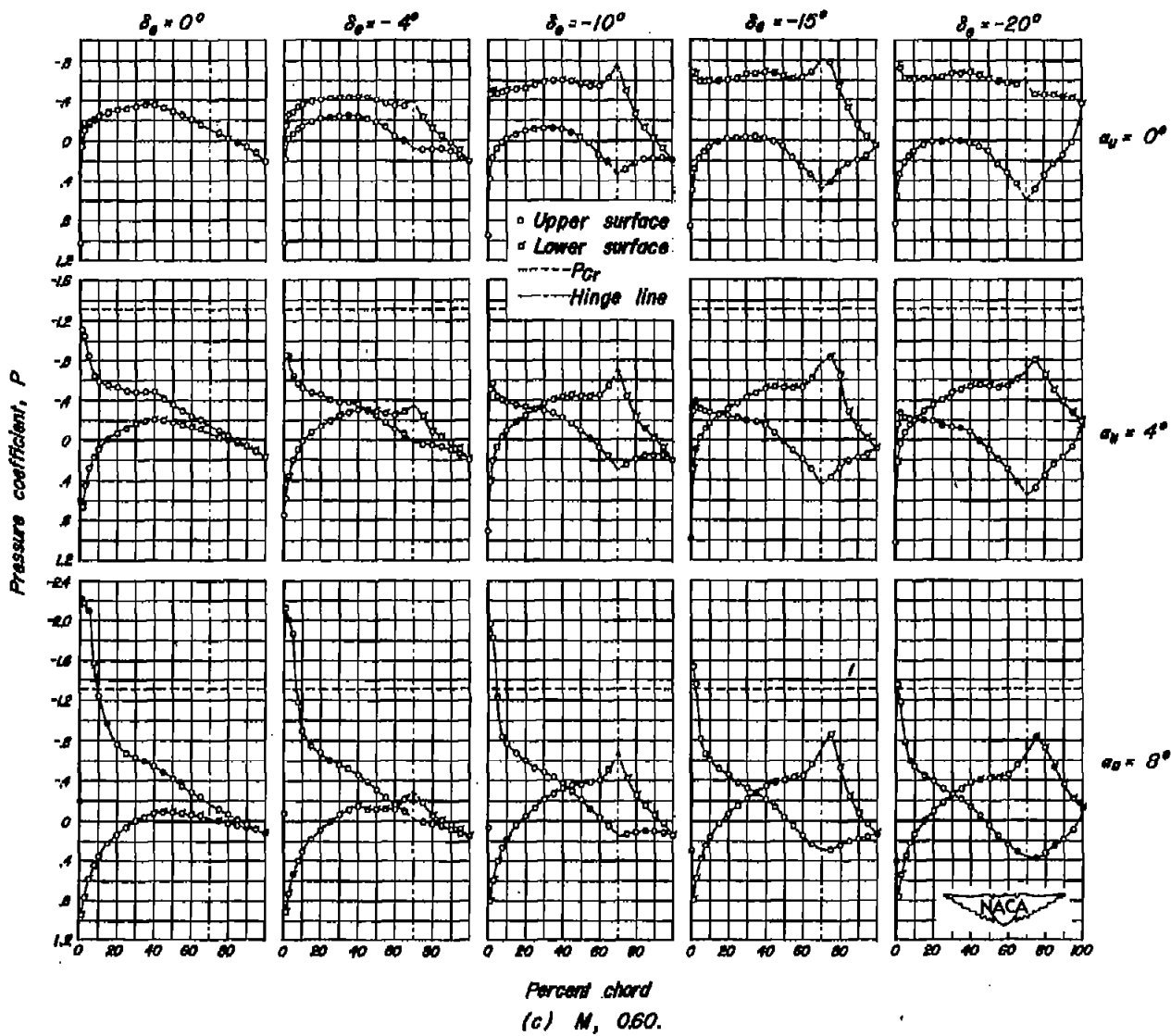


Figure 12.— Continued.

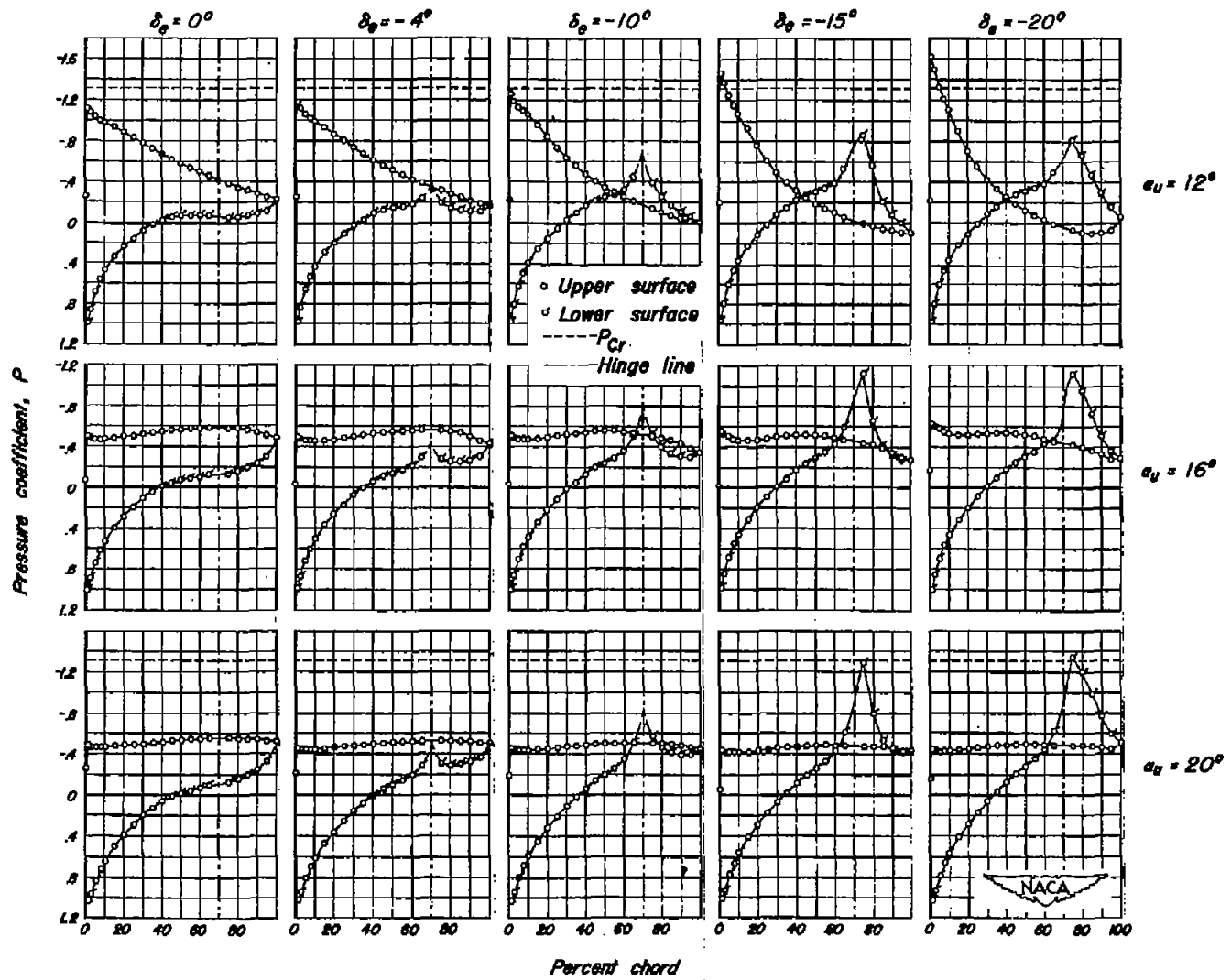
(d) $M, 0.60$, concluded.

Figure 12. — Continued.

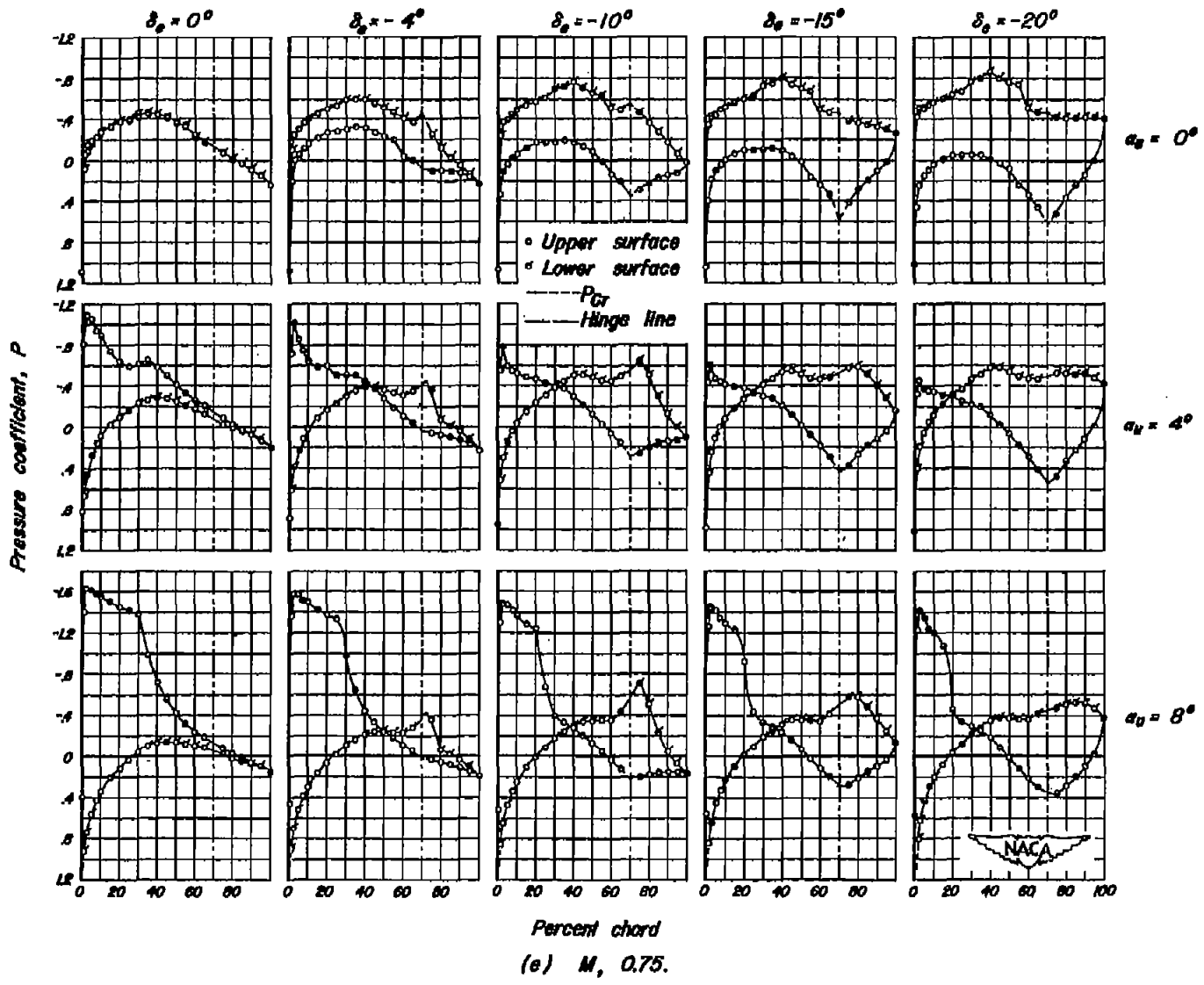


Figure 12.— Continued.

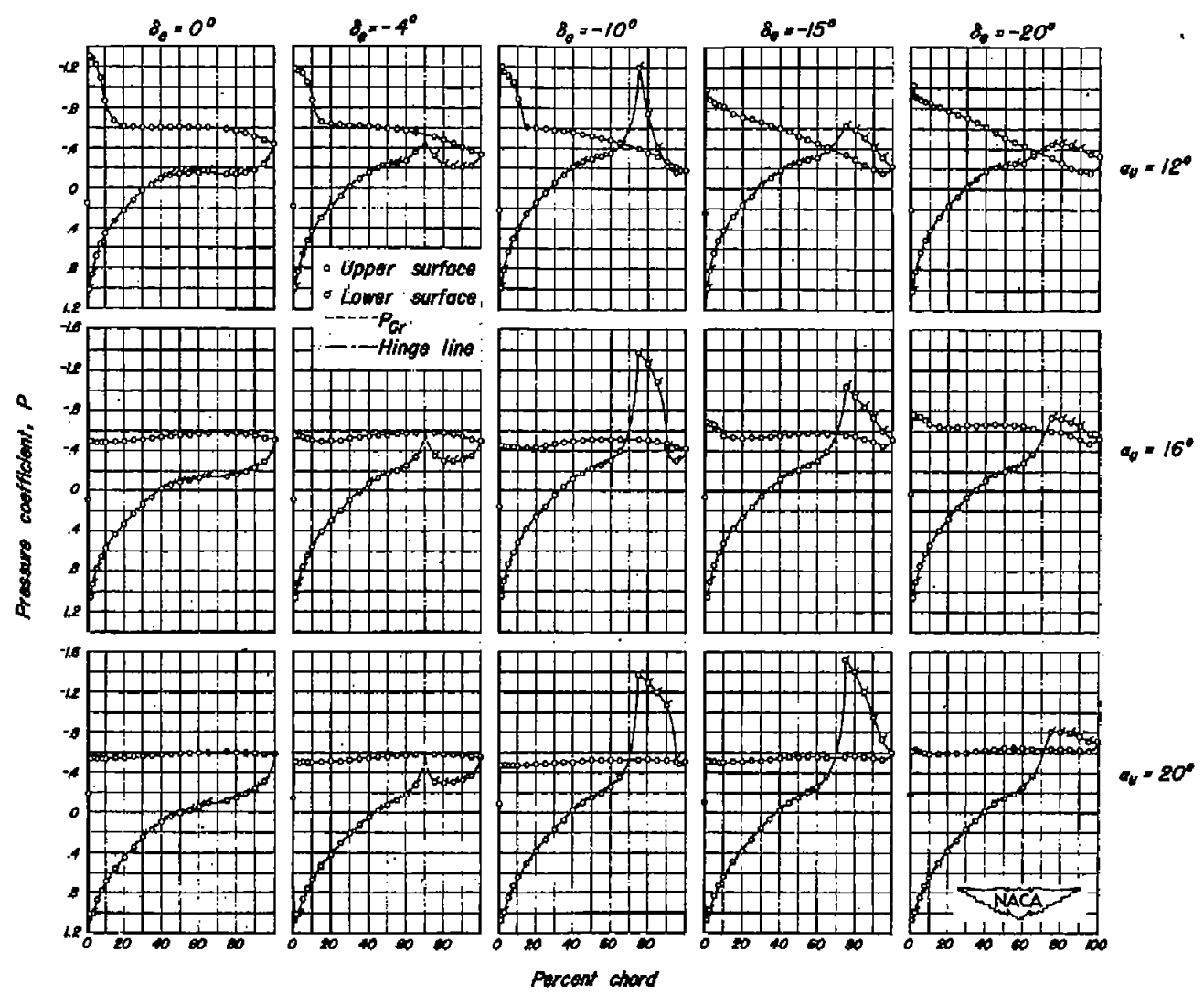


Figure 12.— Continued.

(f) $M, 0.75$, concluded.

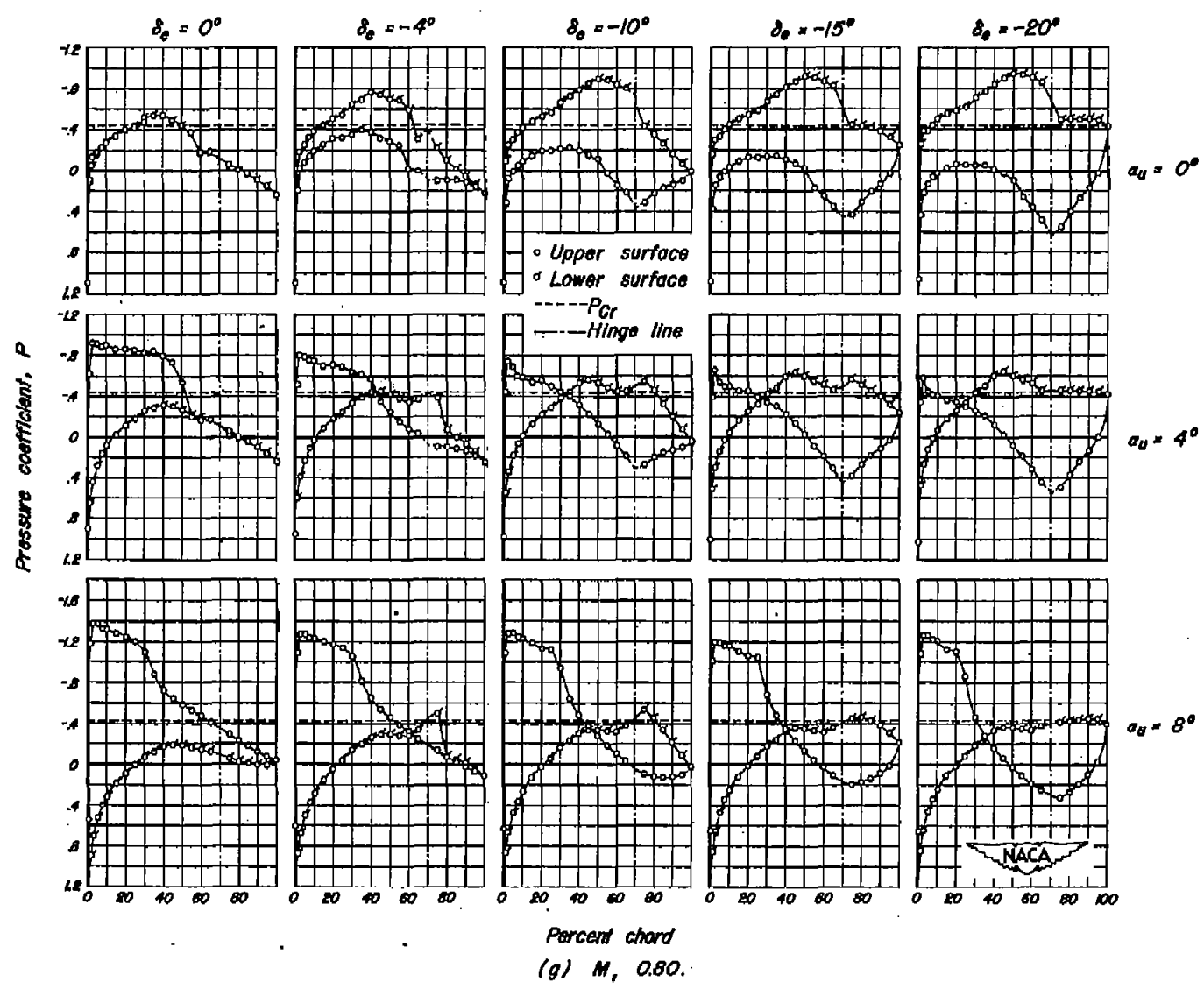


Figure 12.— Continued.

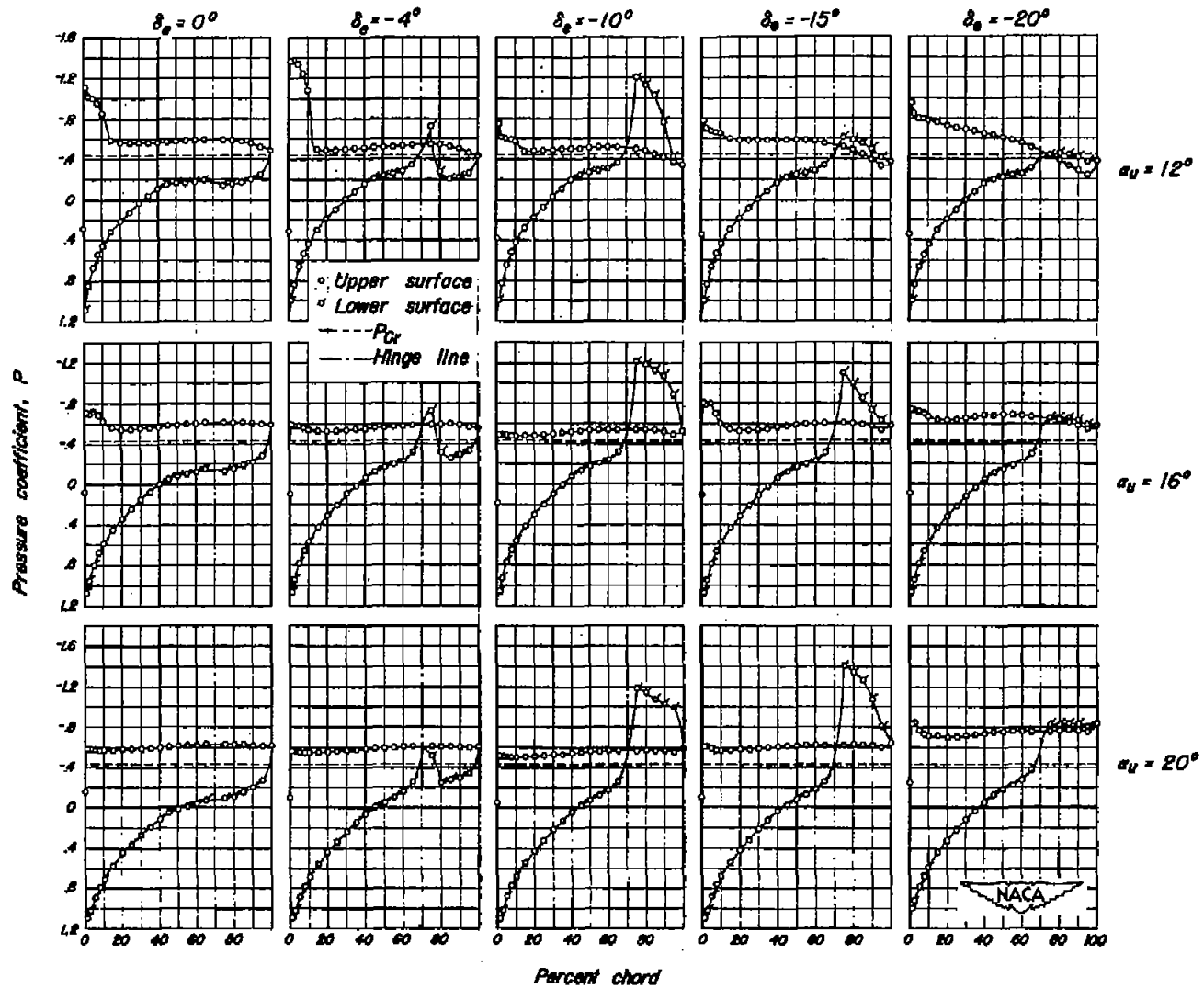


Figure 12. — Continued.

(h) $M, 0.80$, concluded.

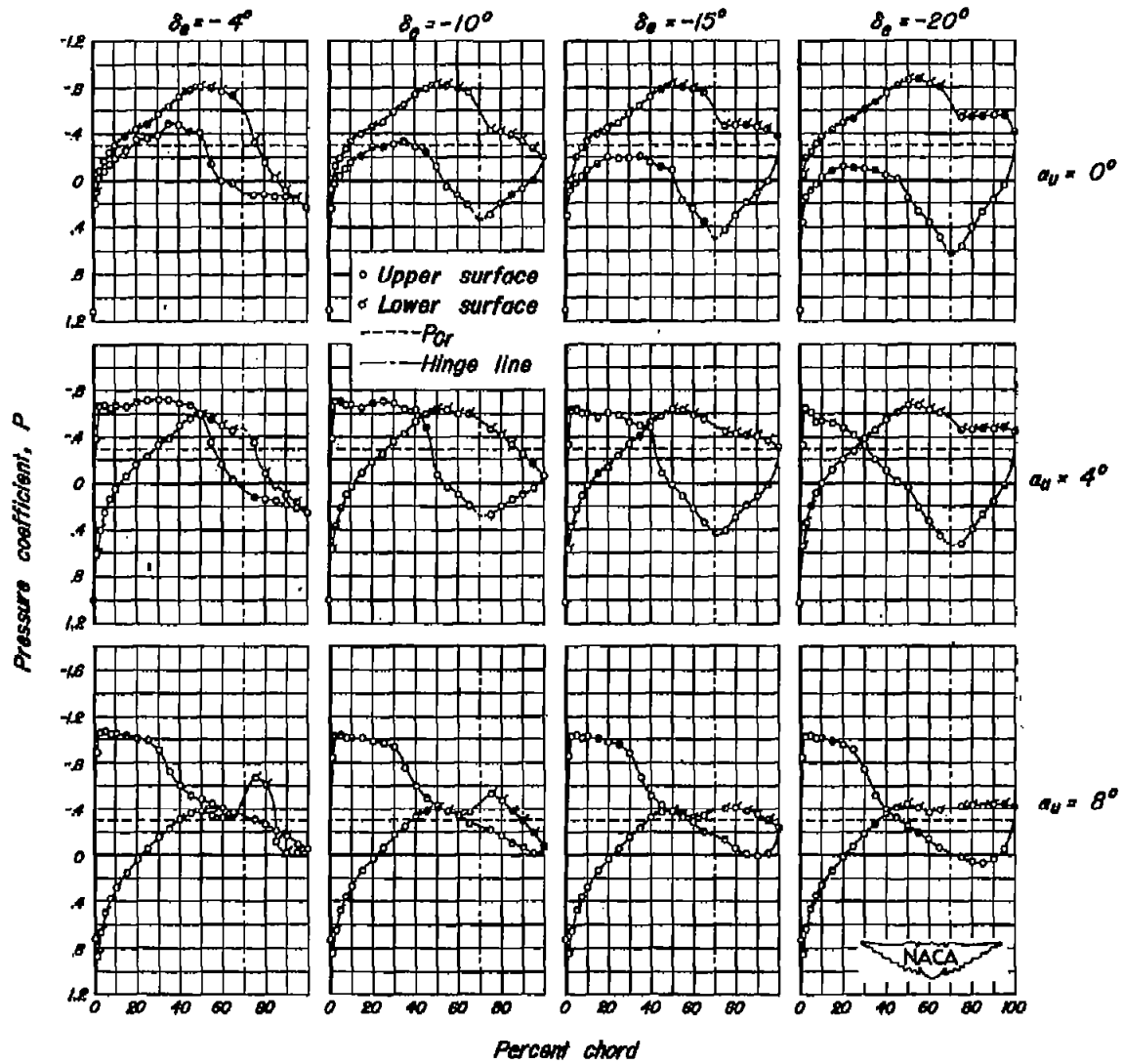
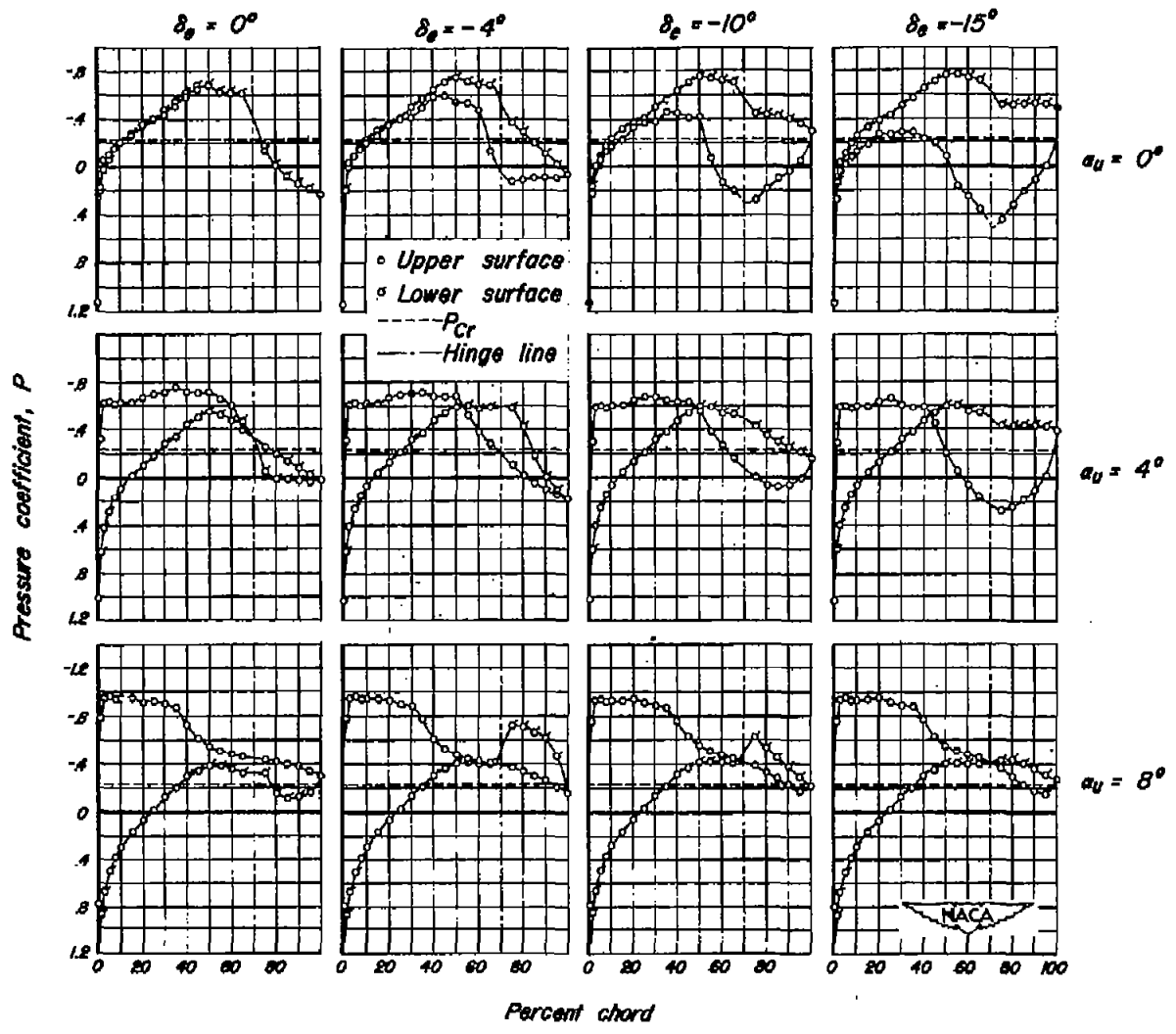


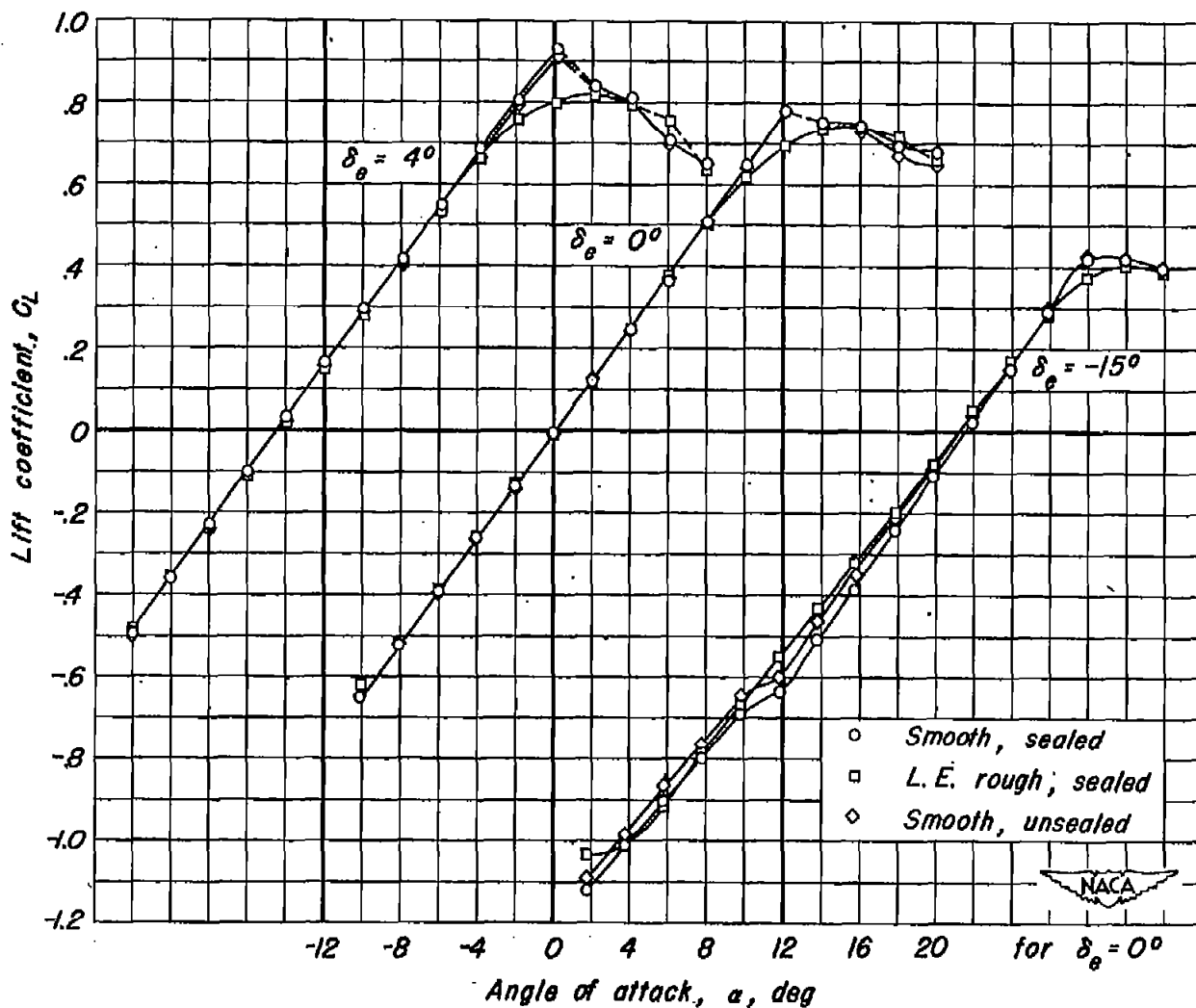
Figure 12.— Continued.

(1) $M, 0.85.$



(j) $M, 0.88.$

Figure 12. — Concluded.



(a) $M, 0.21$.

Figure 13.— The independent effects of leading-edge roughness and removal of the elevator-nose seal on the variation of lift coefficient with angle of attack. $\delta_1, 0^\circ$; $R, 2,000,000$.

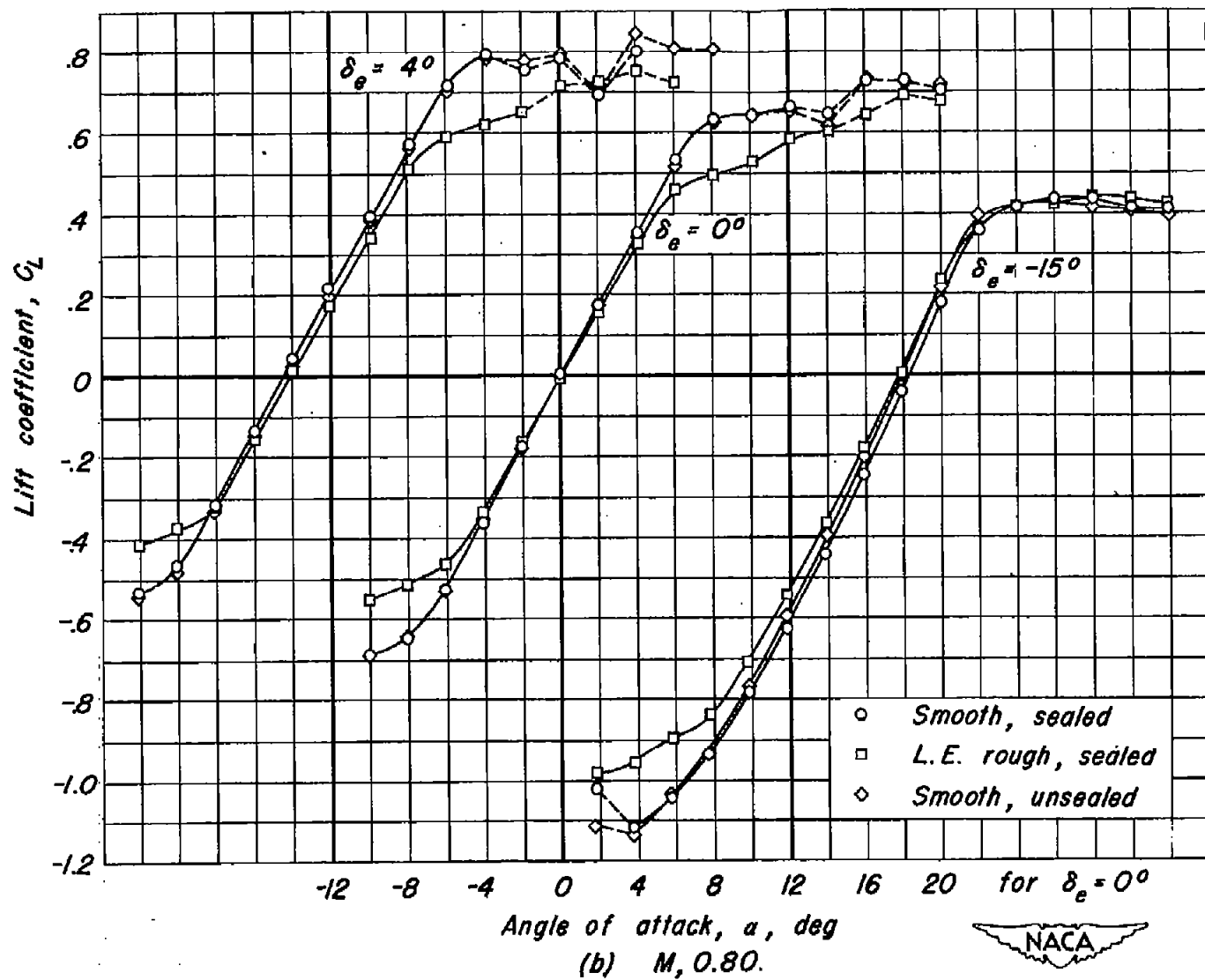


Figure 13. — Continued.

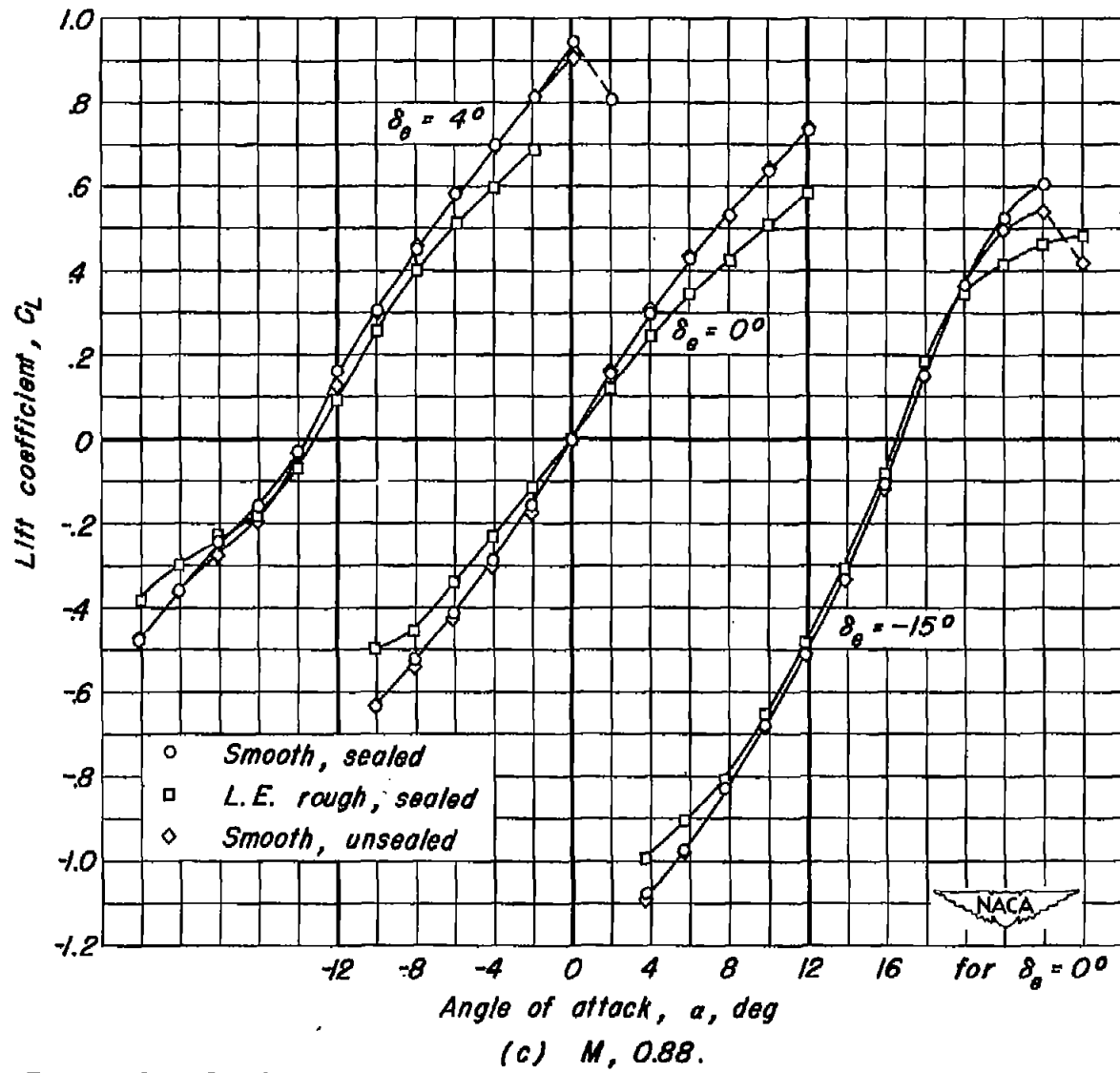


Figure 13. - Concluded.

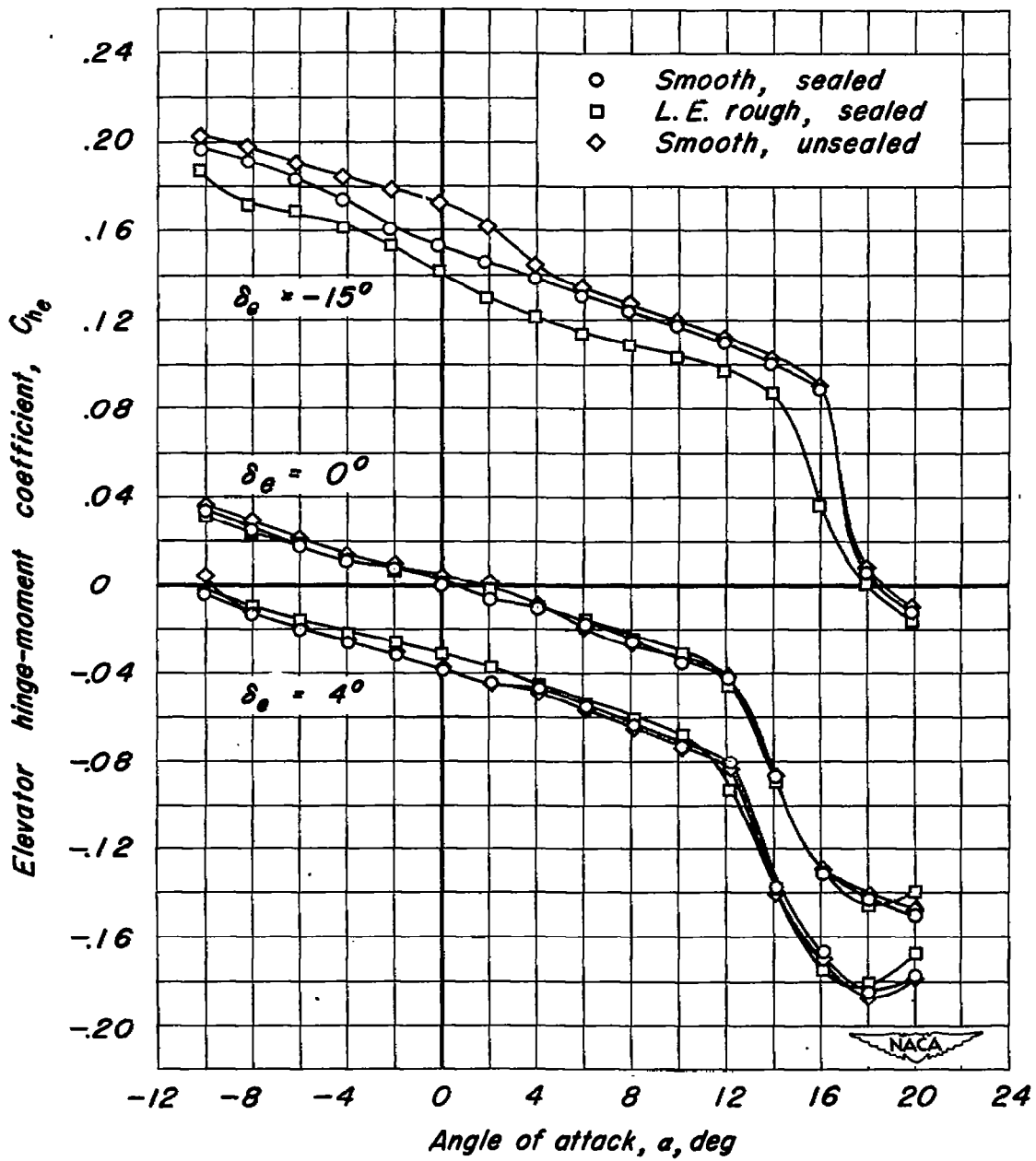
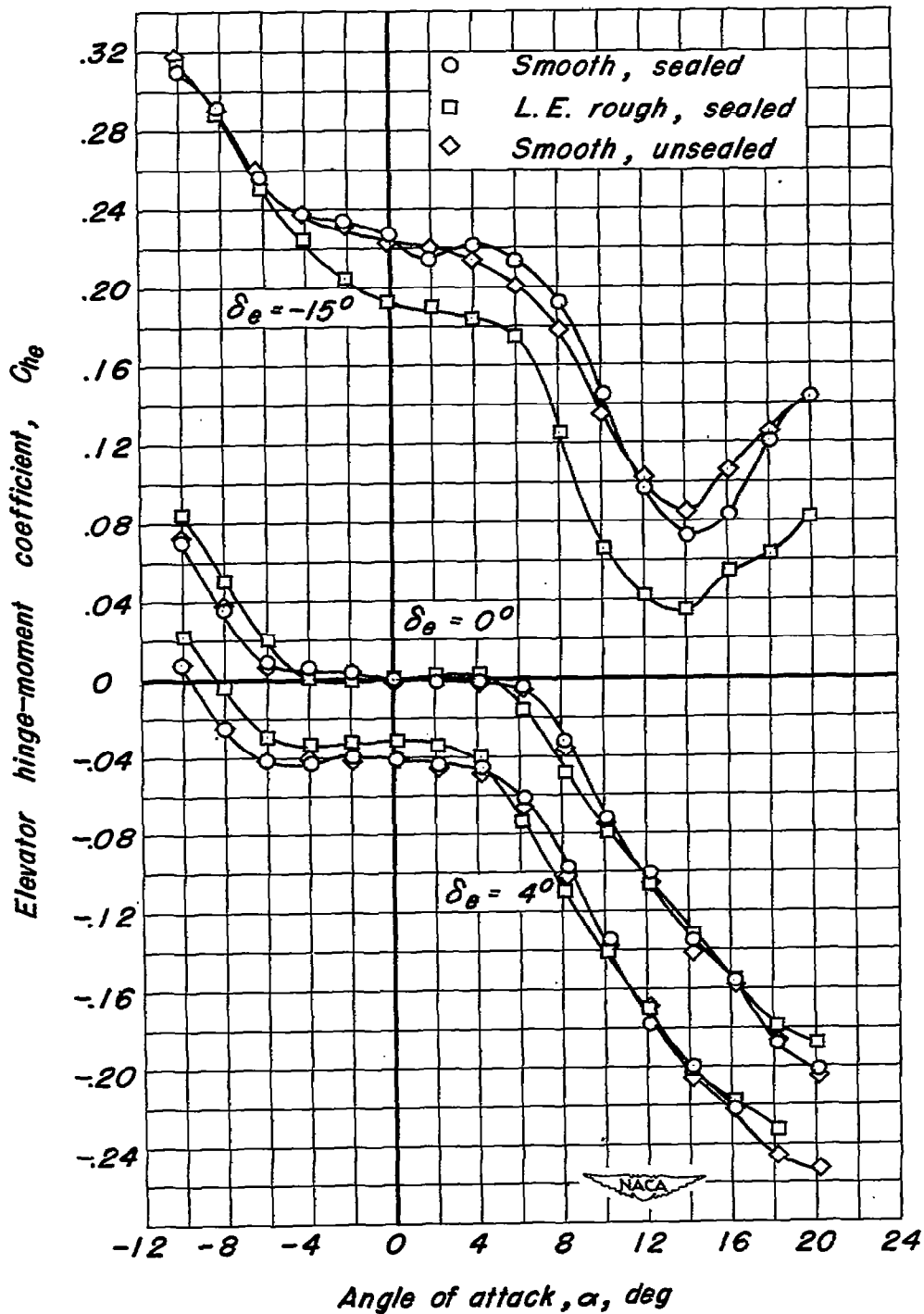
(a) $M, 0.21$.

Figure 14.— The independent effects of leading-edge roughness and removal of the elevator-nose seal on the variation of elevator hinge-moment coefficient with angle of attack. $\delta_t, 0^\circ$; $R, 2,000,000$.



(b) $M, 0.80.$

Figure 14. - Continued.

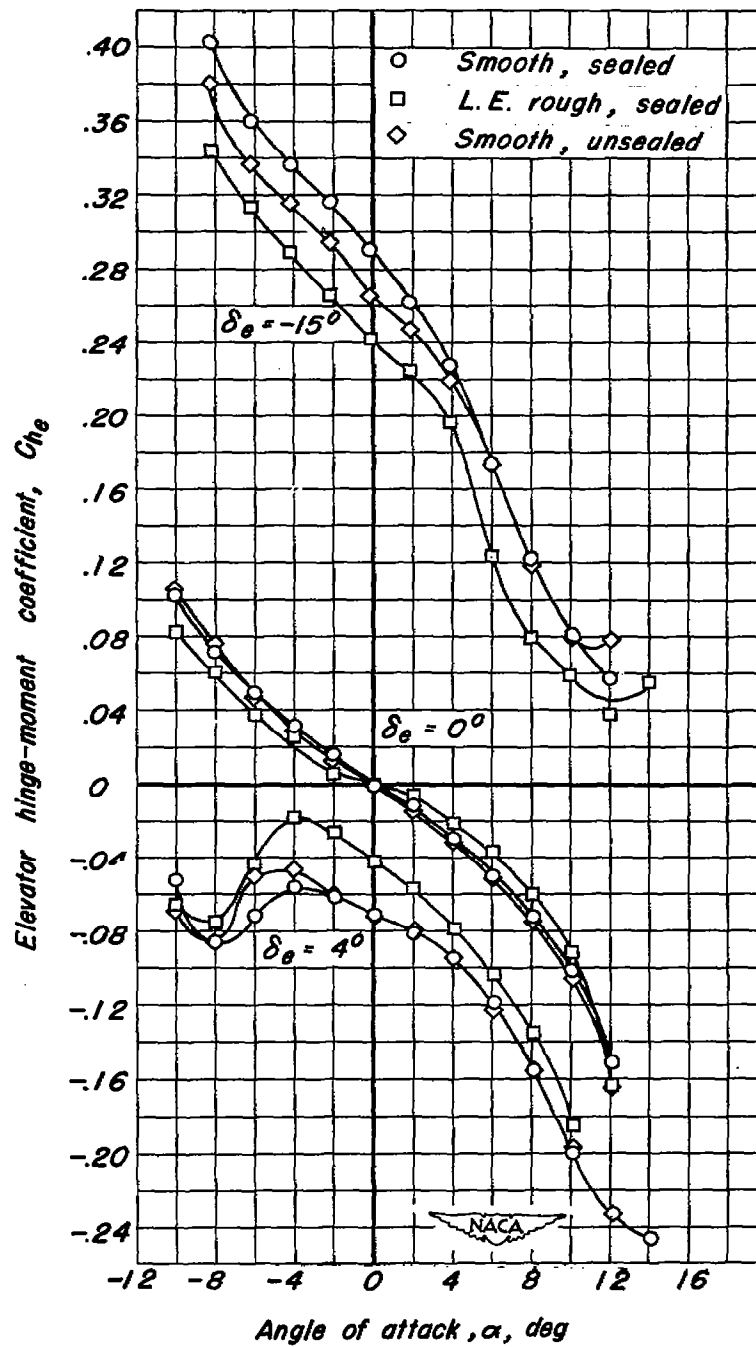
(c) $M, 0.88.$

Figure 14. — Concluded.

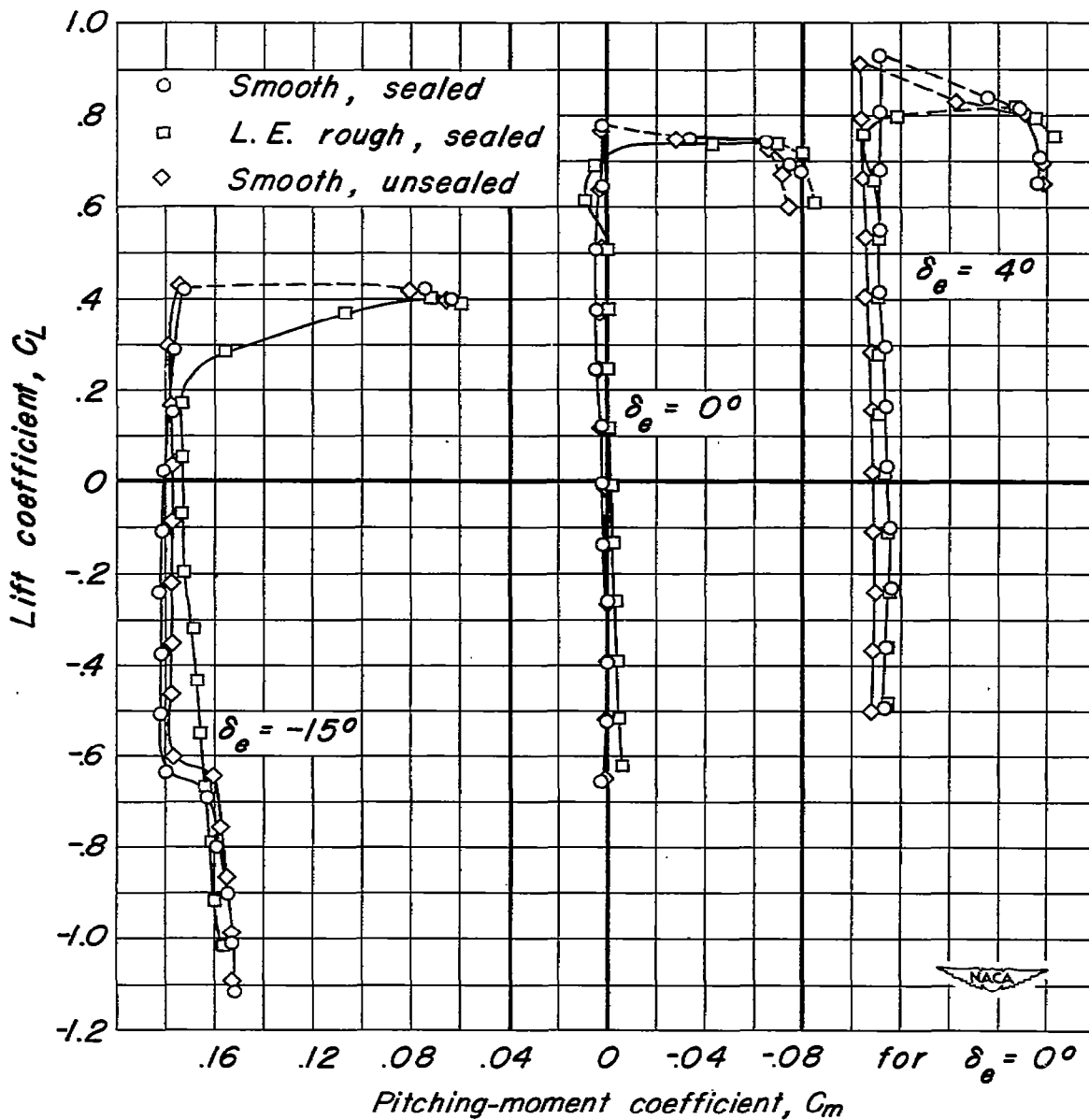
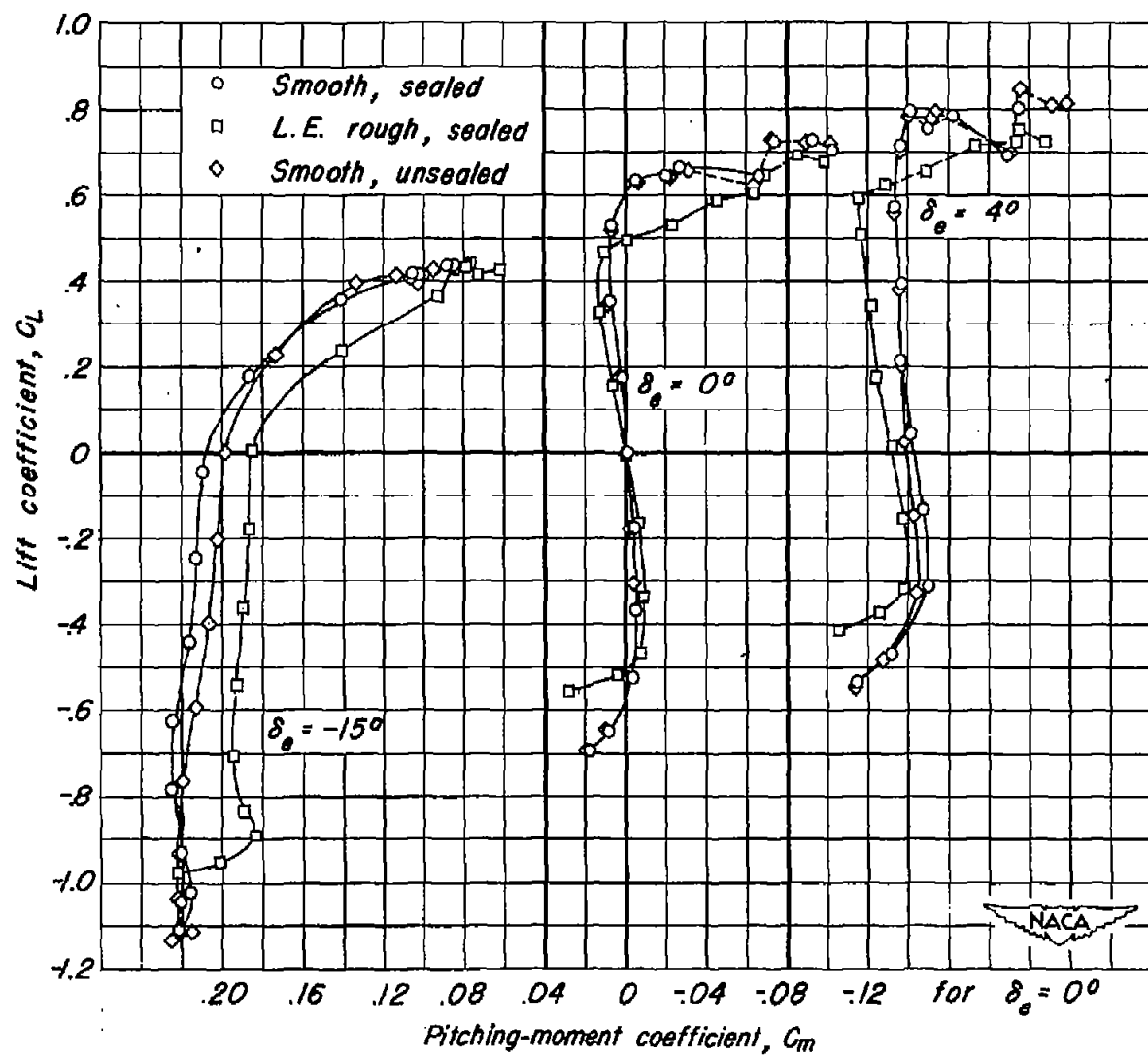
(a) $M, 0.21$.

Figure 15. — The independent effects of leading-edge roughness and removal of the elevator-nose seal on the variation of lift coefficient with pitching-moment coefficient. $\delta_t, 0^\circ$; $R, 2,000,000$.



(b) $M, 0.80$.

Figure 15. — Continued.

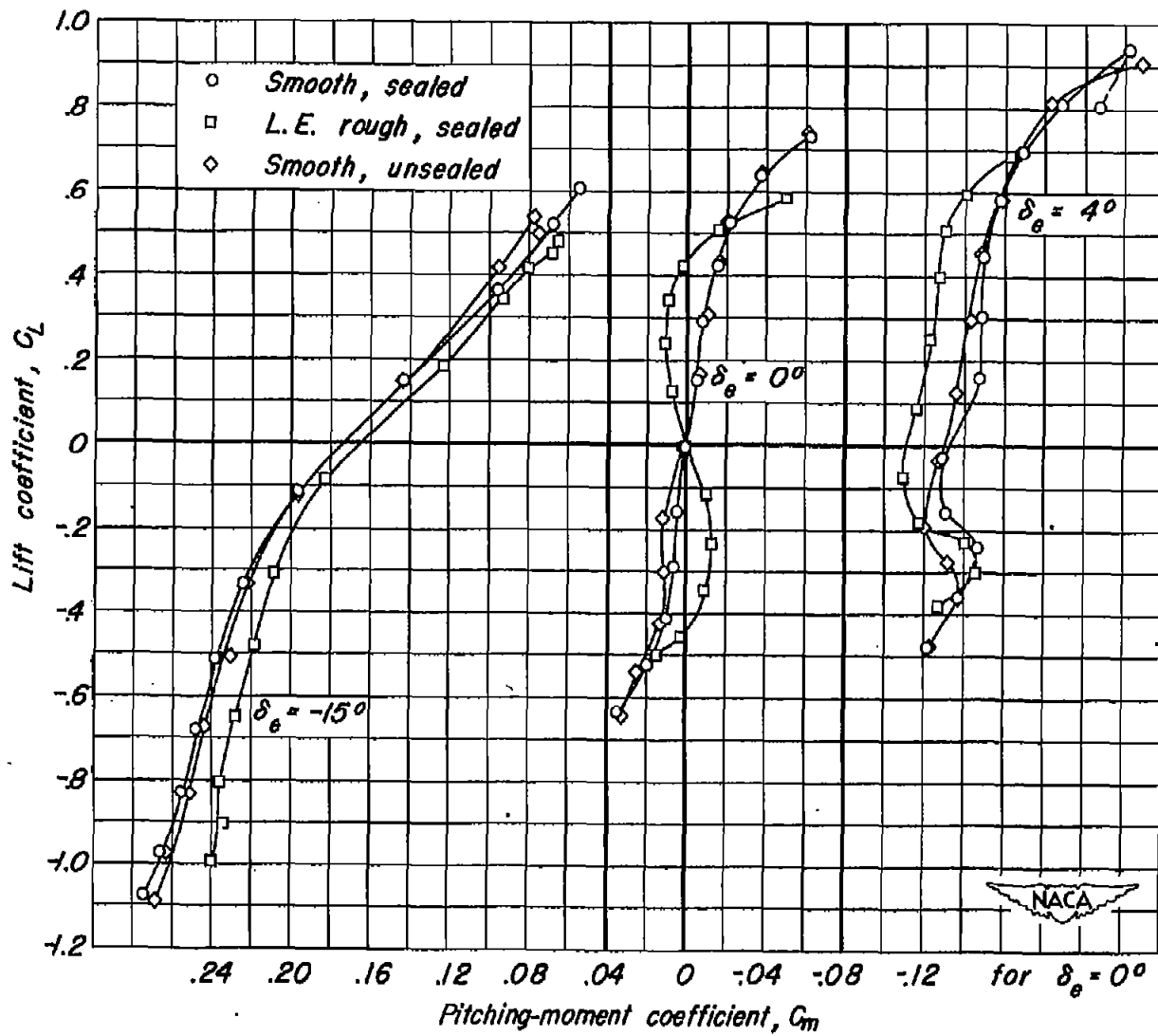


Figure 15. — Concluded.

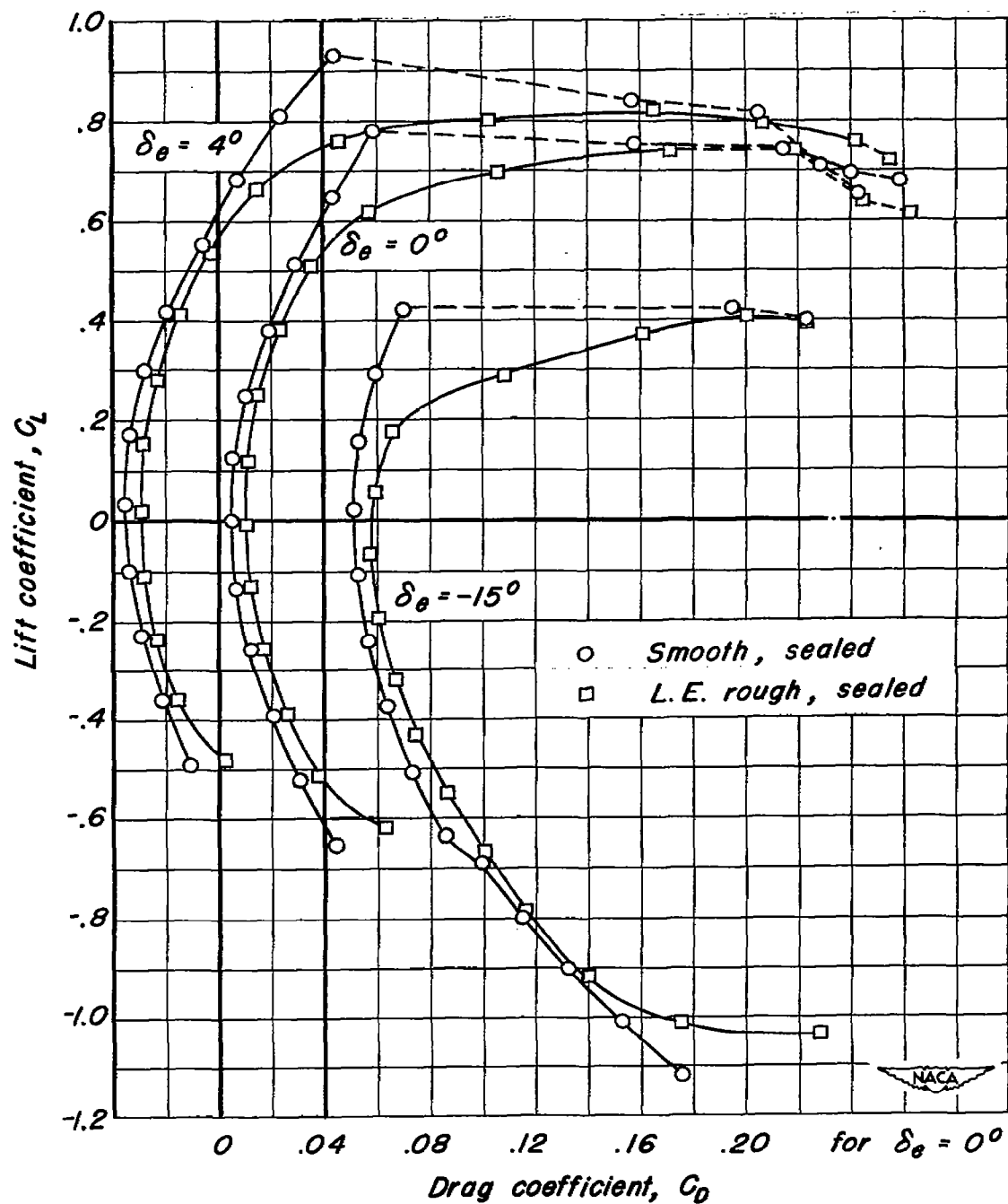
(a) $M, 0.21$.

Figure 16.— The effect of leading-edge roughness on the variation of lift coefficient with drag coefficient. $\delta_1, 0^\circ$; $R, 2,000,000$.

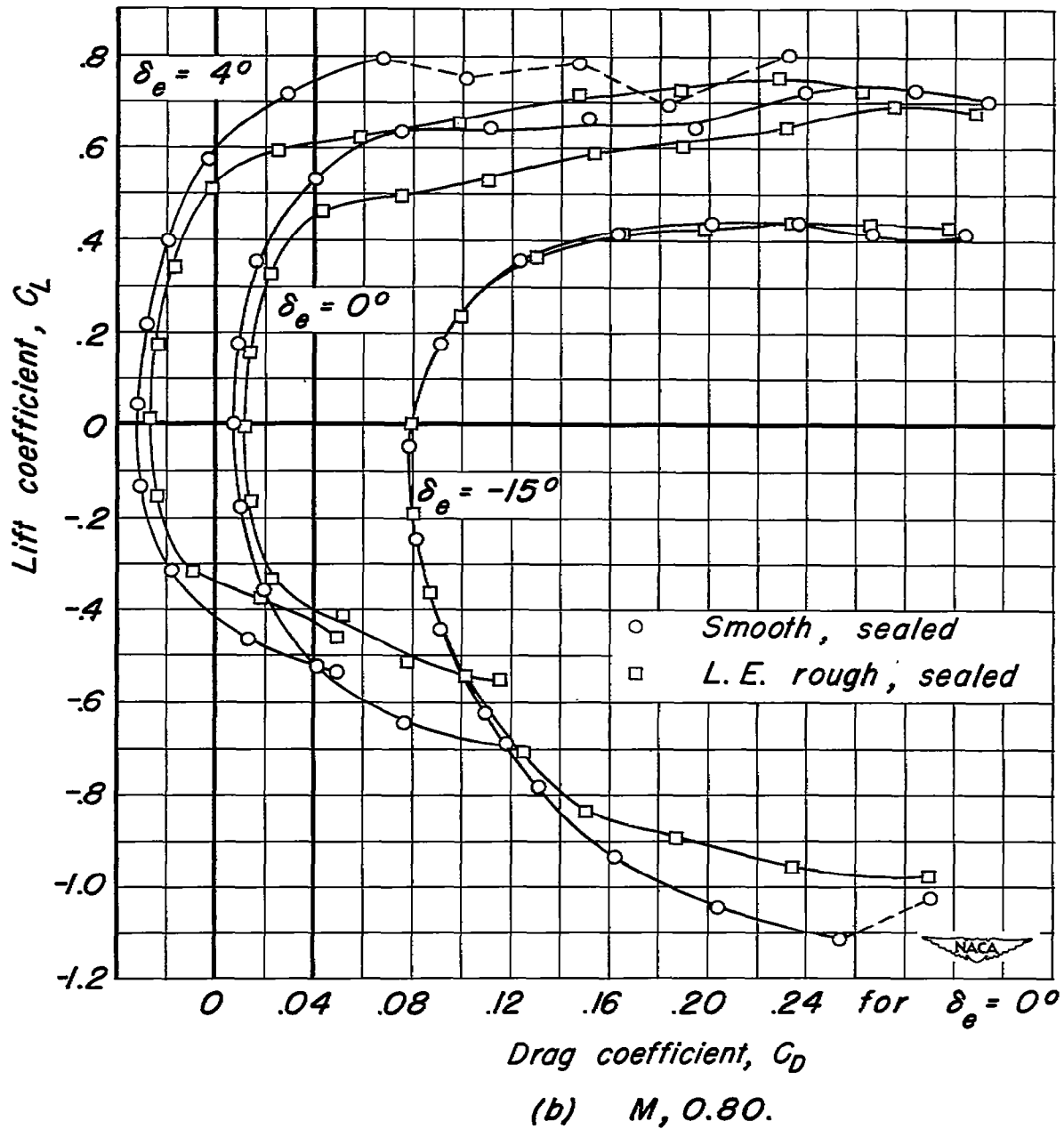
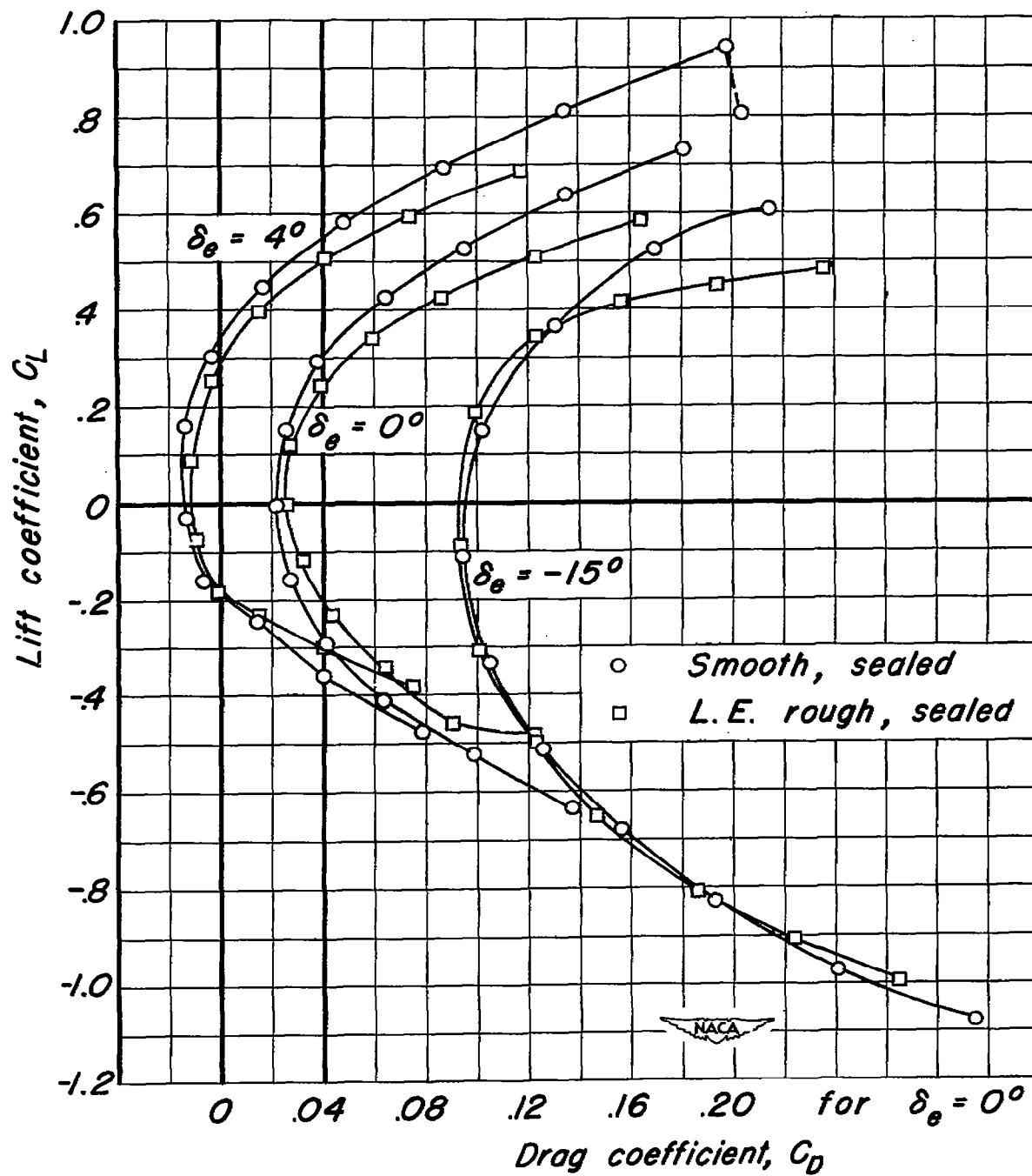


Figure 16. — Continued.



(c) $M, 0.88.$

Figure 16. — Concluded.

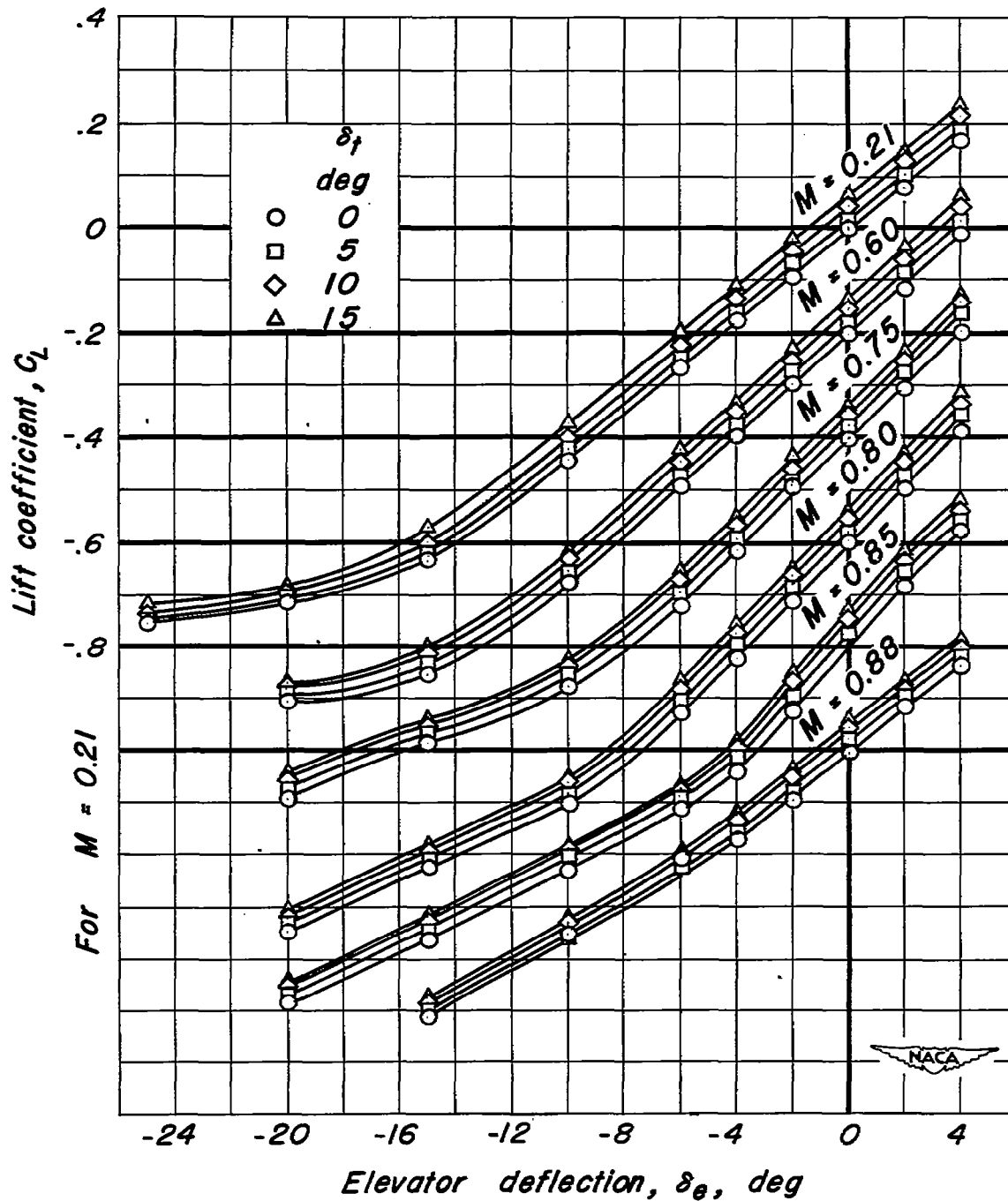


Figure 17. — The variation of lift coefficient with elevator deflection. $\alpha_u, 0^\circ$; $R, 2,000,000$.

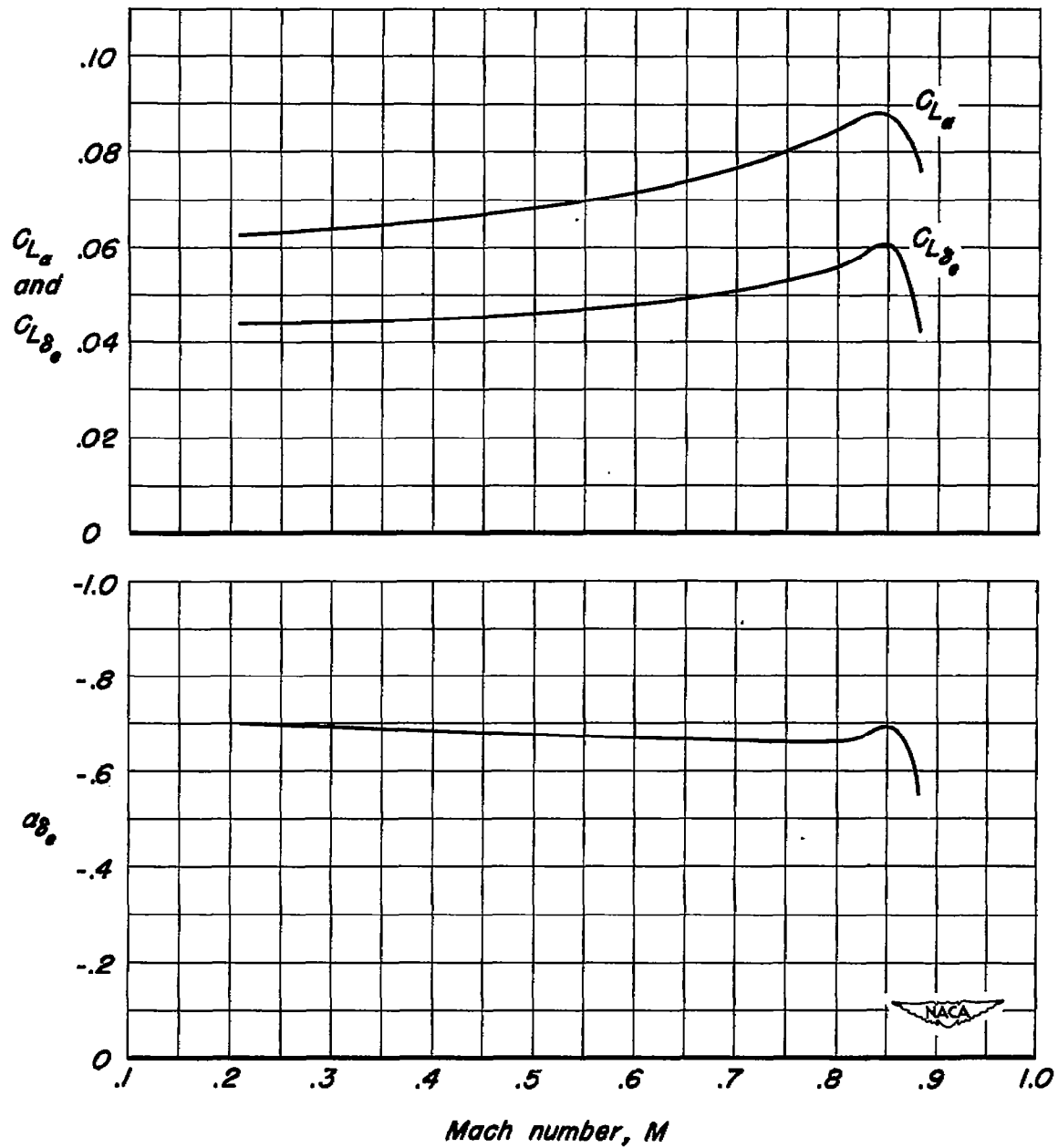
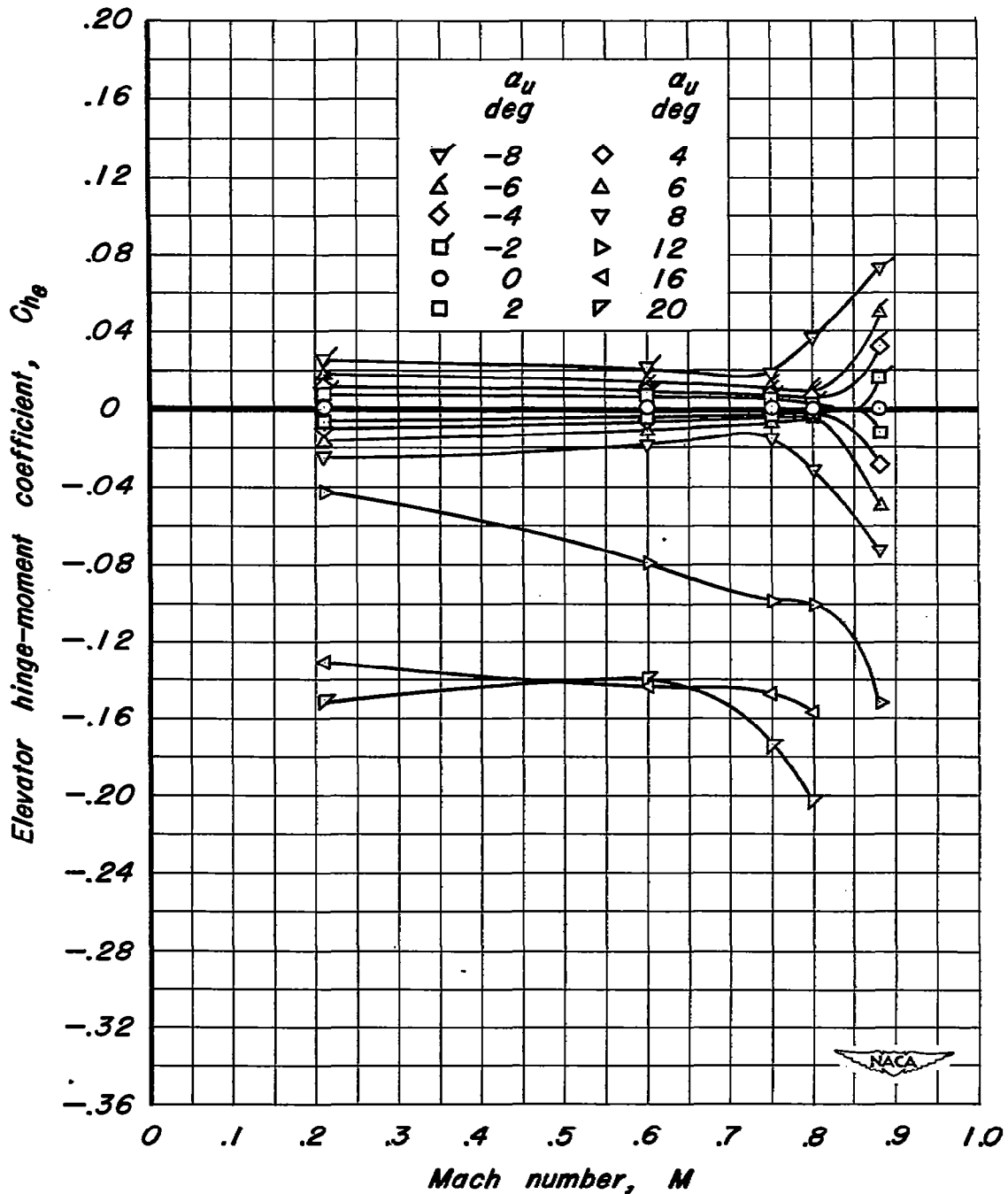
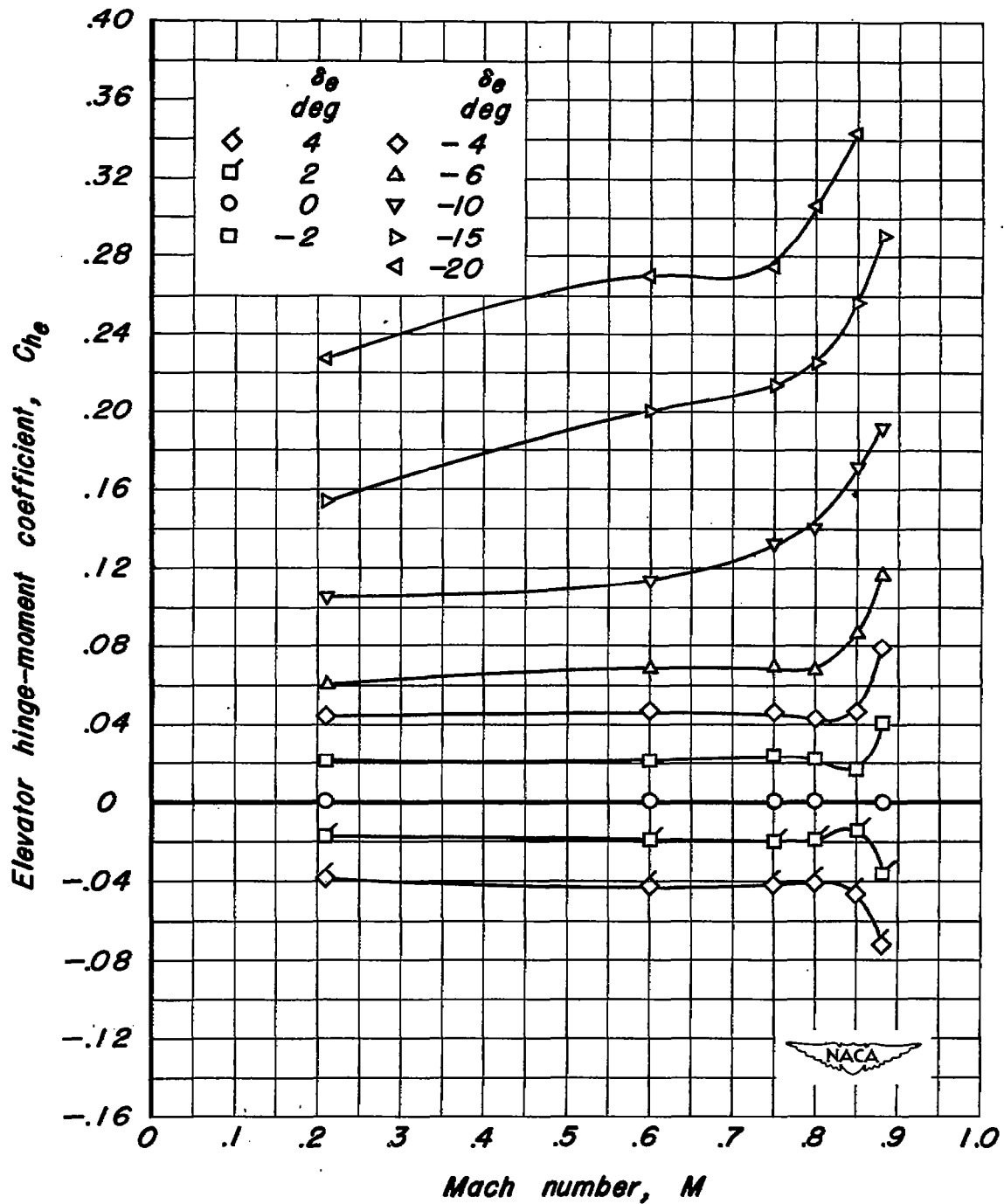


Figure 18.- The variations of lift parameters C_{L_α} , C_{L_β} , and α_{β_0} with Mach number. R , 2,000,000.



(a) $\delta_\theta, 0^\circ$

Figure 19.— The variation of elevator hinge-moment coefficient with Mach number. $\delta_t, 0^\circ$; $R, 2,000,000$.



(b) $\alpha_u, 0^\circ$.

Figure 19.— Concluded.

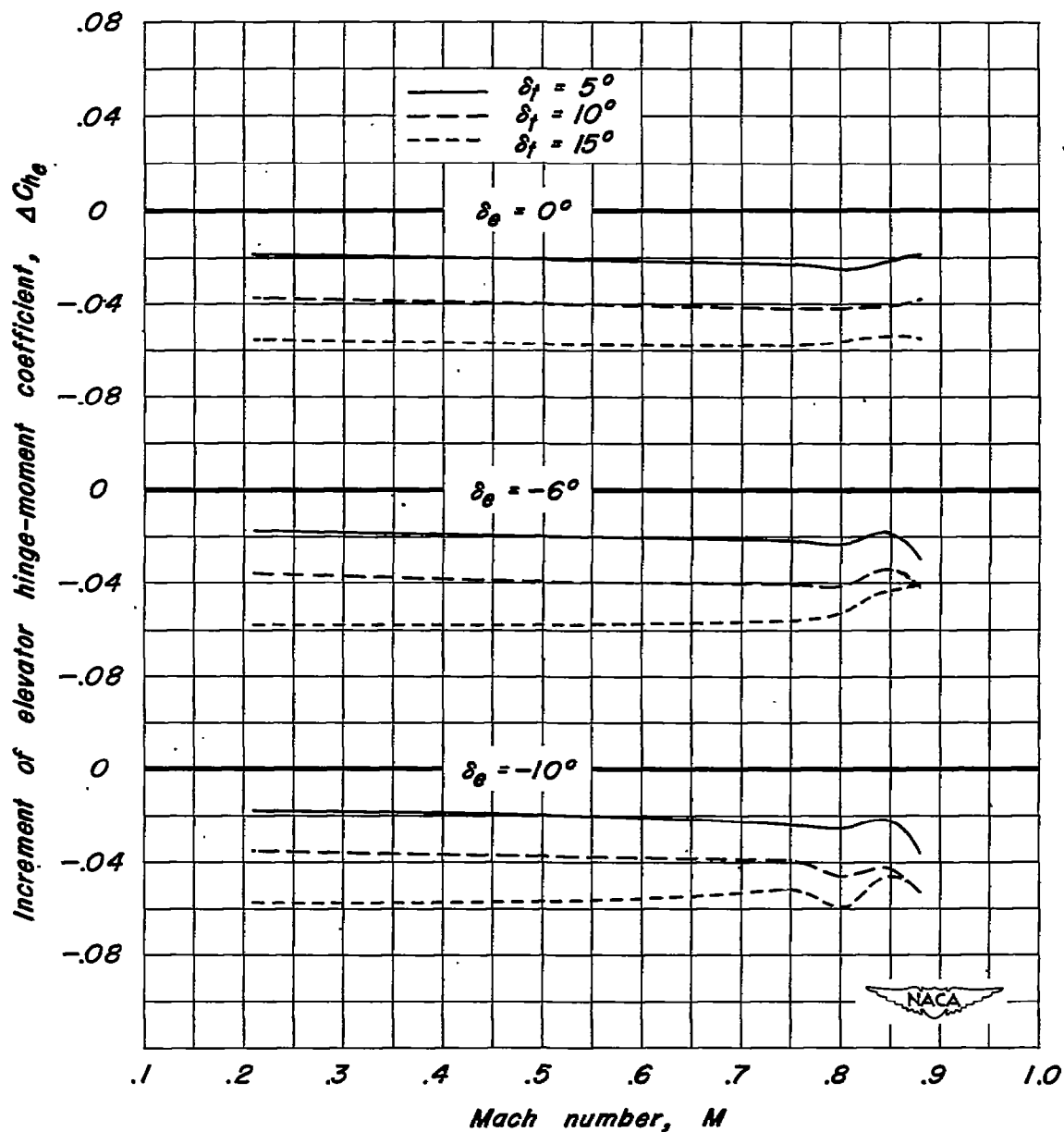


Figure 20. — The variation of increment of elevator hinge-moment coefficient due to tab deflection with Mach number. $\alpha_u, 0^\circ$; $R, 2,000,000$.

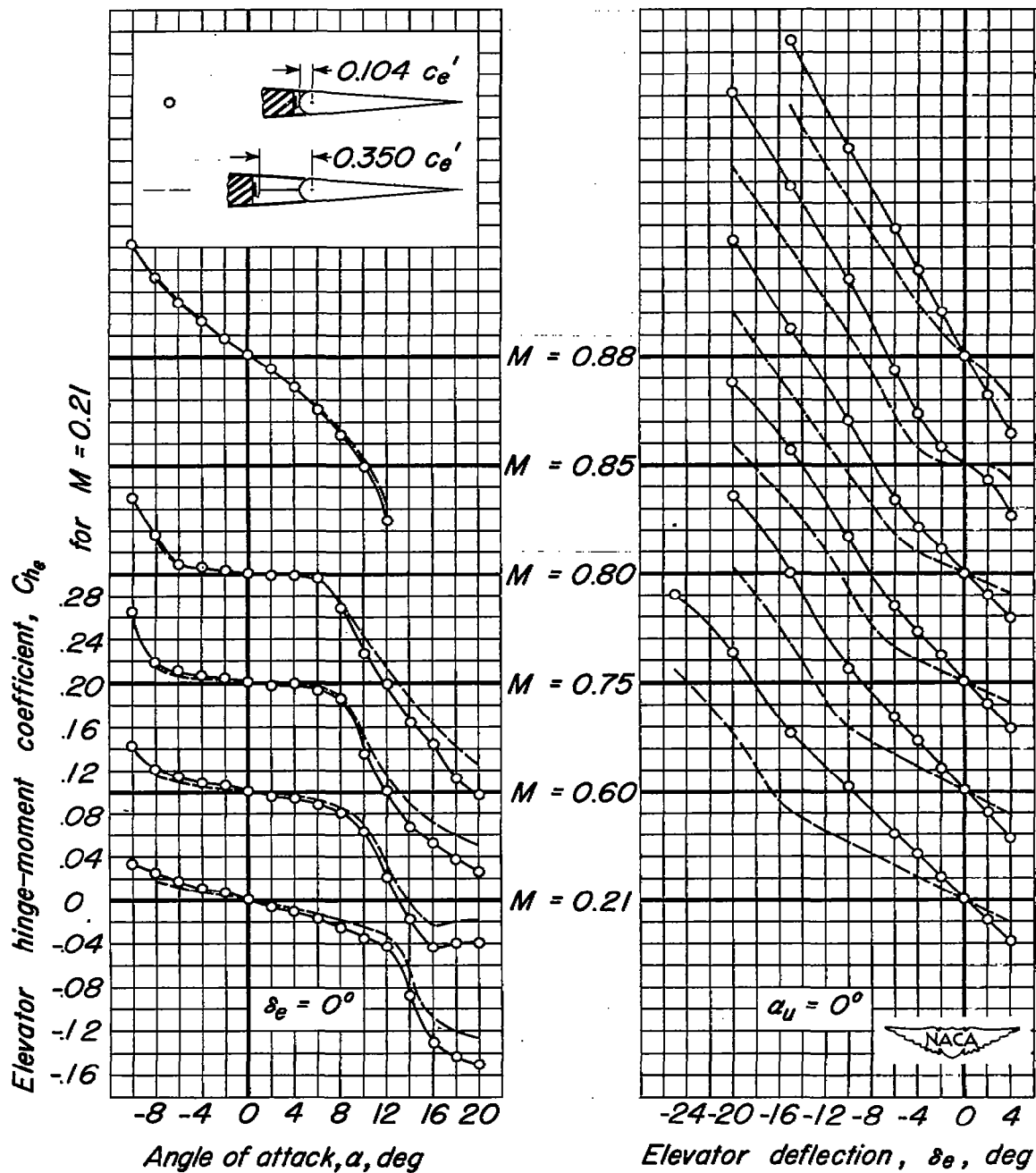


Figure 21. — The computed effect of a sealed, internal, aerodynamic balance on the variation of elevator hinge-moment coefficient with angle of attack and with elevator deflection. $\delta_t, 0^\circ$; $R, 2,000,000$.

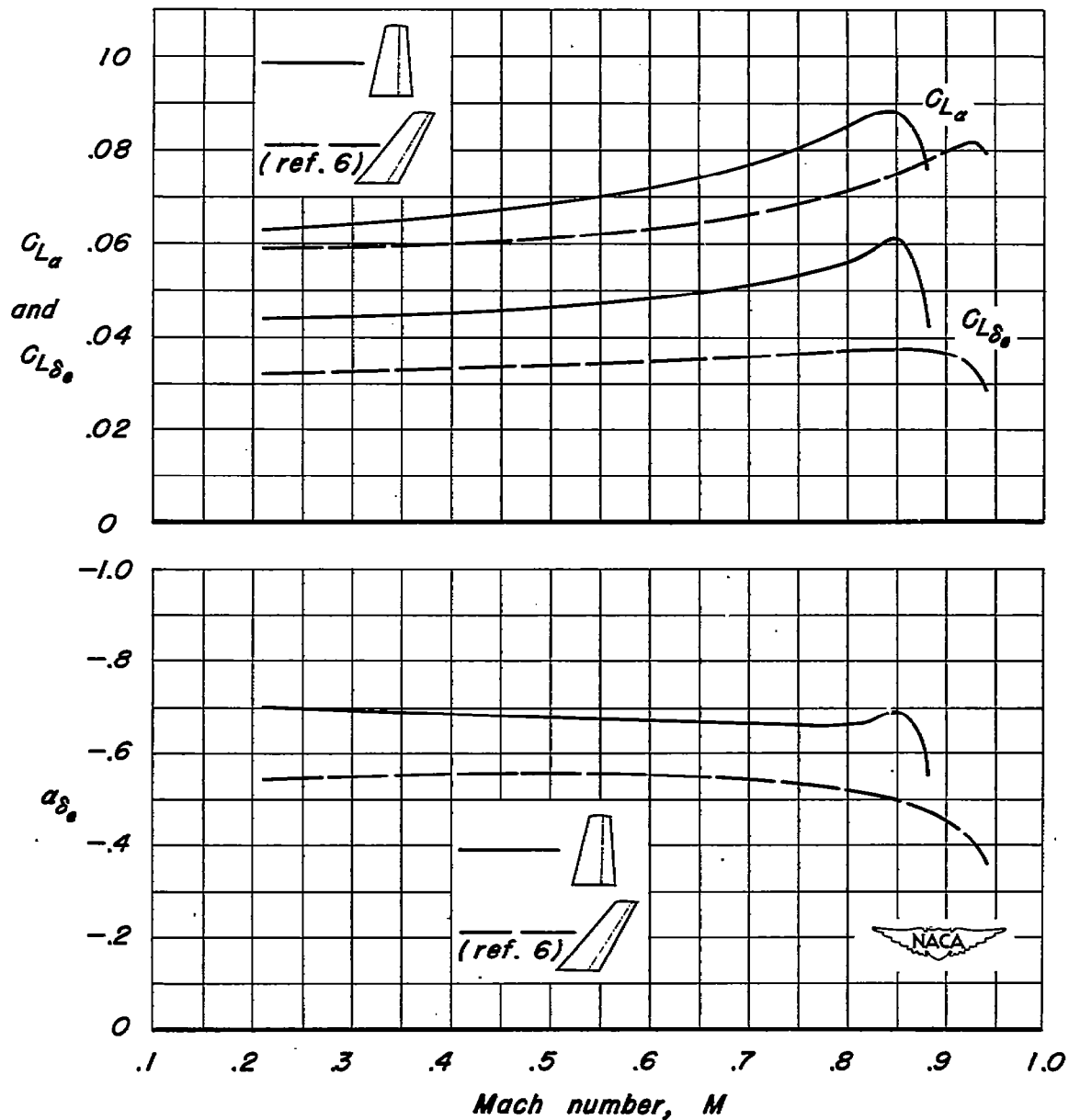


Figure 22.-The variations of the parameters $C_{L\alpha}$, $C_{L\delta_0}$, and α_{δ_0} with Mach number for two horizontal tails: one with the hinge line normal to the plane of symmetry and one with the quarter-chord line having 35° of sweepback. $\delta_1, 0^\circ$; $R, 2,000,000$.

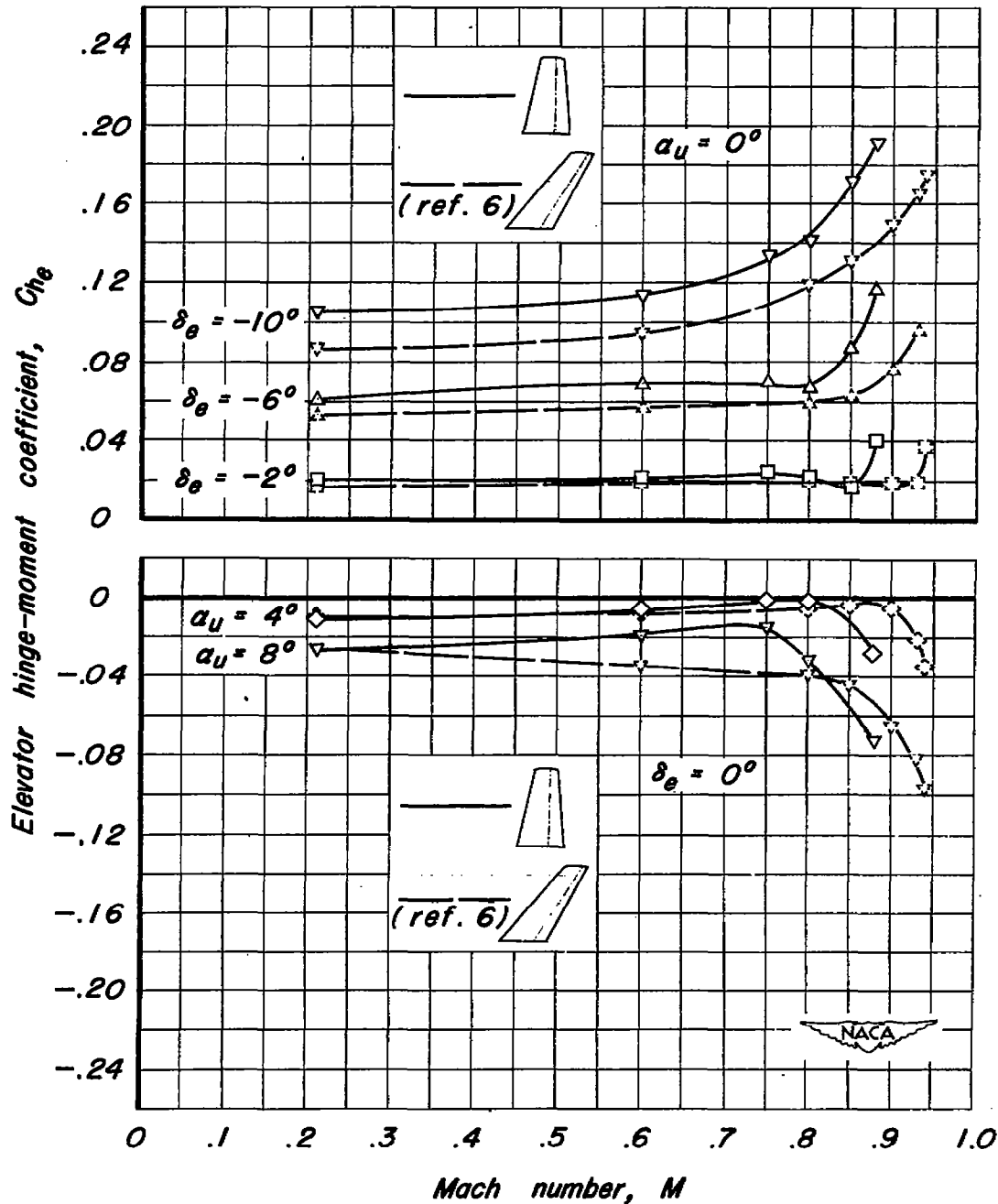


Figure 23.- The variation of elevator hinge-moment coefficient with Mach number for two horizontal tails: one with the hinge line normal to the plane of symmetry and one with the quarter-chord line having 35° of sweepback. $\delta_t, 0^\circ$; $R, 2,000,000$.

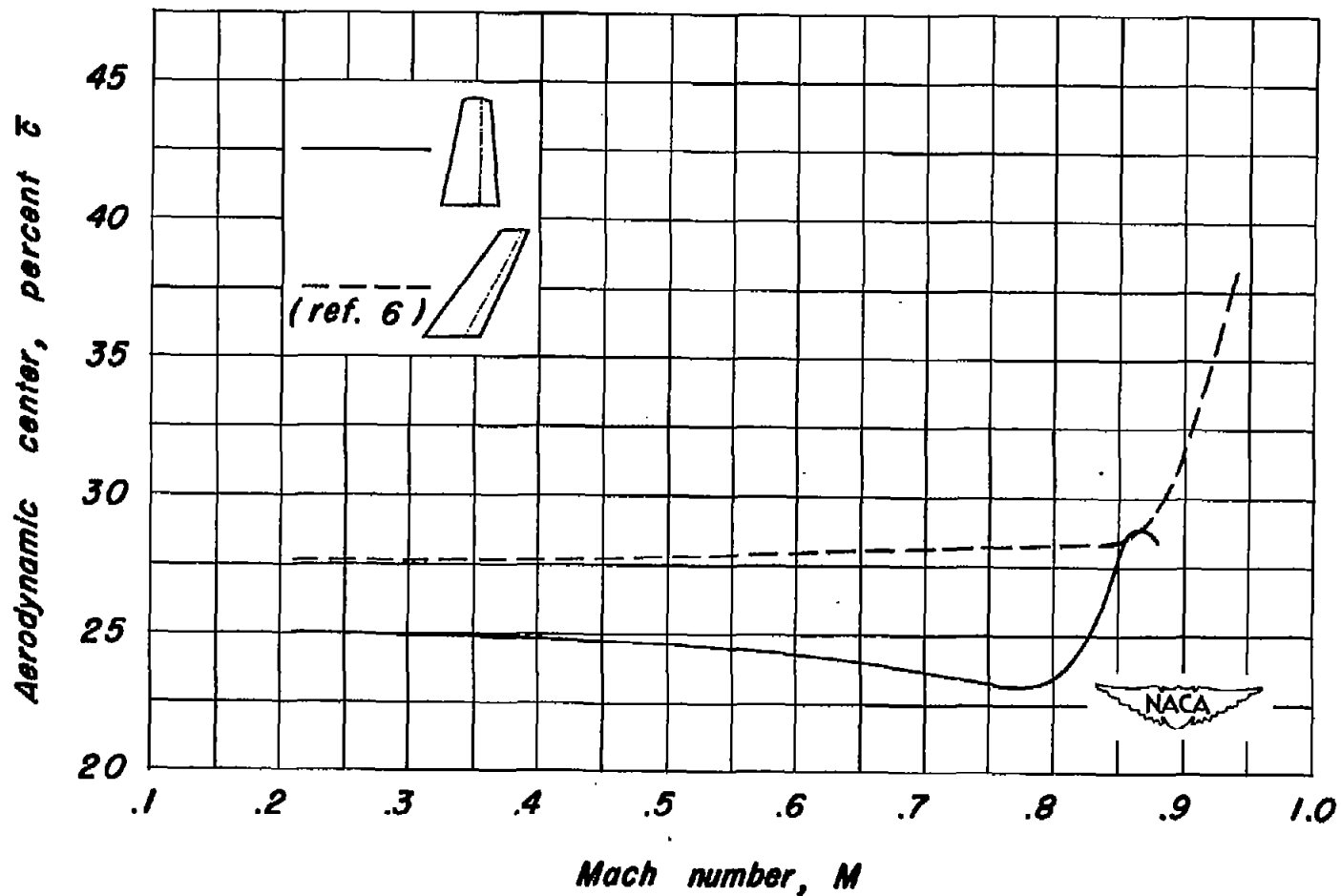


Figure 24.- The variations of aerodynamic-center location for two horizontal tails: one with the hinge line normal to the plane of symmetry and one with the quarter-chord line having 35° of sweepback. $C_L, 0$; $\delta_e, 0^\circ$; $\delta_1, 0^\circ$; $R, 2,000,000$.

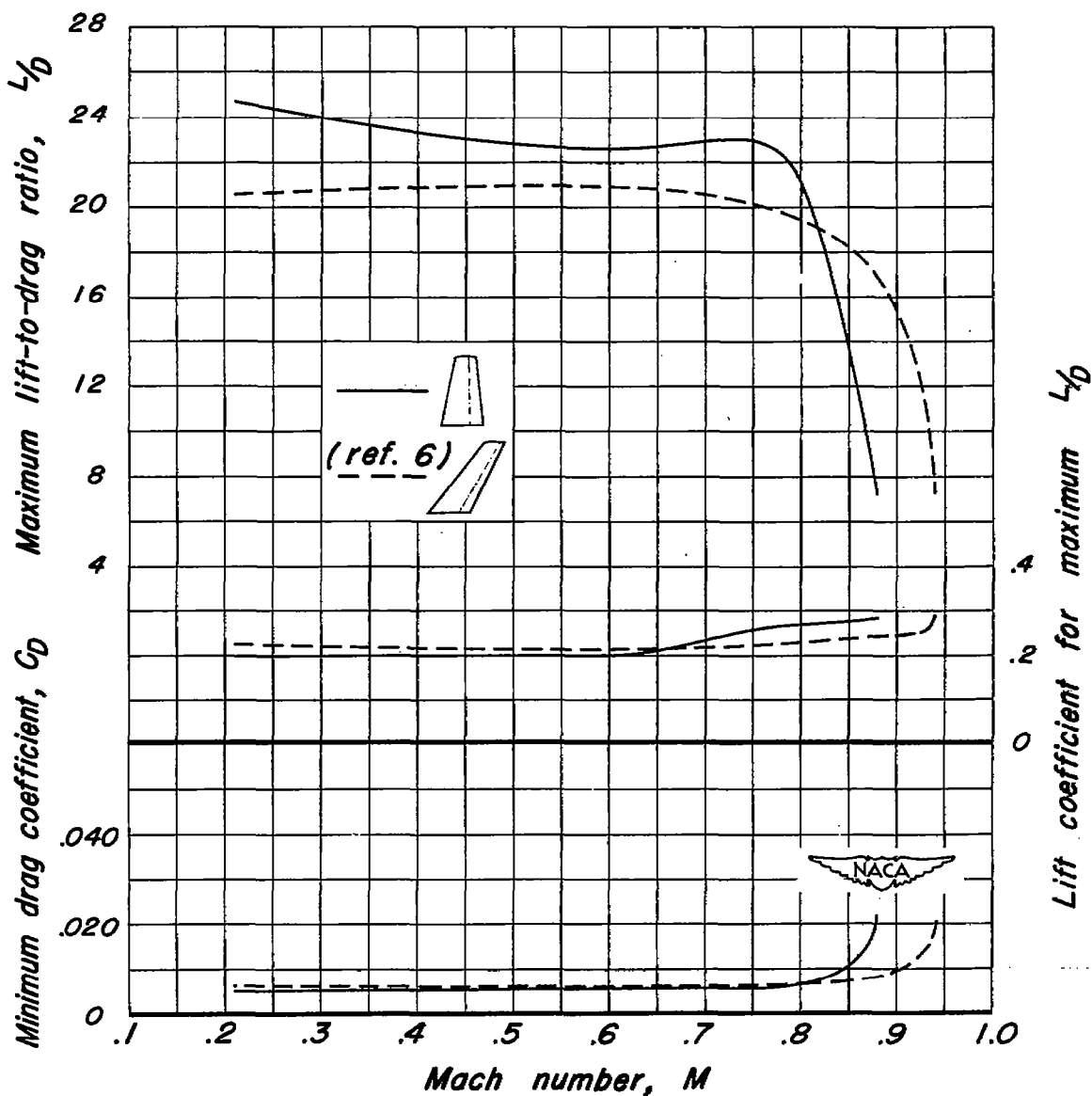


Figure 25.- The variations of maximum lift-drag ratio, of lift coefficient for maximum lift-drag ratio, and of minimum drag coefficient with Mach number for two horizontal tails: one with the hinge line normal to the plane of symmetry and one with the quarter-chord line having 35° of sweepback. $\delta_e, 0^\circ$; $\delta_f, 0^\circ$; $R, 2,000,000$.

NASA Technical Library



3 1176 01434 4817